OPTICAL WIRELESS COMMUNICATIONS WITH OPTICAL POWER AND DYNAMIC RANGE CONSTRAINTS

A Dissertation
Presented to
The Academic Faculty

by

Zhenhua Yu

In Partial Fulfillment
of the Requirements for the Degree
Doctor of Philosophy in the
School of Electrical and Computer Engineering

Georgia Institute of Technology
May 2014

OPTICAL WIRELESS COMMUNICATIONS WITH OPTICAL POWER AND DYNAMIC RANGE CONSTRAINTS

Approved by:

Dr. G. Tong Zhou, Advisor
School of Electrical and Computer Engineering
Georgia Institute of Technology

Dr. Robert J. Baxley, Co-advisor
Information and Communications Laboratory
Georgia Tech Research Institute

Dr. Gee-Kung Chang
School of Electrical and Computer Engineering
Georgia Institute of Technology

Dr. Xiaoli Ma
School of Electrical and Computer Engineering
Georgia Institute of Technology

Dr. John R. Barry
School of Electrical and Computer Engineering
Georgia Institute of Technology

Dr. Grady Tuell
Electro-Optical Systems Laboratory
Georgia Tech Research Institute

Date Approved: March 26, 2014

To my grandparents, mom, and wife

ACKNOWLEDGEMENTS

First I would like to thank my advisors Dr. G. Tong Zhou and Dr. Robert J. Baxley. They brought me into the world of academia, taught me how to strive for excellence in my academic pursuits and helped me to develop critical thinking and presenting skills. I knew Dr. Zhou since she initiated Georgia Tech Shanghai program in 2006. I am very proud of my Georgia Tech Shanghai experience and feel very lucky to have received so much personal attention, advice and support from Dr. Zhou. Dr. Zhou's dedication, leadership, entrepreneurship and her courage to overcome the difficulties will always inspire me in my career.

I would also like to thank the other members of my Ph.D. dissertation reading committee: Dr. Gee-Kung Chang, Dr. Xiaoli Ma, Dr. John R. Barry, and Dr. Grady Tuell. Their support and suggestions have greatly improved the quality of this dissertation.

Special thanks go to Wallace H. Coulter Foundation and CEO Ms. Sue Van, who sponsored my tuition and expenses when I studied in Georgia Tech Shanghai Program. Otherwise, I would not have the opportunity to start my research in Georgia Tech.

I would also like to thank Texas Instruments Leadership University program that sponsored my research. I'm especially grateful to Dr. Arthur J. Redfern and Dr. Lei Ding who supervised me in the summer of 2013 when I did internship in Texas Instruments.

Finally, I would like to thank my friends from Georgia Tech Shanghai program and members in my research group: Dr. Qi Zhou, Hayang Kim, Marie Shinotsuka, Andrew Harper, Malik Muhammad Usman Gul, Brian Beck, Yiming Kong, Qingsong Wen, Kai Ying, Hyunwook Cho, and Seksan Laitrakun.

TABLE OF CONTENTS

LIST OF TABLES

LIST OF FIGURES

SUMMARY

Along with the rapidly increasing demand for wireless data while more and more crowded radio frequency (RF) spectrum, optical wireless communications (OWC) become a promising candidate to complement conventional RF communications, especially for indoor short and medium range data transmissions. Single carrier modulation waveforms such as on-off keying (OOK), pulse-position modulation (PPM), M-ary pulse-amplitude modulation (M-PAM), and M-ary quadrature amplitude modulation (M-QAM) have been applied to OWC in a relatively straightforward way, but they suffer from the frequency-selective OWC channel as the data rates increase. Orthogonal frequency division multiplexing (OFDM) is considered for OWC due to its ability to boost achievable data rates. OFDM can utilize the available modulation bandwidth of LEDs with adaptive bit and energy loading of different frequency subbands. However, the average emitted optical power and dynamic range of optical intensity are two major constraints in OWC. OFDM waveforms exhibits high upper and lower peak-to-average power ratios (PAPRs). To make the lower peak of OFDM signal above the turn-on voltage (TOV), a DC is often added to the original zero-mean OFDM signal. This operation, however, contradicts the average optical power constraints. Large upper PAPR and lower PAPR of OFDM also make it easy to violate the dynamic range of LEDs, resulting clipping and nonlinear distortions.

In this dissertation, we analyze and design optical power and dynamic range constrained optical wireless communication systems, for which OFDM is our major subject. We first derive distributions of upper PAPR and lower PAPR of OWC-OFDM signals. Then we analyze the clipped OFDM signals in term of error vector magnitude (EVM), signal-to-distortion ratio (SDR), and achievable data rates under both

optical power and dynamic range constraints. The next part of this dissertation is the OFDM system design for visible light communications (VLC) considering illumination requirement. In recent ten years, the fast growing solid-state lighting (SSL) technology has fueled the research on VLC, which is a subcategory of OWC, thanks to its duality of illumination and communication. We investigate the illumination-to-communication efficiency (ICE) in VLC-OFDM, and design the brightness control and flickering mitigation schemes for VLC-OFDM. In the end, to reduce the complexity of driving circuits of LEDs , we propose using delta-sigma modulators in VLC-OFDM systems to convert continuous magnitude OFDM symbols into two-level LED driver signals without loss of the communication theory advantages of OFDM.

CHAPTER I

INTRODUCTION

1.1 Motivations

With the rapidly growing demand for data in wireless communications and the significant increase of the number of users, the radio frequency (RF) spectrum become one of the scarcest resources in the world [3]. Motivated by the more and more crowed RF spectrum, optical wireless communications (OWC) has been identified as a promising candidate to complement conventional RF communication, especially for indoor short and medium range data transmission [45, 31]. OWC utilizes optical spectrum, which includes infrared (IR) and visible light to convey information in free space. Most practical OWC systems use light emitting diodes (LEDs) or laser diodes (LDs) as transmitter and PIN photodiode or avalanche photodiode (APD) as receiver. OWC has many advantages including low-cost front-ends, energy-efficient transmission, high security, huge (THz) bandwidth, no electromagnetic interference, etc.. The use of optical free-space emissions to provide indoor wireless communications can be traced back to the work of Gfeller and Bapst in 1979 [38]. Since then, most of the research on OWC are based on IR spectrum. Kanh and Barry reviewed their pioneering work on wireless infrared communications in reference [47]. In recent ten years, the use of visible light spectrum to transmit informations, namely, visible light communications (VLC), becomes the buzzword in academia [58, 41, 56, 37], industry [4] and standardization [63, 2] due to increasing popularity of solid-state lighting (SSL) technology. The white illumination LEDs, with their long lifetimes and energy efficiencies at least ten times greater than incandescent bulbs, will become the dominant light sources in the next few years. VLC modulate white LEDs at high rates in a way

that is imperceptible to humans. Therefore, VLC can enable the dual functionality of illumination and communication simultaneously. The VLC market is projected to have a compound annual growth rate of 82% from 2013 to 2018 and to be worth over $6 billion per year by 2018 [4].

In this dissertation, we focus on OWC based on intensity modulation (IM) / direct detection (DD), which means that the modulation signal has to be both real valued and unipolar [47]. Orthogonal frequency division multiplexing (OFDM) [10] is applied to OWC thanks to its ability to boost the achievable data rates. OFDM can combat inter-symbol-interference (ISI) efficiently with simple single-tap equalizers in the frequency domain [70]. OFDM supports adaptive bit and energy loading of different subcarriers according to the channel quality [20]. OFDM can also avoid low-frequency noises caused by ambient light and the DC wander effect in electrical circuits. OFDM is powerful to support multiple access implementation as subcarriers can be allocated to different users resulting in orthogonal frequency division multiple access (OFDMA). There are promising results reported in [48, 23, 12, 68] using OFDM.

However, applying OFDM to OWC has to deal with some challenges. On one hand, the average emitted optical power and dynamic range of optical intensity are two major constraints in OWC. The average optical power is limited due to the eye safety requirements in infrared communications, and the the brightness/dimming control in VLC. LED has a minimum threshold value known as the turn-on voltage (TOV) which is the onset of current flow and light emission. In addition, to ensure not overheating the LED, the alternative currents (AC) must be controlled below the corresponding maximum permissible AC current. As a result, the driving current/voltage has to be within a certain dynamic range. On the other hand, OFDM waveforms exhibits high upper and lower peak-to-average power ratios (PAPR). To make the lower peak of OFDM signal above the TOV, a DC is often added to

the original zero-mean OFDM signal. This operation, however, contradicts the average optical power constraints. Large upper PAPR and lower PAPR of OFDM also make it easy to violate the dynamic range of LEDs, resulting clipping and nonlinear distortions. For VLC system, since the primary function is providing illumination, two-level modulation signal, such as OOK and PPM, are more favored because their driving circuits are simple and it is easy for them to control the brightness and mitigate flickering. Clipped OFDM signals, however, may cause optical power wander and flickering. The brightness control scheme for dynamic range constrained OFDM transmission is still unknown. Moreover, driving circuits of a white LED has to support continuous magnitude inputs, and the mixed-signal digital-to-analog converter (DAC) design is complicated. Modification of driving circuits of white LEDs will be not beneficial to the application and commercialization of VLC. Therefore, our research on optical power and dynamic range constrained optical wireless communications is well motivated.

1.2 Objectives

In this dissertation, we focus on analyzing and designing optical power and dynamic range constrained optical wireless communication systems, for which OFDM will be our major subject.

PAPR is an important metric widely used to quantify the variations of OFDM waveforms. Although the distribution of PAPR of complex-valued RF-OFDM baseband signals has been extensively studied in references [16, 61, 39, 46], the distribution of upper PAPR and lower LPAPR of real-valued OWC-OFDM are still unknown. A number of papers [14, 60, 59, 62] have studied the clipping effects on the RF-OFDM signals. However, clipping in the OWC system has two important differences: (i) the RF baseband signal is complex-valued whereas time-domain signals in the OWC system are real-valued; (ii) the main power limitation for OWC is average optical power

and dynamic optical power, rather than average electrical power and peak power as in RF communication. Therefore, most of the theory and analyses developed for RF OFDM are not directly applicable to optical OFDM. We will derive the individual distribution and joint distribution of upper PAPR and lower PAPR of OWC-OFDM. We will analyze the performance of the clipped OFDM signals in terms of error vector magnitude (EVM), signal-to-distortion ratio (SDR), and achievable data rates under both average optical power and dynamic range constraints.

VLC-OFDM system design considering illumination requirement and dynamic range constraint is also our objective. In this thesis, we will investigate the illumination-to-communication efficiency (ICE) in VLC-OFDM. We will design the brightness control and flickering mitigation schemes for VLC-OFDM. OFDM transmission increases the complexity of circuits in the front-end of VLC. In this dissertation, we will try to address the above mentioned issues for OFDM in VLC applications.

1.3 Outline

The rest of the dissertation is organized as follows:

In Chapter 2, optical wireless communications are introduced and the fundamental intensity modulation and direct detection models are reviewed. We study the cause of optical power and dynamic range constraints for OWC system. The motivation of applying OFDM to OWC is discussed as well.

Chapter 3 to Chapter 6 analyze the performance of optical real-valued OFDM for general OWC system. In Chapter 3, upper PAPR (UPAPR) and lower PAPR (LPAPR) of real-valued OFDM signals are defined. The individual distribution of UPAPR and LPAPR, and the joint distribution of UPAPR and LPAPR are derived. In Chapter 4, the error vector magnitude (EVM) is adopted as the figure of metric to quantify the nonlinear-distortions. We derive EVM of DC-biased optical OFDM (DCO-OFDM) and asymmetrically clipped optical OFDM (ACO-OFDM) undergoing

clipping distortions, and compare with lower bounds given dynamic range constraints. In Chapter 5, achievable data rates of DCO-OFDM and ACO-OFDM are derived and compared, under the same optical power and dynamic range constraints. Both AWGN channel and frequency-selective channel are considered.

Chapter 6 to Chapter 9 focus on OFDM for visible light communications, taking the illumination function into considerations. In Chapter 6, we quantify the illumination-to-communication conversion efficiency (ICE) and clarify how UPAPR and LPAPR are related to efficiency in VLC systems. We also present a method to improve the efficiency of VLC-OFDM systems. In Chapter 7, the brightness control in dynamic range constrained VLC-OFDM is investigated. Illumination function in turn place a constraint on the average amplitude of the OFDM signal in VLC. We combine two bipolar-to-unipolar models, namely, linear scaling & biasing model, and clipping & biasing model, with the biasing adjustments and pulse width modulation (PWM) schemes. The performance are demonstrated and compared. Clipping can cause the performance degradation of communication as well as illumination. In Chapter 8, we propose an iterative clipping method considering brightness control and flicker mitigation. We investigate the performance in terms of error vector magnitude (EVM) as well as computational complexity. In Chapter 9, we propose the use of delta-sigma modulators in VLC-OFDM systems to convert continuous magnitude OFDM symbols into LED driver signals. The proposed system has the communication theory advantages of OFDM along with the practical analog and optical advantages of simple two level driver signals.

In the end, Chapter 10 summarizes the main contributions of this dissertation and provides a few suggestions for future research.

CHAPTER II

BACKGROUND

2.1 Optical wireless communication (OWC)

Optical wireless communications (OWC) leverage optical spectrum, which includes infrared (IR) and visible light, to wirelessly transmit information. In OWC, simple low-cost intensity modulation and direct detection (IM / DD) techniques are employed, which means that only the signal intensity is modulated and there is no phase information. At the transmitter, the light emitting diodes (LEDs) or laser diodes (LDs) convert the amplitude of the electrical signal to the intensity of the optical signal, while at the receiver, the photodiodes (PDs) or image sensors generate the electrical signal proportional to the intensity of the received optical signal. IM/DD requires that the electric signal must be real-valued and unipolar (positive-valued). With rapidly growing wireless data demand and the saturation of radio frequency (RF) spectrum, OWC has become a promising candidate to complement conventional RF communication, especially for indoor and medium range data transmission. OWC has many advantages including low-cost front-ends, energy-efficient transmission, huge (THz) bandwidth, no electromagnetic interference, etc..

A number of modulation techniques have been employed for OWC. These modulation schemes include on-off keying (OOK), pulse position modulation (PPM), pulse amplitude modulation (PAM), orthogonal frequency division multiplexing (OFDM), and color-shift keying (CSK) [31].

Visible light communication (VLC) is a category of OWC, which uses visible light between 375 nm and 780 nm. VLC [58] relies on white LEDs which already provide illumination and are quickly becoming the dominant lighting source to transmit data.

Visible light is safe for human and has no eye safety constraints like infrared. VLC has potential applications in a number of areas. These include smart lighting, indoor localization, vehicles and transportation, underwater communication, etc.. Recently, VLC is drawing intense attention from standardization groups. The VLC consortium (VLCC) was founded in 2003 in Japan which contributes to research, development, and standardization of VLC. The VLCC has added a visible light physical layer to the existing IrDA infra-red standard. In 2010, the task group IEEE 802.15.7 published the P802.15.7 draft standard [63].

2.2 Intensity modulation and direct detection

In RF wireless communications, the baseband signals are up-converted to a designated RF carrier, and sent to the air via antennas at transmitter. Receiver employs one or more antennas, each followed by a down-converter, which includes a local oscillator and a mixer, to generate baseband signals.

In optical wireless communications, the baseband signals are up-converted to optical carriers at the transmitter, and the receiver down-convert optical signal into baseband electric signal. The electric-optic and optic-electric conversions do not rely on expensive oscillators and mixers, but only low-cost LEDs and photodiodes. The most feasible up-conversion scheme is intensity modulation (IM), in which the desired waveform is modulated onto the instantaneous power of the optical carrier. The most practical down-conversion is direct detection (DD), where a photodiode produces a current proportional to the optical intensity. In IM/DD, only magnitude information, but no phase, can be modulated.

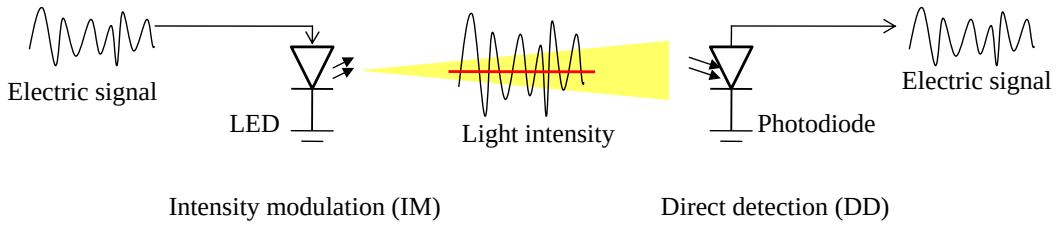

Figure 1: Intensity modulation and direct detection in OWC

Fig. 1 shows the basic concept of intensity modulation and direct detection in OWC. The received signal is the instantaneous current in the receiving photodetector, which is proportional to the integral over the photodetector surface of the total instantaneous optical power at each location.

2.2.1 Optical components

The LED consists of a chip of semiconducting material doped with impurities to create a p-n junction. As in other diodes, current flows easily from the p-side, or anode, to the n-side, or cathode, but not in the reverse direction. The wavelength of the light emitted depends on the band gap energy of the materials forming the p-n junction.

For infrared wireless communications, the use 780-950 nm optical band is preferred due to the availability of low cost optoelectronic components. The modulation bandwidth can be tens of kilohertz to tens of megahertz [47].

For visible light communications, the primary function is providing illumination. Thus, the LED has to emit white light, which includes the whole visible light spectrum from 375 to 780 nm (400 and 800 THz). There are basically two types of white LED: R-G-B LED, and phosphorescent LED. The R-G-B LED consists of red, green, and blue chips and combines the three lights in a correct proportion to generate white light. R-G-B LED has relative higher modulation bandwidth (20MHz) and can support wavelength division multiplexing (WDM), but the cost is relatively high.

Phosphorescent LED uses the blue LED chip coated with a yellow phosphor, which is the most popular white LED in the market due to its low cost. However, the slow response of phosphor limits the modulation bandwidth of the phosphorescent white LEDS to only few MHZ. A blue filtering can be operated at the receiver to increase the modulation bandwidth to 20MHz. As an example, the frequency response of emitted white light and the blue part of a typical white light (Luxeon STAR) LED is shown in Fig. 2 [50].

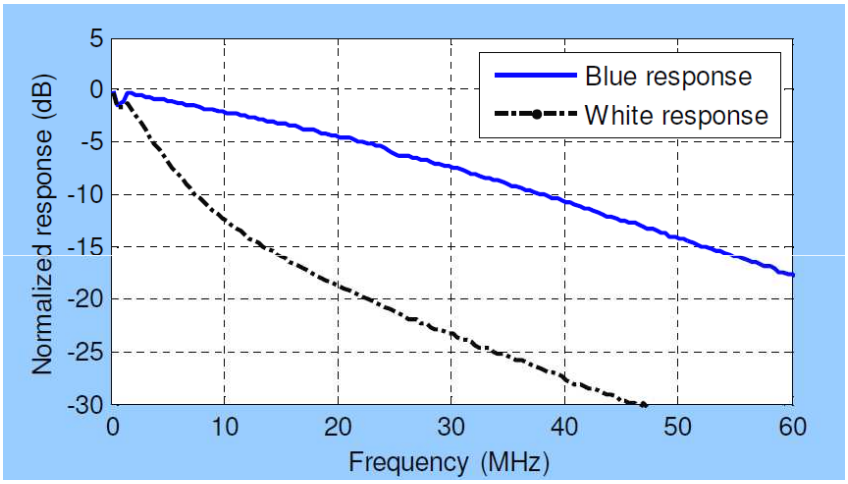

Figure 2: Frequency response of emitted white light and the blue part of a typical white light (Luxeon STAR) LED [50].

A photodiode is a p-n junction or PIN structure. When a photon of sufficient energy strikes the diode, it creates an electron, hole pair. A photodiode is designed to operate in reverse bias. There are two widely adopted types: ordinary positive-intrinsic-negative photodiodes and avalanch photodiodes (APD's). APD's are favored when there is little ambient-induced shot noise because their structure can overcome more preamplifier thermal noise. A photodiode has more modulation bandwidth than LED, which is not a concern in OWC.

Besides, optical filters, concentrators, and preamplifier are normally required at

the receiver to increase the signal-to-noise power ratio (SNR).

2.2.2 Propagation models

The channel in OWC can be modeled as a baseband linear system [47]

$$r(t) = y(t) \otimes h(t) + w(t), \tag{1}$$

where $y(t)$ denotes the transmitted signal, $r(t)$ denotes the received signal, $h(t)$ denotes the channel impulse response, and $w(t)$ denotes the additive noise, receptively. $\otimes$ is convolution operation. Let $H(f)$ denote the frequency response of channel,

$$H(f) = \int_{-\infty}^{\infty} h(t) e^{-j2\pi ft} dt \tag{2}$$

For OWC channel, if we only consider the line-of-sight (LOS) propagation path, the channel DC gain $H(0)$ is given by [47]

$$H(0)_{\text{LOS}} = \begin{cases} \frac{A}{d^2} R(\theta) T_s(\psi) g(\psi) \cos(\psi), & 0 \leq \psi \leq \Psi_c \\ 0, & \psi \geq \Psi_c \end{cases} \tag{3}$$

where θ denotes the angle of emission with respect to transmitter, ψ denotes the angle with respect to the receiver, d represents the distance between the transmitter and the receiver, Ψ_c is the receiver filed of view (FOV), A is the collection area in the receiver, $T_S(\psi)$ is the transmission gain of the optical filter, $g(\psi)$ is the transmission gain of the concentrator, $R(\theta)$ denotes the Lambertian radiant intensity:

$$R(\theta) = \frac{(m+1)\cos^m(\theta)}{2\pi}, \tag{4}$$

where m is the order of Lambertian emission mode number, which is related to the transmitter semi-angle $\Theta_{1/2}$ by

$$m = -\ln 2 / \ln(\cos \Theta_{1/2}) \tag{5}$$

The multi-path propagation is dominated by diffuse reflection. The light reflected from each surface element follows a Lambertian distribution, independent of the angle

of incidence. Given a particular source $\mathcal{S}$ and receiver $\mathcal{R}$ in a room, the paper [47] modeled the impulse response of multi-path channel as an infinite sum

$$h(t;\mathcal{S},\mathcal{R}) = \sum_{k=0}^{\infty} h^{(k)}(t;\mathcal{S},\mathcal{R}), \tag{6}$$

where $h^{(k)}(t)$ is the response of the light undergoing exactly k reflections, which is calculated recursively from $h^{(k-1)}(t)$

$$h^{(k)}(t;\mathcal{S},\mathcal{R}) = \sum_{i=1}^{N} h^{(0)}(t;\mathcal{S},E_i) \otimes h^{(k-1)}(t;E_i,\mathcal{R}), \tag{7}$$

where E_i, $i = 1, 2, \ldots, N$ denotes the small elements of reflecting surfaces. Figure 3 shows the channel responses drawn from experiments [47].

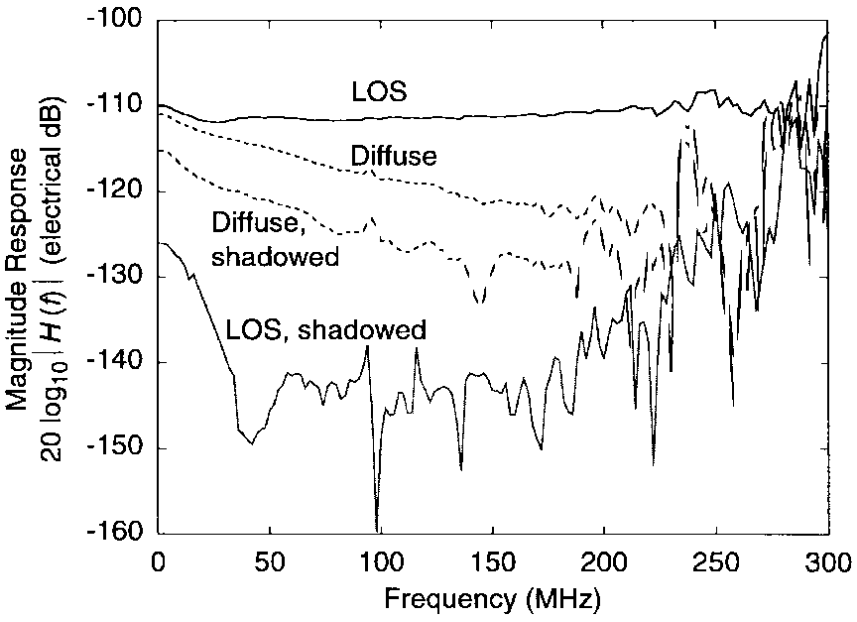

(a)

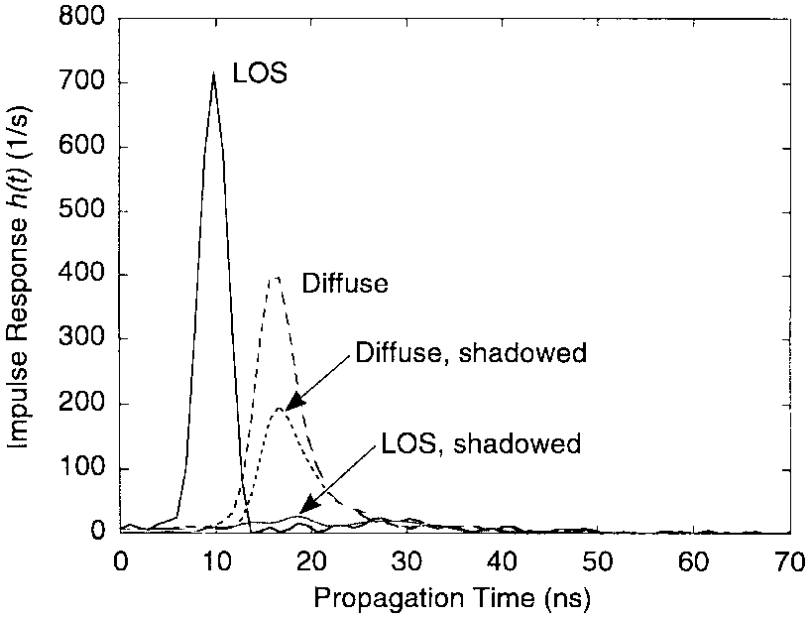

(b)

Figure 3: Response of nondirected-LOS and nondirected-non-LOS channels. Measurements were performed in a 5.5m × 7.5 m × 3.5 m. (a) Frequency responses. (b) Impulse responses. [47]

The noise in IM/DD OWC channel is usually modeled to be Gaussian and signal-independent. There are two major noise sources: shot noise due to ambient light, and thermal noise. The noise variance can be written as

$$\sigma_w^2 = \sigma_{\text{shot}}^2 + \sigma_{\text{thermal}}^2 \tag{8}$$

2.3 Optical power and dynamic range constraints

In RF system, the baseband signal is normally complex-valued, and there is a constraint placed on the average squared amplitude of the baseband signal as

$$\lim_{T \longrightarrow \infty} \frac{1}{2T} \int_{-T}^{T} |x(t)|^2 dt \leq P_{i,avg} \tag{9}$$

Besides, the power amplifier is indispensable device in RF system, which place a peak power constraint on baseband signal as

$$|y(t)|^2 \leq P_{i,sat} \tag{10}$$

In OWC system, the constraints become average optical power and dynamic range of LEDs. Since the LED input $y(t)$ represents instantaneous optical intensity. The average optical power constraint can be expressed as

$$\lim_{T \longrightarrow \infty} \frac{1}{2T} \int_{-T}^{T} y(t) dt \leq I_{avg} \tag{11}$$

We place the average optical power constraint on the input of LED for several reasons. For OWC system using infrared , the uncontrolled average optical power may cause safety issues to human. The infrared radiation can pass through the human cornea and be focused by the lens onto the retina, where it can potentially induce thermal damage. For OWC system using visible light, brightness control is essential for the illumination function. As a result, the average optical power is determined by the illumination level.

Dynamic range constraints come from the nonlinearity of LED. Figure 4 is the nonlinear transfer characteristics of a high power Infrared LED (OSRAM,SFH 4230).

LED has a minimum threshold value known as the turn-on voltage (TOV) which is the onset of current flow and light emission. In addition, to ensure not overheating the LED, the DC and AC currents must be controlled below the corresponding maximum permissible DC current and maximum permissible AC current.

In paper [29], the authors proposed a predistortor to linearize the LED [see Figure 5]. The relation between the forward voltage and the current through the LED is modeled by a polynomial using the least-square curve fitting technique. The solid line illustrates the linearized transfer characteristic. Assuming v_{in} is the input signal amplitude and $i_{\text{out}-\text{pd}}$ is the desired output current known form the linear response. Then, the original input amplitude, v_{in}, is adjusted to produce $v_{\text{out}-\text{pd}}$ which produces the correct output current amplitude, $i_{\text{out}-\text{pd}}$, that gives the overall predistorted-LED chain a linear response. With predistortion, the input-output characteristic of the LED can be linearized, but only within a limited interval $[I_L, I_H]$, where I_L denotes the turn on voltage/current and I_H denotes the saturation input voltage/current [29]. Therefore, the OWC is a dynamic range limited system. The input signal outside this range will be clipped.

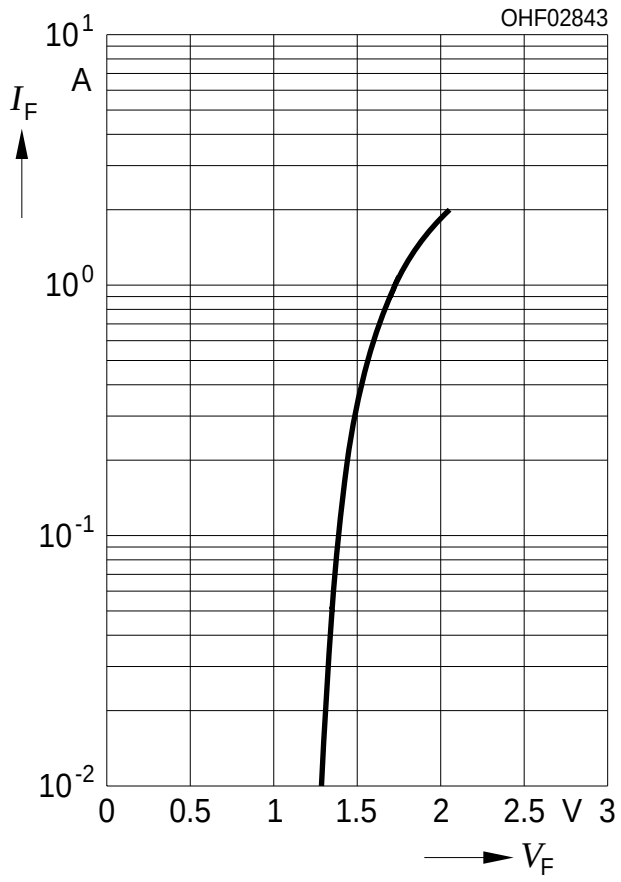

Figure 4: Nonlinear transfer characteristics of a high power IR LED (OSRAM,SFH 4230).

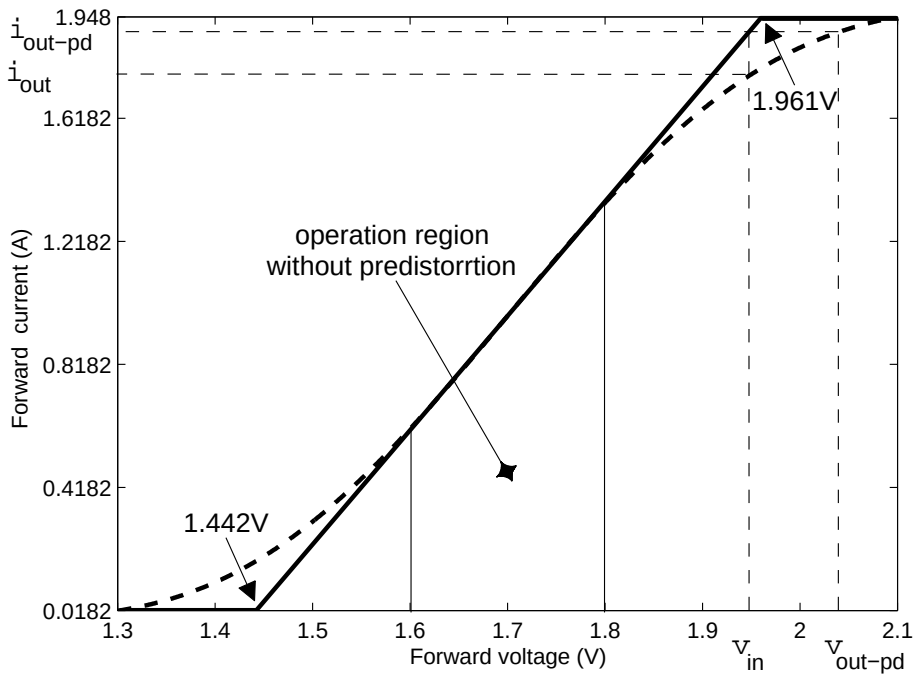

Figure 5: Nonlinear and linearized LED transfer characteristic [29].

2.4 Modulation techniques

2.4.1 Single carrier modulation

2.4.1.1 Amplitude modulation

In amplitude modulation, the binary bits are mapped into different signal amplitudes. On-off keying (OOK) and M-ary pulse amplitude modulation (M-PAM) are two examples of AM employed in OWC.

OOK is the simplest modulation in OWC. OOK transmits the bit 1 by "turning on" the optical intensity and transmits the bit 0 by "turning off" the optical intensity. When transmitting the bit 0, the optical intensity is not necessarily turned off completely, but dimmed at a lower level relatively to the "turning on" when transmitting the bit 1.

M-PAM conveys the bits information by M different positive amplitudes. In each symbol, $\log_2 M$ bits are coded and mapped into one of the M magnitudes according

the M-PAM mapper. Actually, OOK is a special case of M-PAM with $M = 2$.

2.4.1.2 Pulse-position modulation (PPM)

In L-ary pulse-position modulation scheme, each symbol interval of duration is divided into L subintervals, or chips. Information is sent by transmitting a on-zero optical intensity in a single chip, while other chip intervals remain "off". Each of the chips is non-overlapping in time, so each symbol is orthogonal of all the others.

Fig. 6 shows the examples OOK and 2-PPM waveforms.

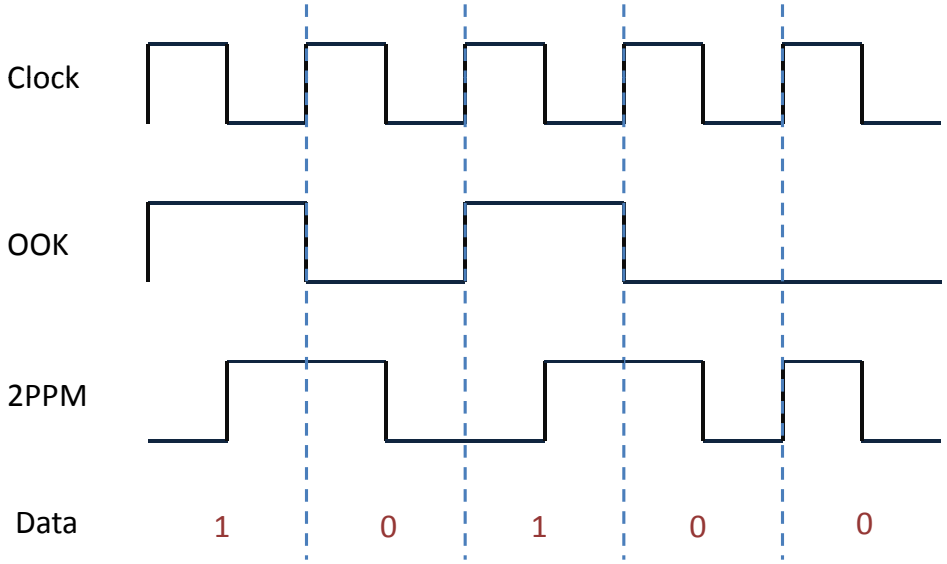

Figure 6: Examples of OOK and 2-PPM waveforms

2.4.2 Orthogonal frequency division multiplexing (OFDM)

Orthogonal frequency division multiplexing (OFDM) has been considered for OWC thanks to its ability to boost data rates and efficiently combat inter-symbol interference [44, 8, 32, 10, 36]. In an OFDM system, a discrete time-domain signal $\mathbf{x} = [x[0], x[1], \ldots, x[N-1]]$ is generated by applying the inverse DFT (IDFT) operation to a frequency-domain signal $\mathbf{X} = [X_0, X_1, \ldots, X_{N-1}]$ as

$$x[n] = \text{IDFT}(X_k) = \frac{1}{\sqrt{N}} \sum_{k=0}^{N-1} X_k \exp(j2\pi kn/N), \quad 0 \leq n \leq N-1, \tag{12}$$

where $j = \sqrt{-1}$ and N are the size of IDFT, assumed to be an even number in this dissertation. In an OWC system using LED, the IM/DD schemes require that the electric signal be real-valued and unipolar (positive-valued). Fig. 7 shows the OFDM system model in optical wireless communications.

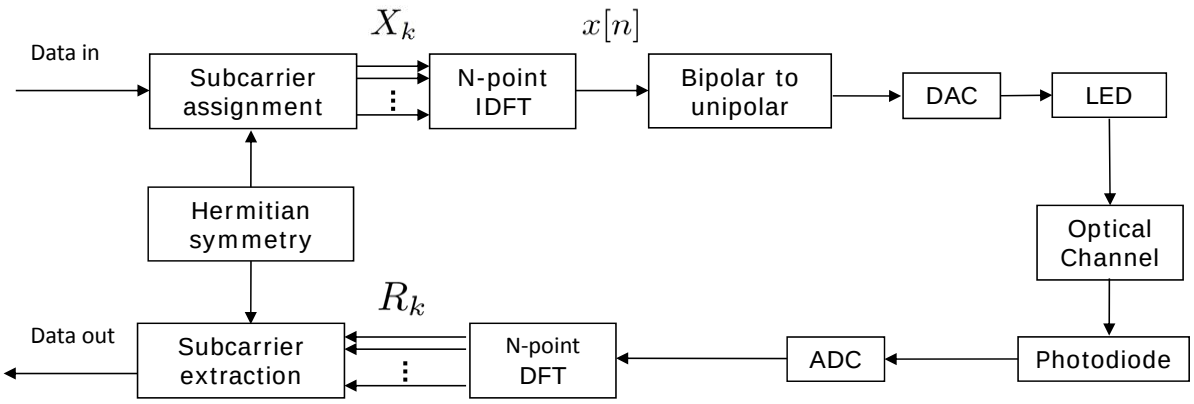

Figure 7: OFDM system model in IM/DD optical wireless communications.

According to the property of IDFT, a real-valued time-domain signal $x[n]$ corresponds to a frequency-domain signal X_k that is Hermitian symmetric, i.e.,

$$X_k \quad = \quad X^*_{N-k}, \quad 1 \leq k \leq N-1, \tag{13}$$

where $*$ denotes complex conjugate. The 0th and $N/2$th subcarrier are null; i.e., $X_0 = 0$, $X_{N/2} = 0$. According to the Central Limit Theorem, $x[n]$ is approximately Gaussian distributed with zero mean and variance σ_x^2 with probability density function (pdf)

$$f_x(z) = \frac{1}{\sigma_x}\phi\left(\frac{z}{\sigma_x}\right), \tag{14}$$

where $\phi(x) = \frac{1}{\sqrt{2\pi}}e^{-\frac{1}{2}x^2}$ is the pdf of the standard Gaussian distribution. As a result, the time-domain OFDM signal $x[n]$ tends to occupy a large dynamic range and is bipolar.

Based on the subcarrier arrangement, and bipolar-to-uniploar conversion, DC-biased optical OFDM (DCO-OFDM) and asymmetrically clipped optical OFDM

(ACO-OFDM) have been discussed in the literature for creating real-valued unipolar OFDM signal for OWC.

(1) DC-biased optical OFDM (DCO-OFDM) [44]

In DCO-OFDM, subcarriers of the frequency-domain signal $\mathbf{X}^{(D)}$ are arranged as

$$\mathbf{X}^{(D)} = [0 \quad X_1^{(D)} \quad X_2^{(D)} \quad \dots \quad X_{N/2-1}^{(D)} \quad 0 \quad X_{N/2-1}^{*(D)} \quad \dots \quad X_2^{*(D)} \quad X_1^{*(D)}] \quad (15)$$

where the 0th and $N/2$th subcarriers are null (do not carry data). Equation (15) reveals Hermitian symmetry with respect to $k = N/2$. Let $\mathcal{K}_d$ denote the set of data-carrying subcarriers with cardinality $|\mathcal{K}_d|$. The set of data-carrying subcarriers for DCO-OFDM is $\mathcal{K}_d^{(D)} = \{1, 2, \dots, N/2-1, N/2+1, \dots, N-2, N-1\}$ and $|\mathcal{K}_d^{(D)}| = N-2$. The time-domain signal $x^{(D)}[n]$ can be obtained as

$$x^{(D)}[n] = \frac{2}{\sqrt{N}} \sum_{k=1}^{N/2-1} \left(\Re(X_k^{(D)}) \cos(2\pi kn/N) - \Im(X_k^{(D)}) \sin(2\pi kn/N) \right), \quad (16)$$

which is real-valued. The unipolar signal $y^{(D)}[n]$ is obtained by adding a biasing to

$$y^{(D)}[n] = x^{(D)}[n] + B. \quad (17)$$

(2) Asymmetrically clipped optical OFDM (ACO-OFDM) [8]

In ACO-OFDM, only odd subcarriers of the frequency-domain signal $\mathbf{X}^{(\mathbf{A})}$ carry data

$$\mathbf{X}^{(\mathbf{A})} = [0 \quad X_1^{(A)} \; 0 \; X_3^{(A)} \; \dots \; 0 \; X_{N/2-1}^{(A)} \; 0 \; X_{N/2-1}^{*(A)} \; \dots \; 0 \; X_3^{*(A)} \; 0 \; X_1^{*(A)}], \quad (18)$$

and $\mathbf{X}^{(\mathbf{A})}$ meets the Hermitian symmetry condition. The set of data-carrying subcarriers for ACO-OFDM is $\mathcal{K}_d^{(A)} = \{1, 3, \dots, N-1\}$ and $|\mathcal{K}_d^{(A)}| = N/2$. Thus, the time-domain signal $x^{(A)}[n]$ can be obtained as

$$x^{(A)}[n] = \frac{2}{\sqrt{N}} \sum_{q=0}^{N/4-1} \left(\Re(X_{2q+1}^{(A)}) \cos\left(2\pi(2q+1)n/N\right) - \Im(X_{2q+1}^{(A)}) \sin\left(2\pi(2q+1)n/N\right) \right), \quad (19)$$

which is real-valued. The $x^{(A)}[n]$ satisfies the following negative half symmetry condition:

$$x^{(A)}[n + N/2] = -x^{(A)}[n], \quad n = 0, 1, \dots, N/2-1. \quad (20)$$

Therefore, by clipping the negative parts of $x^{(A)}[n]$ without information loss, we can obtain the unipolar ACO-OFDM signal $y[n]$

$$y^{(A)}[n] = \begin{cases} x^{(A)}[n], & x^{(A)}[n] \geq 0, \\ 0, & \text{otherwise.} \end{cases} \tag{21}$$

Denote by $v[n]$ a generic discrete-time signal that satisfies $v[n+N/2] = -v[n]$, $n = 0, 1, \ldots, N/2-1$ and by $\bar{z}[n]$ its clipped version where the negative values are removed, i.e.,

$$\bar{v}[n] = \begin{cases} v[n], & v[n] \geq 0, \\ 0, & \text{otherwise.} \end{cases} \tag{22}$$

It was proved in [72] that in the frequency-domain,

$$\bar{V}_k = \frac{1}{2} V_k, \quad \forall k \text{ odd.} \tag{23}$$

Since $x^{(A)}[n]$ satisfies (20), we infer based on (23) that

$$Y_k^{(A)} = \frac{1}{2} X_k^{(A)}, \quad \forall k, \tag{24}$$

For ACO-OFDM, no DC-biasing is necessary.

OFDM can efficiently combat ISI-induced frequency-selective channel via one-tap frequency-domain equalization. The paper [15] compared the computational complexity in real operations per bit for receivers employing various modulation schemes, as shown in Table 1.

Table 1: Computational complexity for various modulation schemes [15]

Bit rates (Mbits/s)	50	100	300
DCO-OFDM	45.9	45.9	45.3
ACO-OFDM	50	50	49.6
OOK	272	432	1008

Another benefit of OFDM is that it can enable adaptive modulation and bit-loading on each subcarrier based on the communication system properties. As we discussed, the LEDs act like a low-pass filter. The signal-to-noise power ratio (SNR) at low-frequency subcarriers is higher than SNR at high-frequency subcarriers. OFDM with bit-loading can leverage more frequencies than the 3-dB bandwidth of LED, in which more bits are allocated to low-frequency subcarriers and less bits are allocated to high-frequency subcarriers. The paper [48] generates OFDM signals with bandwidth 180 MHz (3-dB bandwidth of LED is only 20 MHz) to achievable 1 Gbit/s transmission by bit loading. Figure 8 shows the allocations of bits and power on each subcarrier [48].

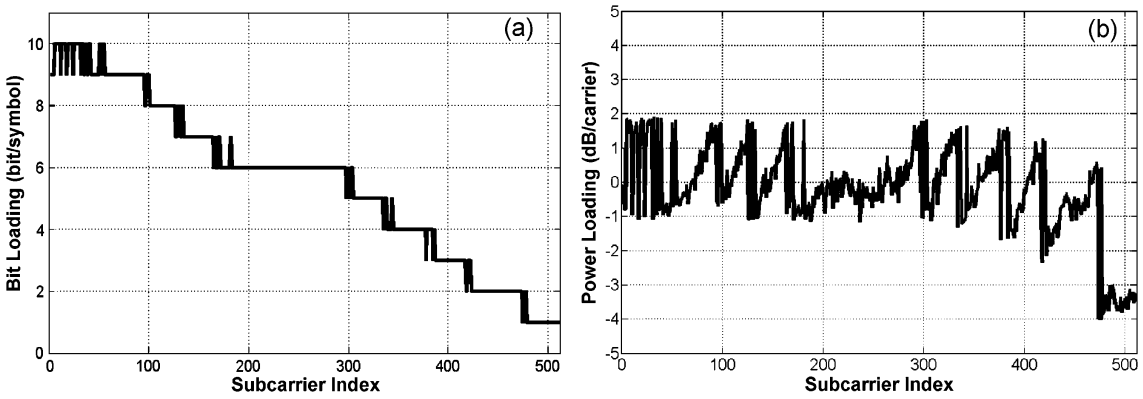

Figure 8: Allocations of bits and power on each subcarrier [48].

However, OFDM waveforms exhibit high peak-to-average-power ratio (PAPR) due to the summation over a large number of terms [67]. The high PAPR or dynamic range of OFDM makes it very sensitive to nonlinear distortions.

CHAPTER III

DISTRIBUTIONS OF UPPER PAPR AND LOWER PAPR OF REAL-VALUED OFDM SIGNALS

Orthogonal frequency-division multiplexing (OFDM) in optical wireless communications (OWC) inherits the disadvantage of high peak-to-average power ratio (PAPR) from OFDM in radio frequency (RF) communications. The upper peak power and lower peak power of real-valued OWC-OFDM signals are both limited by the dynamic constraints of light emitting diodes (LEDs). The efficiency and transmitted electrical power are directly related with the upper PAPR (UPAPR) and lower PAPR (LPAPR) of OWC-OFDM. In this chapter, we will derive the complementary cumulative distribution function (CCDF) of UPAPR and LPAPR, and investigate the joint distribution of UPAPR and LPAPR.

3.1 Introduction

OFDM is also known for its disadvantage of high peak-to-average power ratio (PAPR). Power amplifiers in RF communication systems often have to operate with large power back-off and reduces the power efficiency [17]. The distribution of PAPR of complex-valued RF-OFDM baseband signals has been extensively studied in references [16, 61, 39, 46]. OWC-OFDM inherits the high PAPR from RF-OFDM. However, different from RF-OFDM, OWC-OFDM baseband signals must be real-valued required by IM/DD schemes. Thus, the frequency-domain symbols of OFDM must be Hermitian symmetric to make the time-domain samples real-valued. Additional, rather than peak power constrained in RF-OFDM, OWC-OFDM is dynamic range constrained by the turn-on current and maximum permissible alternating current of

LEDs [29]. Furthermore, eye-safety requirements in infrared communications or illumination requirements in visible light communications place a constraint on the average amplitude of the OWC-OFDM signal. For the real-valued OWC-OFDM signal, the square of the maximum value can be seen as the upper peak power, and the square of the minimum value can be seen as the lower peak power. Upper peak and lower peak have individual constraints in OWC. It has been studied in references [77, 76] that the efficiency and transmitted electrical power are directly related with the upper PAPR (UPAPR) and lower PAPR (LPAPR) of OWC-OFDM. Although the distribution of PAPR of real-valued OFDM was shown in reference [73, 53], to the best of our knowledge, the distribution of UPAPR and LPAPR are still unknown.

In this chapter, we will derive the complementary cumulative distribution function (CCDF) of UPAPR and LPAPR, and the joint distribution of UPAPR and LPAPR, assuming that OWC-OFDM time-domain signals are independent and identically Gaussian distributed for large number of subcarriers. Simulated results are provided to examine our theoretical analysis.

3.2 Review of PAPR in RF-OFDM

In RF-OFDM systems, let $\{X_k\}_{k=0}^{N-1}$ denote the frequency-domain OFDM signal, where k is the subcarrier index and N is the number of subcarriers. The Nyquist-rate sampled time-domain OFDM signal $\{x[n]\}_{n=0}^{N-1}$ is generated by applying inverse discrete Fourier transform (IDFT) to the frequency-domain signal:

$$x[n] = \frac{1}{\sqrt{N}} \sum_{k=0}^{N-1} X_k e^{j2\pi kn/N}, \quad 0 \le k \le N-1, \tag{25}$$

where $j = \sqrt{-1}$ and n is the discrete-time index. It is well-known that the OFDM time-domain signal has high peak-to-average power ratio (PAPR) [17], which is defined as

$$\text{PAPR} = \frac{\max\limits_{0 \le n \le N-1} |x[n]|^2}{E[|x[n]|^2]}, \tag{26}$$

where $E[\cdot]$ stands for the statistical expectation. For a large N, $\{x[n]\}_{n=0}^{N-1}$ are asymptotically independent and approximately complex Gaussian distributed, and the real part and the imaginary part of $x[n]$ are asymptotically independent [61]. Then, the complementary cumulative distribution function (CCDF) of the PAPR can be shown to be [16, 61]

$$Pr\{\text{PAPR} > r\} = 1 - (1 - e^{-r})^N. \tag{27}$$

3.3 PAPR in OWC-OFDM

In OWC systems, intensity modulation (IM) is employed at the transmitter. The forward signal drives the LED which in turn converts the magnitude of the input electric signal into optical intensity. Direct detection (DD) is employed at the receiver. A photodiode (PD) transforms the received optical power into the amplitude of an electrical signal.

IM/DD schemes require the baseband signal in the VLC to be real-valued. Thus, complex-valued RF-OFDM in (25) cannot be used in VLC directly. According to the property of the inverse Fourier transform, a real-valued time-domain signal $x[n]$ corresponds to a frequency-domain signal X_k that is Hermitian symmetric; i.e., $X_k = X_{N-k}^*, 1 \leq k \leq N-1$, where $*$ denotes complex conjugate. The 0th and $N/2$th subcarrier are null; i.e., $X_0 = 0$, $X_{N/2} = 0$. Then we can obtain the real-valued time-domain signal $x[n]$ as

$$\begin{aligned} x[n] &= \frac{2}{\sqrt{N}} \sum_{k=1}^{N/2-1} \left(\Re(X_k) \cos\left(\frac{2\pi kn}{N}\right) - \Im(X_k) \sin\left(\frac{2\pi kn}{N}\right) \right), \\ & n = 0, 1, \ldots, N-1, \end{aligned} \tag{28}$$

where $\Re(\cdot)$ denotes the real part of X_k, and $\Im(\cdot)$ denotes the imaginary part of X_k. Since the DC component is zero ($X_0 = 0$), $x[n]$ has zero mean. According to the Central Limit Theorem, for a large N, $\{x[n]\}_{n=0}^{N-1}$ are asymptotically independent and approximately Gaussian distributed. According to the definition of PAPR in

(26), the PAPR of real-valued OFDM signal $x[n]$ is given by

$$\mathcal{P} \triangleq \frac{\max\limits_{0\le n\le N-1} x^2[n]}{\sigma_x^2}. \tag{29}$$

Assume $x[n]$ is independent and identically distributed, the CCDF of $\mathcal{P}$ can be shown as [73]

$$\begin{aligned} & \mathrm{CCDF}_{\mathcal{P}}\{r_p\} = Pr\{\mathcal{P} > r_p\} \qquad (30)\\ = \;& 1 - Pr\{\mathcal{P} \le r_p\} \\ = \;& 1 - Pr\{-\sigma_x\sqrt{r_p} \le x[n] \le \sigma_x\sqrt{r_p}, 0 \le n \le N-1\} \\ = \;& 1 - [Pr\{-\sigma_x\sqrt{r_p} \le x[0] \le \sigma_x\sqrt{r_p}\}]^N \\ = \;& 1 - [\Phi(\sqrt{r_p}) - \Phi(-\sqrt{r_p})]^N, \end{aligned}$$

where $\Phi(x) = \int_{-\infty}^{x} \phi(t)dt$.

For the real-valued bipolar signal $\{x[n]\}_{n=0}^{N-1}$, the square of the maximum value $\left(\max\limits_{0\le n\le N-1} x[n]\right)^2$ can be seen as the upper peak power, and the square of the minimum value $\left(\min\limits_{0\le n\le N-1} x[n]\right)^2$ can be seen as the lower peak power. Let us define the upper PAPR (UPAPR) of $x[n]$ as

$$\mathcal{U} \triangleq \frac{\left(\max\limits_{0\le n\le N-1} x[n]\right)^2}{\sigma_x^2}, \tag{31}$$

and define the lower PAPR (LPAPR) of $x[n]$ as

$$\mathcal{L} \triangleq \frac{\left(\min\limits_{0\le n\le N-1} x[n]\right)^2}{\sigma_x^2}. \tag{32}$$

Accordingly, we can derive the CCDF of UPAPR as

$$\begin{aligned} & \mathrm{CCDF}_{\mathcal{U}}\{r_u\} = Pr\{\mathcal{U} > r_u\} \qquad (33) \\ = \;& 1 - Pr\{\mathcal{U} \leq r_u\} \\ = \;& 1 - Pr\{x[n] \leq \sigma_x\sqrt{r_u}, 0 \leq n \leq N-1\} \\ = \;& 1 - [Pr\{x[0] \leq \sigma_x\sqrt{r_u}\}]^N \\ = \;& 1 - \Phi^N(\sqrt{r_u}), \end{aligned}$$

and the CCDF of LPAPR is derived as

$$\begin{aligned} & \mathrm{CCDF}_{\mathcal{L}}\{r_l\} = Pr\{\mathcal{L} > r_l\} \qquad (34) \\ = \;& 1 - Pr\{\mathcal{L} \leq r_l\} \\ = \;& 1 - Pr\{x[n] \geq -\sigma_x\sqrt{r_l}, 0 \leq n \leq N-1\} \\ = \;& 1 - [Pr\{x[0] \geq -\sigma_x\sqrt{r_l}\}]^N \\ = \;& 1 - \Phi^N(\sqrt{r_l}). \end{aligned}$$

Note that the UPAPR and the LPAPR have the same CCDF. Fig. 9 shows the simulated CCDF of UPAPR and LPAPR with various constellation orders and numbers of subcarriers. In this chapter, all the simulation results are taken from 100000 OFDM symbols with 4-QAM, 64-QAM, and 256-QAM constellations. Theoretical results are plotted as well to examine our analysis. We can observe that the distribution of $\mathcal{U}$ and $\mathcal{L}$ are independent of the constellations orders and increase with more subcarriers. When $N = 128$, slight differences can be found between the simulated results and the theoretical values. When $N = 1024$, the simulated results match the theoretical values very well because the central limit theory holds better.

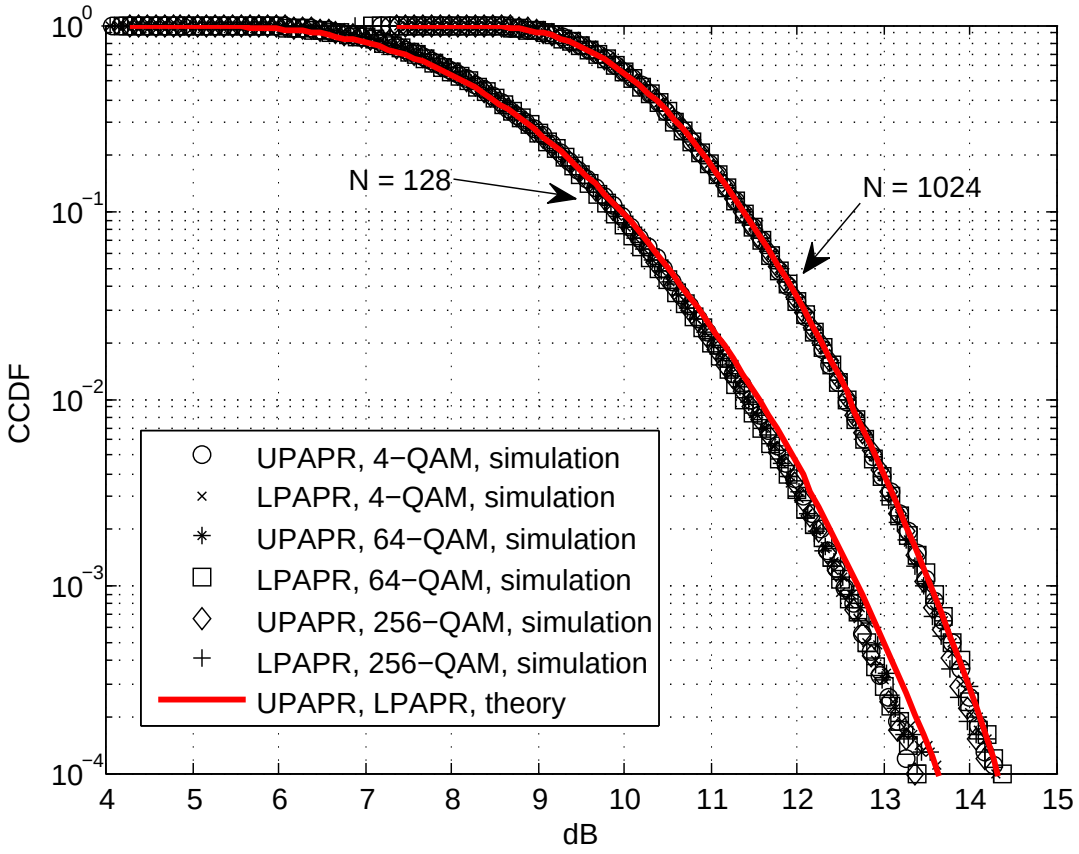

Figure 9: CCDF of UPAPR and LPAPR with various constellation orders and numbers of subcarriers.

From the definitions of UPAPR and LPAPR, we can see that UPAPR and LPAPR are not independent distributed. Therefore, it is necessary to know the joint cumulative distribution function of UPAPR and LPAPR, which can be obtained as

$$\begin{aligned} & F_{\mathcal{L},\mathcal{U}}(r_l, r_u) = Pr\{\mathcal{L} \leq r_l, \mathcal{U} \leq r_u\} \qquad (35) \\ = \; & Pr\{-\sigma_x\sqrt{r_l} \leq x[n] \leq \sigma_x\sqrt{r_u}, 0 \leq n \leq N-1\} \\ = \; & [Pr\{-\sigma_x\sqrt{r_l} \leq x[0] \leq \sigma_x\sqrt{r_u}]^N \\ = \; & [\Phi(\sqrt{r_u}) - \Phi(-\sqrt{r_l})]^N. \end{aligned}$$

The joint PDF of UPAPR and LPAPR is

$$\begin{aligned} & f_{\mathcal{L},\mathcal{U}}(r_l, r_u) \\ = & \frac{\partial^2 F_{\mathcal{L},\mathcal{U}}(r_l, r_u)}{\partial r_l \partial r_u} \\ = & \frac{\phi(\sqrt{r_u})\phi(\sqrt{r_l})}{4\sqrt{r_l r_u}} N(N-1)[\Phi(\sqrt{r_u}) - \Phi(-\sqrt{r_l})]^{N-2}. \end{aligned} \tag{36}$$

3.4 Linear scaling and biasing

LEDs place dynamic range constraints $[I_L, I_H]$ on the input signal, where I_L denotes turn-on current and I_H denotes the maximum input current [29]. The Dynamic range can be denoted by $D \triangleq I_H - I_L$. Since I_L is positive, the bipolar signal $x[n]$ cannot serve as the input of LEDs directly. The forward signal $y[n]$ can be obtained from the OFDM signal $x[n]$ after both a linear scaling and a biasing operation; i.e.,

$$y[n] = \epsilon x[n] + B, \quad 0 \leq n \leq N-1, \tag{37}$$

where ϵ denotes the scaling factor used to control the input power back-off

$$\Lambda \triangleq \frac{D^2}{\epsilon^2 \sigma_x^2}, \tag{38}$$

and B denotes the biasing level. ϵ and B are both real-valued. The resulting signal, $y[n]$, has a mean value B and a variance $\sigma_y^2 = E[\epsilon^2]\sigma_x^2$. Let us define biasing ratio as

$$\chi \triangleq \frac{B - I_L}{D}. \tag{39}$$

Without loss of generality, we only consider biasing ratio in the range $0 \leq \chi \leq 0.5$, because any forward signal $s[n]$ with biasing ratio $0.5 < \chi \leq 1$ can be created from $y[n]$, which has biasing ratio $0 \leq 1-\chi \leq 0.5$ and is within the dynamic range $[I_L, I_H]$, by $s[n] = I_H + I_L - y[n]$.

3.4.1 Symbol-invariant scaling factor

Assume that the scaling factor ϵ or input power back-off Λ is fixed for all OFDM symbols. Given the biasing ratio χ and the input power back-off Λ, it is useful to

know the probability that the input OFDM symbol $\{y[n]\}_{n=0}^{N-1}$ is beyond the dynamic range of LEDs, which is given by

$$
\begin{aligned}
& Pr\{\{y[n]\}_{n=0}^{N-1} \text{ is out of dynamic range} \mid \Lambda, \chi\} \qquad (40)\\
= \;& Pr\{y[n] > I_H, \text{or } y[n] < I_L \mid \Lambda, \chi\} \\
= \;& Pr\left\{x[n] > \frac{I_H - B}{\epsilon}, \text{or } x[n] < \frac{I_L - B}{\epsilon} \mid \Lambda, \chi\right\} \\
= \;& 1 - Pr\left\{\frac{I_L - B}{\epsilon} \leq \{x[n]\}_{n=0}^{N-1} \leq \frac{I_H - B}{\epsilon} \mid \Lambda, \chi\right\} \\
= \;& 1 - Pr\left\{\frac{I_L - B}{\epsilon\sigma_x} \leq \frac{\{x[n]\}_{n=0}^{N-1}}{\sigma_x} \leq \frac{I_H - B}{\epsilon\sigma_x} \mid \Lambda, \chi\right\} \\
= \;& 1 - Pr\left\{-\chi\sqrt{\Lambda} \leq \frac{\{x[n]\}_{n=0}^{N-1}}{\sigma_x} \leq (1-\chi)\sqrt{\Lambda}, \right\} \\
= \;& 1 - Pr\{\mathcal{L} \leq \chi^2\Lambda, \text{and } \mathcal{U} \leq (1-\chi)^2\Lambda\} \\
= \;& 1 - F_{\mathcal{L},\mathcal{U}}(\chi^2\Lambda, (1-\chi)^2\Lambda),
\end{aligned}
$$

where $(I_L - B)/\epsilon\sigma_x = -\chi\sqrt{\Lambda}$ and $(I_H - B)/\epsilon\sigma_x = (1-\chi)\sqrt{\Lambda}$ are obtained from the Eqs. (38) (39). We can see that the probability in Eq. (40) depends on the joint distribution of UPAPR and LPAPR. Fig. 10 shows simulated and theoretical results for 128 subcarriers. Fig. 11 shows simulated and theoretical results for 1024 subcarriers. We can observe that the joint distribution of UPAPR and LPAPR is independent of constellations, and the simulated results match the theoretical values well. For a biasing ratio $\chi \in [0, 0.5]$, lower biasing ratio requires larger input power back-off to achieve the same probability.

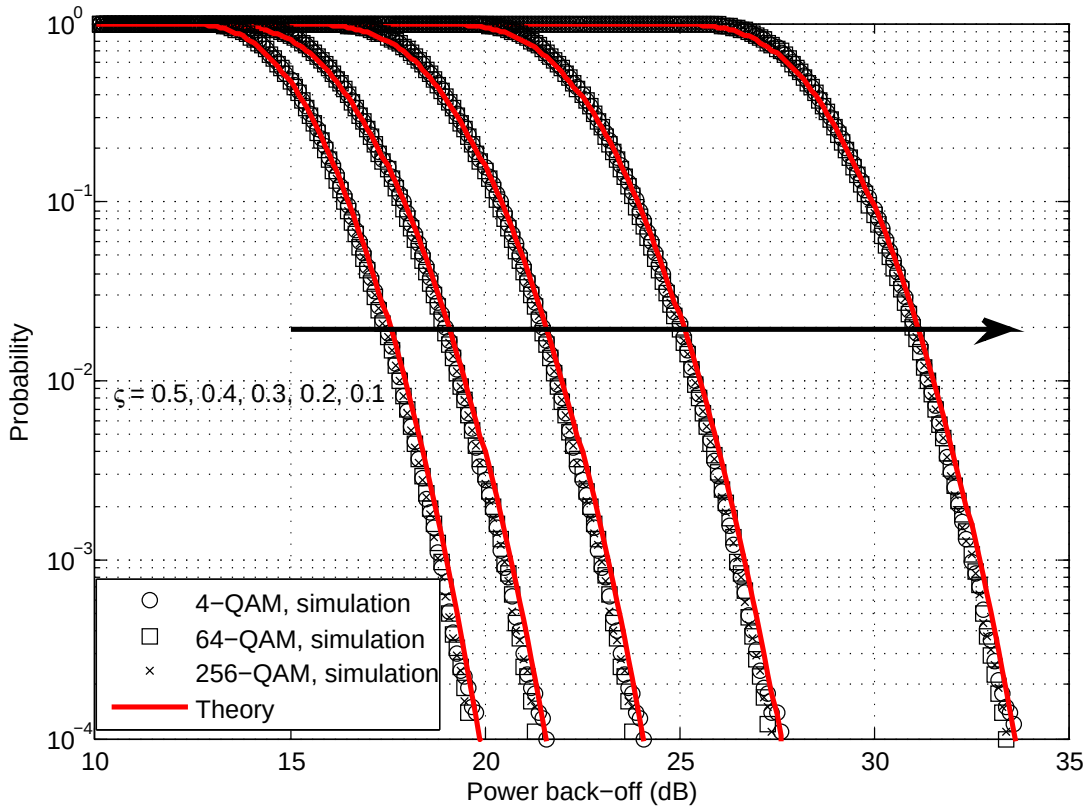

Figure 10: Probability that the input symbol $\{y[n]\}_{n=0}^{N-1}$ is beyond the dynamic range of LEDs given power back-off and biasing ratio (128 subcarriers).

3.4.2 Symbol-variant scaling factor

Assume that the scaling factor ϵ can be adjusted symbol by symbol. The variance σ_y^2 can be maximized by selecting ϵ with the greatest value for each OFDM symbol. To ensure $y[n]$ is within the dynamic range of the LED, we can obtain an ϵ with the greatest value as

$$\epsilon = \min \left\{ \frac{I_H - B}{\max\limits_{0 \le n \le N-1} x[n]}, \frac{I_L - B}{\min\limits_{0 \le n \le N-1} x[n]} \right\} \tag{41}$$

We can obtain the variance of $y[n]$ as

$$\begin{aligned} \sigma_y^2 &= \sigma_x^2 E[\epsilon^2] \\ &= D^2 E_{\mathcal{U},\mathcal{L}}\left[\min\left\{\frac{(1-\zeta)^2}{\mathcal{U}}, \frac{\zeta^2}{\mathcal{L}}\right\}\right] \\ &= D^2 \int_0^\infty \int_0^\infty \min\left\{\frac{(1-\zeta)^2}{r_u}, \frac{\zeta^2}{r_l}\right\} f_{\mathcal{L},\mathcal{U}}(r_l, r_u) dr_l dr_u, \end{aligned} \tag{42}$$

where $f_{\mathcal{L},\mathcal{U}}(r_l, r_u)$ is the joint PDF of UPAPR and LPAPR from Eq. (36). We can observe that the variance σ_y^2 depends on three factors: biasing ratio, upper PAPR of the OFDM signal and lower PAPR of the OFDM signal. Note that the dynamic range D is a fixed value, which is determined by characteristics of LEDs. The scaling factor ϵ varies symbol by symbol since $\mathcal{U}$ and $\mathcal{L}$ are both random variables. Fig. 12 is a plot of the variance σ_y^2 versus the biasing ratio with normalized dynamic range. The plots demonstrate that our theoretical analysis matches the simulated results very well. The variances are identical for all three constellation orders since the distributions of LPAPR and UPAPR are independent of constellations. The variance decrease with increasing subcarriers because both the UPAPR and LPAPR will increase when there are more subcarriers. Since the OFDM signal has a symmetric distribution, the maximum variance occurs at biasing ratio 0.5 when the OFDM signal is biased around the middle point of the dynamic range.

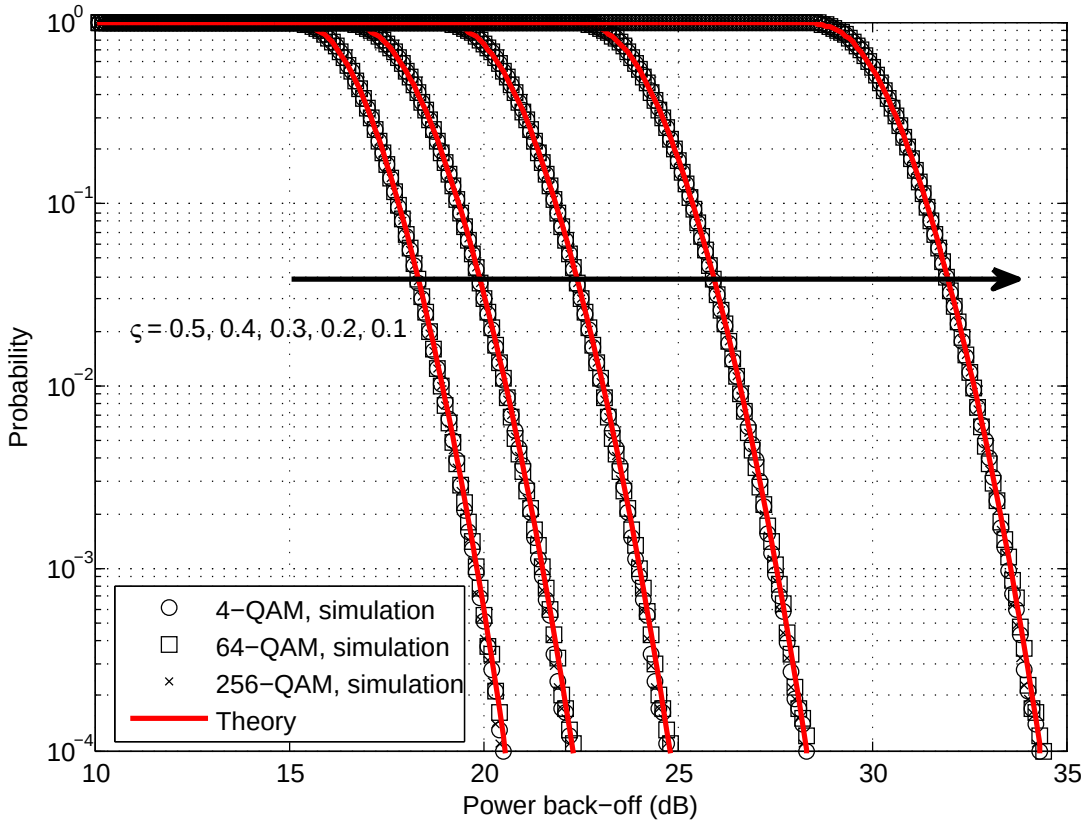

Figure 11: Probability that the input symbol $\{y[n]\}_{n=0}^{N-1}$ is beyond the dynamic range of LEDs given power back-off and biasing ratio (1024 subcarriers).

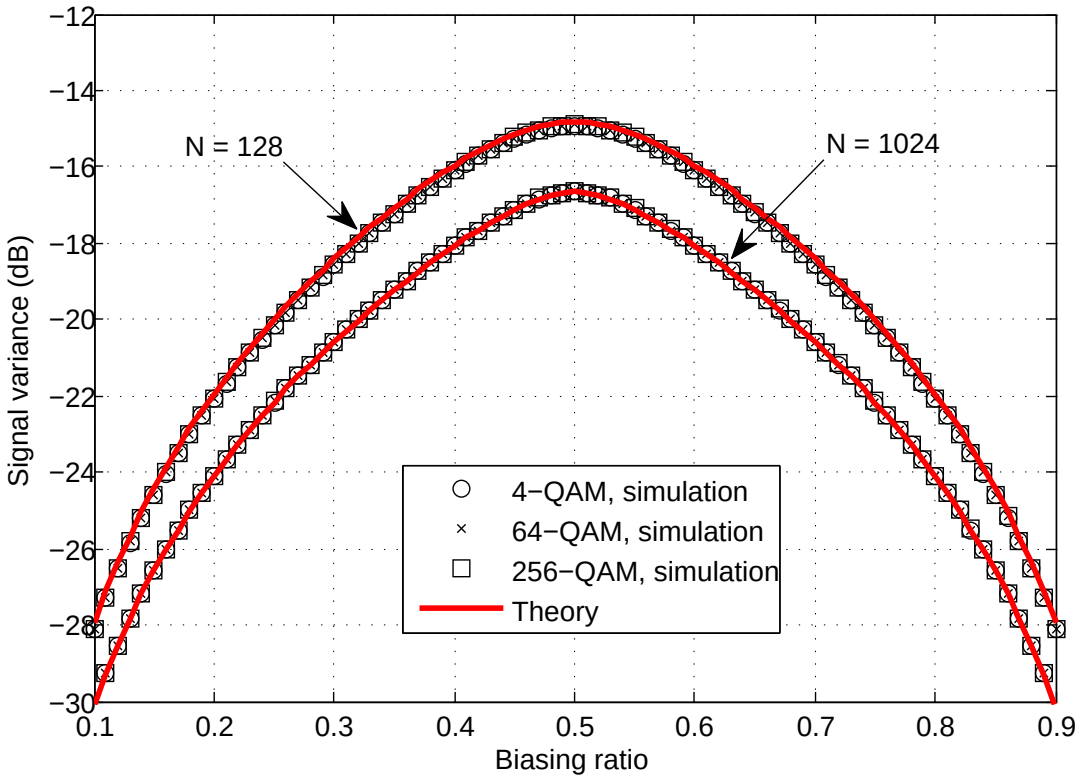

Figure 12: Variance σ_y^2 as a function of the biasing ratio with normalized dynamic range.

3.5 Conclusions

In this chapter, we derived the CCDF and the joint distribution of UPAPR and L-PAPR. The performance of OWC-OFDM with dynamic range and average amplitude constraints are shown to be directly related with UPAPR and LPAPR. Simulation results matched the theoretical analysis well.

CHAPTER IV

ERROR VECTOR MAGNITUDE (EVM) ANALYSIS OF CLIPPED OFDM SIGNALS IN OWC

A major disadvantage of OFDM is the large dynamic range of its time-domain waveforms, making OFDM vulnerable to nonlinearity of light emitting diodes. DC-biased optical OFDM (DCO-OFDM) and asymmetrically clipped optical OFDM (ACO-OFDM) are two popular OFDM techniques developed for the OWC. EVM is a commonly used metric to characterize distortions. We will describe an approach to numerically calculate the EVM for DCO-OFDM and ACO-OFDM. We will derive the optimum biasing ratio in the sense of minimizing EVM for DCO-OFDM. In addition, we will formulate the EVM minimization problem as a convex linear optimization problem and obtain an EVM lower bound against which to compare the DCO-OFDM and ACO-OFDM techniques. We will prove that the ACO-OFDM can achieve the lower bound.

4.1 Introduction

One disadvantage of OFDM is its high peak-to-average-power ratio (PAPR) due to the summation over a large number of terms [67]. The high PAPR or dynamic range of OFDM makes it very sensitive to nonlinear distortions. In OWC, the LED is the main source of nonlinearity. The nonlinear characteristics of LED can be compensated by digital pre-distortion (DPD) [29], but the dynamic range of any physical device is still limited. The input signal outside this range will be clipped. A number of papers [14, 60, 59, 62] have studied the clipping effects on the RF-OFDM signals. However, clipping in the OWC system has two important differences: (i) the RF baseband signal is complex-valued whereas time-domain signals in the OWC system

are real-valued; (ii) the main power limitation for OWC is average optical power and dynamic optical power, rather than average electrical power and peak power as in RF communication. Therefore, most of the theory and analyses developed for RF OFDM are not directly applicable to optical OFDM.

Error vector magnitude (EVM) is a frequently used performance metric in modern communication standards. In [30, 29], the EVM is measured by simulations for varying power back-off and biasing levels. In this chapter, we will describe an approach to numerically calculate the EVM for DCO-OFDM and ACO-OFDM, and derive the optimum biasing ratio for DCO-OFDM. We will formulate the EVM minimization problem as a convex linear optimization problem and obtain an EVM lower bound. In this chapter, we assume that the LED has been turned on by a bias tee. Hence, the dynamic constraints become $[0, D]$.

4.2 Clipping and biasing model

In order to fit into the dynamic range of the LED, clipping is often necessary, i.e.,

$$\bar{x}[n] = \begin{cases} c_u, & x[n] > c_u \\ x[n], & c_l \leq x[n] \leq c_u \\ c_l, & x[n] < c_l \end{cases}, \tag{43}$$

where c_u denotes the upper clipping level, and c_l denotes the lower clipping level. In order for the LED input to be non-negative, we may need to add a DC bias B to the clipped signal $\bar{x}[n]$ to obtain

$$\bar{y}[n] = \bar{x}[n] + B. \tag{44}$$

For $\bar{y}[n] \geq 0$, we need $B = -c_l$. To facilitate the analysis, we define the clipping ratio γ and the biasing ratio ς as

$$\gamma \triangleq \frac{(c_u - c_l)/2}{\sigma_x}, \tag{45}$$

$$\varsigma \triangleq \frac{B}{c_u - c_l} = \frac{-c_l}{c_u - c_l} \tag{46}$$

Thus, the upper and lower clipping levels can be written as

$$c_u = 2\sigma_x\gamma(1-\varsigma), \quad c_l = -2\sigma_x\gamma\varsigma. \tag{47}$$

The ratios γ and ς can be adjusted independently causing c_u and c_l to vary.

Clipping in the time-domain gives rise to distortions on all subcarriers in the frequency domain. On the other hand, DC-bias only affects the DC component in the frequency-domain. The clipped and DC-biased signal $\bar{y}[n]$ is then converted into analog signal and subsequently modulate the intensity of the LED. At the receiver, the photodiode, or the image sensor, converts the received optical signal to electrical signal and transforms it to digital form. The received sample can be expressed as

$$r[n] = (\bar{x}[n] + B) \otimes h[n] + w[n], \tag{48}$$

where $h[n]$ is the impulse response of the wireless optical channel, $w[n]$ is AWGN, and $\otimes$ denotes convolution. By taking the DFT of Equation (48), we can obtain the received data on the kth subcarrier as

$$R_k = \bar{X}_k H_k + W_k, \quad k \neq 0, \tag{49}$$

where H_k is the channel frequency response on the kth subcarrier.

In DCO-OFDM, we first obtain a clipped signal $\bar{x}^{(D)}[n]$, and then add DC-bias $B = -c_l$ to obtain the LED input signal

$$\bar{y}^{(D)}[n] = \bar{x}^{(D)}[n] + B = \begin{cases} c_u - c_l, & x^{(D)}[n] > c_u \\ x^{(D)}[n] - c_l, & c_l \leq x^{(D)}[n] \leq c_u \\ 0, & x^{(D)}[n] < c_l \end{cases} \tag{50}$$

In the frequency domain,

$$\bar{Y}_k^{(D)} = X_k^{(D)} + C_k, \forall k \neq 0, \tag{51}$$

where C_k is clipping noise on the kth subcarrier.

For ACO-OFDM, no DC-biasing is necessary and thus the biasing ratio $\varsigma = 0$. We obtain the LED input signal $\bar{y}^{(A)}[n]$ via

$$\bar{y}^{(A)}[n] = \begin{cases} c_u, & x^{(A)}[n] > c_u \\ x^{(A)}[n], & 0 \leq x^{(A)}[n] \leq c_u \\ 0, & x^{(A)}[n] < 0 \end{cases} \tag{52}$$

Equation (52) can be regarded as a 2-step clipping process, whereby we first remove those negative values in $x^{(A)}[n]$, and then replace those $x^{(A)}[n]$ values that exceed c_u by c_u. Since $x^{(A)}[n]$ satisfies (20), we infer based on (23) that

$$Y_k^{(A)} = \frac{1}{2} X_k^{(A)} + C_k, \quad \forall k \text{ odd}. \tag{53}$$

As an example, suppose that we need to transmit a sequence of eight quadrature phase-shift keying (QPSK) symbols. Table 2 shows the subcarrier arrangement for DCO-OFDM, whereas Table 3 shows the subcarrier arrangement for ACO-OFDM. The time-main signals $x^{(D)}[n]$ and $x^{(A)}[n]$ and the corresponding LED input signals $y^{(D)}[n]$ and $y^{(A)}[n]$ are shown in Figure 13. We see that in $x^{(A)}[n]$, the last 16 values are a repetition of the first 16 values but with the opposite sign. It takes ACO-OFDM more bandwidth than DCO-OFDM to transmit the same message, although ACO-OFDM is less demanding in terms of dynamic range requirement of the LED and power consumption.

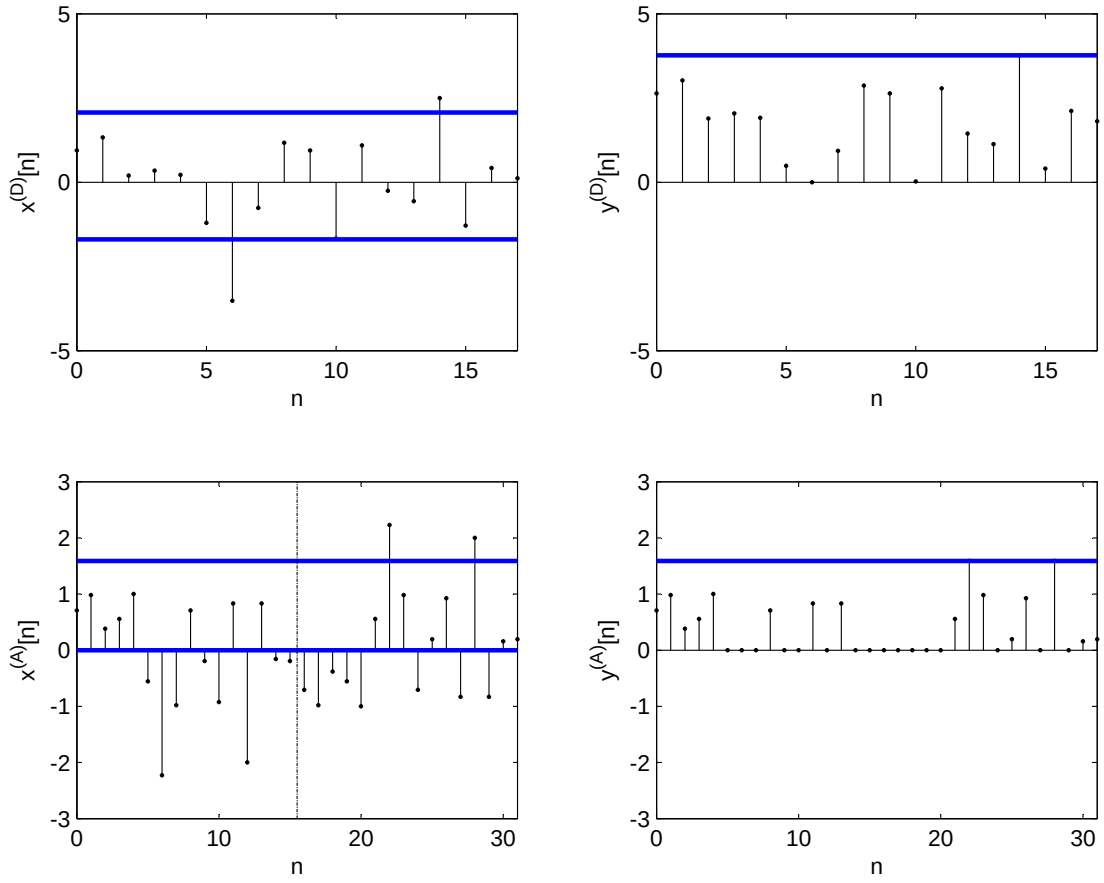

Figure 13: An example of $x^{(D)}[n]$, $y^{(D)}[n]$, $x^{(A)}[n]$ and $y^{(A)}[n]$ to convey a sequence 8 QPSK symbols. For DCO-OFDM, $\gamma = 1.41 = 3$ dB, $\varsigma = 0.45$, $c_l = -1.70$, $c_u = 2.07$, $B = 1.70$; For ACO-OFDM, $\gamma = 0.79 = -2$ dB, $\varsigma = 0$, $c_l = 0$, $c_u = 1.59$, $B = 0$

Table 2: DCO-OFDM subcarrier arrangement for transmitting eight QPSK symbols—an example

k	0	1	2	3	4	5	6	7	8
$X_k^{(D)}$	0	$1+j$	$1-j$	$-1-j$	$1+j$	$1-j$	$-1+j$	$-1-j$	$1-j$
k	9	10	11	12	13	14	15	16	17
$X_k^{(D)}$	0	$1+j$	$-1+j$	$-1-j$	$1+j$	$1-j$	$-1+j$	$1+j$	$1-j$

Table 3: ACO-OFDM subcarrier arrangement for transmitting eight QPSK symbols—an example

k	0	1	2	3	4	5	6	7
$X_k^{(A)}$	0	$1+j$	0	$1-j$	0	$-1-j$	0	$1+j$
k	8	9	10	11	12	13	14	15
$X_k^{(A)}$	0	$1-j$	0	$-1+j$	0	$-1-j$	0	$1-j$
k	16	17	18	19	20	21	22	23
$X_k^{(A)}$	0	$1+j$	0	$-1+j$	0	$-1-j$	0	$1+j$
k	24	25	26	27	28	29	30	31
$X_k^{(A)}$	0	$1-j$	0	$-1+j$	0	$1+j$	0	$1-j$

4.3 EVM calculation

EVM is a figure-of-merit for distortions. Let $\mathbf{X}^\dagger = [X_0^\dagger, X_1^\dagger, \ldots, X_{N-1}^\dagger]$ denote the N-length DFT of the modified time-domain signal $\mathbf{x}^\dagger$. EVM can be defined as

$$\xi(\mathbf{X}^{(r)}, \mathbf{X}^\dagger) \triangleq \sqrt{\frac{E\left[\sum_{k\in\mathcal{K}_d} |X_k^{(r)} - X_k^\dagger|^2\right]}{E\left[\sum_{k\in\mathcal{K}_d} |X_k^{(r)}|^2\right]}}, \tag{54}$$

where $\mathbf{X}^{(r)} = [X_0^{(r)}, X_1^{(r)}, \ldots, X_{N-1}^{(r)}]$ denotes the reference constellation.

4.3.1 DCO-OFDM

In DCO-OFDM, clipping in the time-domain generates distortions on all the subcarriers. We denote the clipping error power by $\bar{P}_{\gamma,\varsigma}^{(D)} = \sum_{k\in\mathcal{K}_d^{(D)}} E[|X_k^{(D)} - \bar{X}_k^{(D)}|^2]$. Since the sum distortion power on the 0th and $N/2$th subcarriers is small relative to the total distortion power of N subcarriers, according to the Parseval's theorem, we

can approximate $\bar{P}_{\gamma,\varsigma}^{(D)}$ as

$$\begin{aligned}\bar{P}_{\gamma,\varsigma}^{(D)} &= \sum_{k\in\mathcal{K}_d^{(D)}} E[|X_k^{(D)} - \bar{X}_k^{(D)}|^2] \approx \sum_{n=0}^{N-1} E[|x^{(D)}[n] - \bar{x}^{(D)}[n]|^2] \qquad (55)\\ &= N\left(\int_{c_u}^{\infty}(z-c_u)^2\frac{1}{\sigma_x}\phi\left(\frac{z}{\sigma_x}\right)dz + \int_{-\infty}^{c_l}(z-c_l)^2\frac{1}{\sigma_x}\phi\left(\frac{z}{\sigma_x}\right)dz\right)\\ &= N\sigma_x^2\Big(1+4\gamma^2(1-\varsigma)^2 - 2\gamma(1-\varsigma)\phi\big(2\gamma(1-\varsigma)\big) - 2\gamma\varsigma\phi\big(2\gamma\varsigma\big)\\ &\quad -\Phi\big(2\gamma(1-\varsigma)\big) - 4\gamma^2(1-\varsigma)^2\Phi\big(2\gamma(1-\varsigma)\big) + \Phi\big(-2\gamma\varsigma\big) + 4\gamma^2\varsigma^2\Phi\big(-2\gamma\varsigma\big)\Big),\end{aligned}$$

where $\Phi(x) = \int_{-\infty}^{x}\phi(t)dt$. Thus, we obtain the EVM for the DCO-OFDM scheme as

$$\begin{aligned}\xi_{\gamma,\varsigma}^{(D)} &= \sqrt{\frac{\bar{P}_{\gamma,\varsigma}^{(D)}}{N\sigma_x^2}} \qquad (56)\\ &= \Big(1+4\gamma^2(1-\varsigma)^2 - 2\gamma(1-\varsigma)\phi\big(2\gamma(1-\varsigma)\big) - 2\gamma\varsigma\phi\big(2\gamma\varsigma\big)\\ &\quad -\Phi\big(2\gamma(1-\varsigma)\big) - 4\gamma^2(1-\varsigma)^2\Phi\big(2\gamma(1-\varsigma)\big) + \Phi\big(-2\gamma\varsigma\big) + 4\gamma^2\varsigma^2\Phi\big(-2\gamma\varsigma\big)\Big)^{1/2}.\end{aligned}$$

To find the optimum biasing ratio $\varsigma^\star$, we take the first-order partial derivative and the second-order partial derivative of $\bar{P}_{\gamma,\varsigma}^{(D)}$ with respect to the biasing ratio ς

$$\begin{aligned}\frac{\partial\bar{P}_{\gamma,\varsigma}^{(D)}}{\partial\varsigma} &= N\sigma_x^2\Big(4\gamma\phi\big(2\gamma(1-\varsigma)\big) - 4\gamma\phi\big(2\gamma\varsigma\big) \qquad (57)\\ &\quad -8\gamma^2(1-\varsigma)\Phi\big(2\gamma(\varsigma-1)\big) + 8\gamma^2\varsigma\Phi\big(-2\gamma\varsigma\big)\Big),\\ \frac{\partial^2\bar{P}_{\gamma,\varsigma}^{(D)}}{\partial\varsigma^2} &= N\sigma_x^2\Big(8\gamma^2\Phi\big(2\gamma(\varsigma-1)\big) + 8\gamma^2\Phi\big(-2\gamma\varsigma\big)\Big). \qquad (58)\end{aligned}$$

We can prove that if $\varsigma = 0.5$, $\partial\bar{P}_{\gamma,\varsigma}^{(D)}/\partial\varsigma = 0$. The second-order partial derivative $\partial^2\bar{P}_{\gamma,\varsigma}^{(D)}/\partial\varsigma^2 > 0$ for all ς. Hence, if $\varsigma < 0.5$, $\partial\bar{P}_{\gamma,\varsigma}^{(D)}/\partial\varsigma < 0$. If $\varsigma > 0.5$, $\partial\bar{P}_{\gamma,\varsigma}^{(D)}/\partial\varsigma > 0$. Therefore, $\varsigma^\star = 0.5$ is the optimum biasing ratio which minimizes $\bar{P}_{\gamma,\varsigma}^{(D)}$. By substituting $\varsigma^\star$ into Equation (56) we obtain the EVM for the DCO-OFDM scheme at the optimum biasing ratio as

$$\xi_{\gamma,\varsigma^*}^{(D)} = \sqrt{\frac{\bar{P}_{\gamma,\varsigma^*}^{(D)}}{N\sigma_x^2}} = \sqrt{2(1+\gamma^2)\Phi(-\gamma) - 2\gamma\phi(\gamma)}. \qquad (59)$$

Remarks: (i) $\varsigma^\star = 0.5$ is the optimum biasing ratio for DCO-OFDM, regardless of the clipping ratio. (ii) When $\varsigma = 0.5$, we infer that $c_u = -c_l$, i.e., when the $x^{(D)}[n]$ waveform is symmetrically clipped at the negative and positive tails, the clipping error power is always less than that when the two tails are asymmetrically clipped (i.e., when $c_u \neq c_l$ or when $\varsigma \neq 0.5$).

4.3.2 ACO-OFDM

Denote by $e[n]$, $n = 0, 1, \ldots, N-1$ a generic discrete-time signal with DFT E_k, $k = 0, 1, \ldots, N-1$. When k is odd, E_k can be written as

$$\begin{aligned} E_k &= \frac{1}{\sqrt{N}} \sum_{n=0}^{N-1} e[n] \exp\left(-j2\pi \frac{kn}{N}\right) \qquad (60) \\ &= \frac{1}{\sqrt{N}} \sum_{n=0}^{N/2-1} e[n] \exp\left(-j2\pi \frac{kn}{N}\right) + \frac{1}{\sqrt{N}} \sum_{n=0}^{N/2-1} e[n+N/2] \exp\left(-j2\pi \frac{kn}{N} - jk\pi\right) \\ &= \frac{1}{\sqrt{N}} \sum_{n=0}^{N/2-1} \left(e[n] - e[n+N/2]\right) \exp\left(-j2\pi \frac{kn}{N}\right). \end{aligned}$$

Let $k = 2q+1$, $q = 0, 1, \ldots, N/2-1$, Equation (60) can be further written as

$$\begin{aligned} E_{2q+1} &= \frac{1}{\sqrt{N}} \sum_{n=0}^{N/2-1} \left(e[n] - e[n+N/2]\right) \exp\left(-j2\pi \frac{qn}{N/2} - j2\pi \frac{n}{N}\right) \qquad (61) \\ &= \frac{1}{\sqrt{N}} \sum_{n=0}^{N/2-1} \exp\left(-j2\pi \frac{n}{N}\right) \left(e[n] - e[n+N/2]\right) \exp\left(-j2\pi \frac{qn}{N/2}\right) \end{aligned}$$

Therefore, $\{E_k = E_{2q+1}\}_{q=0}^{N/2-1}$ can be viewed as the DFT coefficients of a new discrete-time sequence $\{\exp\left(-j2\pi \frac{n}{N}\right)\left(e[n] - e[n+N/2]\right)\}_{n=0}^{N/2-1}$. Applying the Parseval's theorem to $\{\exp\left(-j2\pi \frac{n}{N}\right)\left(e[n] - e[n+N/2]\right)\}_{n=0}^{N/2-1}$, we obtain,

$$\sum_{k=\text{odd}} |E_k|^2 = \sum_{q=0}^{N/2-1} |E_{2q+1}|^2 = \frac{1}{2} \sum_{n=0}^{N/2-1} \left(e[n] - e[n+N/2]\right)^2. \qquad (62)$$

In ACO-OFDM, we denote the clipping error power by $\bar{P}_\gamma^{(A)} = \sum_{k \in \mathcal{K}_d^{(A)}} E\left[\left|X_k^{(A)}/2 - \bar{X}_k^{(A)}\right|^2\right]$.

According to (62), we can calculate $\bar{P}_{\gamma}^{(A)}$ as

$$\begin{aligned}
\bar{P}_{\gamma}^{(A)} &= \sum_{k\in\mathcal{K}_d^{(A)}} E\left[\left|X_k^{(A)}/2 - \bar{X}_k^{(A)}\right|^2\right] \qquad (63)\\
&= \frac{1}{2}\sum_{n=0}^{N/2-1} E\left[\left(\frac{x^{(A)}[n]}{2} - \bar{x}^{(A)}[n] - \frac{x^{(A)}[n+N/2]}{2} + \bar{x}^{(A)}[n+N/2]\right)^2\right]\\
&= \frac{N}{4}E\left[\left(x^{(A)}[n] - \bar{x}^{(A)}[n] + \bar{x}^{(A)}[n+N/2]\right)^2\right]\\
&= \frac{N}{4}\int_{-\infty}^{-c_u}(z+c_u)^2\frac{1}{\sigma_x}\phi\left(\frac{z}{\sigma_x}\right)dz + \frac{N}{4}\int_{c_u}^{\infty}(z-c_u)^2\frac{1}{\sigma_x}\phi\left(\frac{z}{\sigma_x}\right)dz\\
&= \frac{N}{2}\sigma_x^2\Big(-2\gamma\phi\left(2\gamma\right) + \Phi\left(-2\gamma\right) + 4\gamma^2\Phi\left(-2\gamma\right)\Big).
\end{aligned}$$

Then we obtain the EVM for the ACO-OFDM scheme as

$$\begin{aligned}
\xi_{\gamma}^{(A)} &= \sqrt{\frac{\bar{P}_{\gamma}^{(A)}}{\sum_{k\in\mathcal{K}_d^{(A)}} E\left[\left|X_k^{(A)}/2\right|^2\right]}} = \sqrt{\frac{4\bar{P}_{\gamma,0}^{(A)}}{N\sigma_x^2}} \qquad (64)\\
&= \sqrt{-4\gamma\phi\left(2\gamma\right) + 2\Phi\left(-2\gamma\right) + 8\gamma^2\Phi\left(-2\gamma\right)}.
\end{aligned}$$

4.4 Lower bound on the EVM

Let us consider the setting

$$\hat{x}[n] = x[n] + c[n], \quad 0 \le n \le N-1, \qquad (65)$$

where $x[n]$ is the original signal, $c[n]$ is a distortion signal, and the resulting $\hat{x}[n]$ is expected to have a limited dynamic range

$$\max(\hat{x}[n]) - \min(\hat{x}[n]) \le 2\gamma\sigma_x. \qquad (66)$$

In (65), all quantities involved are real-valued.

Clipping can produce one such $\hat{x}[n]$ signal, but there are other less straightforward algorithms that can generate other $\hat{x}[n]$ waveforms that also satisfy (66).

In the frequency-domain,

$$\hat{X}_k = X_k + C_k. \qquad (67)$$

Since $x[n]$, $c[n]$, and $\hat{x}[n]$ are all real-valued, X_k, C_k, and $\hat{X}_k$ all should satisfy the Hermitian symmetry condition. Therefore, $c[n]$ has the form

$$c[n] = \frac{2}{\sqrt{N}} \sum_{k=1}^{N/2-1} \Big(\Re(C_k)\cos(2\pi kn/N) - \Im(C_k)\sin(2\pi kn/N) \Big) + \frac{1}{\sqrt{N}} C_0 + \frac{1}{\sqrt{N}} C_{N/2}\cos(\pi n) \tag{68}$$

We are interested in knowing the lowest possible EVM,

$$\xi = \sqrt{\frac{E\left[\sum_{k\in\mathcal{K}_d} |C_k|^2\right]}{E\left[\sum_{k\in\mathcal{K}_d} |X_k|^2\right]}} \tag{69}$$

among all such $\hat{x}[n]$ waveforms. Afterwards, we can compare the EVM from the DCO-OFDM and ACO-OFDM methods to get a sense of how far these algorithms are from being optimum (in the EVM sense).

We formulate the following linear optimization problem:

$$\begin{aligned}
\text{minimize} \quad & \sum_{k\in\mathcal{K}_d} |C_k|^2 \\
\text{subject to} \quad & \max\big(\hat{x}[n]\big) - \min\big(\hat{x}[n]\big) \le 2\gamma\sigma_x \\
& \hat{x}[n] = x[n] + \frac{2}{\sqrt{N}} \sum_{k=1}^{N/2-1} \Big(\Re(C_k)\cos(2\pi kn/N) - \Im(C_k)\sin(2\pi kn/N) \Big) \\
& \qquad\qquad + \frac{1}{\sqrt{N}} C_0 + \frac{1}{\sqrt{N}} C_{N/2}\cos(\pi n), \quad 0 \le n \le N-1 \\
& C_0, C_{N/2} \in \mathbb{R}
\end{aligned} \tag{70}$$

When the distortion of each OFDM symbol is minimized by the above convex optimization approach, the corresponding EVM of $\hat{x}[n]$ (which is proportional to $\sqrt{E\left[\sum_{k\in\mathcal{K}_d} |C_k|^2\right]}$) serves as the lower bound for the given dynamic range $2\gamma\sigma_x$.

4.5 Optimality for ACO-OFDM

In this section, we will prove that the ACO-OFDM scheme achieves the minimum EVM and thus is optimal in the EVM sense.

For ACO-OFDM, let us write $\hat{x}[n] = x^{(A)}[n] + c[n]$, where $c[n]$ is the clipping noise to ensure that $\hat{x}[n]$ has a limited dynamic range as described in (66). In the

frequency-domain, we have $\hat{X}_k = X_k^{(A)} + C_k$, where the $X_k^{(A)}$ subcarriers are laid out as in (18). When k is odd, the objective function in (70) can be written as

$$\sum_{k=\text{odd}} |C_k|^2 \;=\; \frac{1}{2}\sum_{n=0}^{N/2-1} (c[n] - c[n+N/2])^2. \tag{71}$$

The dynamic range constraints in problem (70) can be viewed as two constraints put together.

$$\max\left(x^{(A)}[n] + c[n]\right) - \min\left(x^{(A)}[n] + c[n]\right) \leq 2\gamma\sigma_x, \quad 0 \leq n \leq N/2-1, \tag{72}$$

$$\max\left(x^{(A)}[n] + c[n]\right) - \min\left(x^{(A)}[n] + c[n]\right) \leq 2\gamma\sigma_x, \quad N/2 \leq n \leq N-1. \tag{73}$$

Since $x^{(A)}[n] = -x^{(A)}[n-N/2]$ when $N/2 \leq n \leq N-1$, Equation (73) can be further written as

$$\max\left(x^{(A)}[n] - c[n+N/2]\right) - \min\left(x^{(A)}[n] - c[n+N/2]\right) \leq 2\gamma\sigma_x, \quad 0 \leq n \leq N/2-1. \tag{74}$$

From Equations (71), (72), and (74), the problem (70) can be recast as

$$\begin{aligned} \text{minimize} \quad & \sum_{n=0}^{N/2-1} c^2[n] \\ \text{subject to} \quad & \max\left(x^{(A)}[n] + c[n]\right) - \min\left(x^{(A)}[n] + c[n]\right) \leq 2\gamma\sigma_x, \quad 0 \leq n \leq N/2-1 \end{aligned} \tag{75}$$

which is equivalent to

$$\begin{aligned} \text{minimize} \quad & \sum_{n=0}^{N/2-1} c^2[n] \\ \text{subject to} \quad & x^{(A)}[n] + c[n] \leq 2\gamma\sigma_x, \quad 0 \leq n \leq N/2-1 \\ & x^{(A)}[n] + c[n] \geq 0, \quad 0 \leq n \leq N/2-1 \end{aligned} \tag{76}$$

In Appendix, we prove that the solution $c^\star[n]$ to (76) yields

$$\bar{x}^{(A)}[n] = x^{(A)}[n] + c^\star[n] = \begin{cases} 2\gamma\sigma_x, & x^{(A)}[n] > 2\gamma\sigma_x \\ x^{(A)}[n], & 0 \leq x^{(A)}[n] \leq 2\gamma\sigma_x \\ 0, & x^{(A)}[n] < 0 \end{cases} \tag{77}$$

and thus the ACO-OFDM scheme is optimum in the EVM sense.

4.6 Numerical results

The EVM analyses for DCO-OFDM and ACO-OFDM are validated through computer simulations. In the simulations, we chose the number of subcarriers $N = 512$, and QPSK modulation. One thousand OFDM symbols were generated based on which we calculated the EVM. In order to experimentally determine the optimum biasing ratio for DCO-OFDM, we used biasing ratios ranging from 0.3 to 0.7 in step size of 0.02, and clipping ratios ranging from 5 to 9 dB in step size of 1 dB. Their simulated and theoretical EVM curves are plotted in Figure 14. As expected, the minimum EVM was achieved when the biasing ratio was 0.5, regardless of the clipping ratio. This agrees with the analysis in "EVM calculation" section. The gap between theory and simulation for some cases can be explained by that the 0th subcarrier (DC) dominates the distortions. We compared the EVM for DCO-OFDM with biasing ratio 0.5, EVM for ACO-OFDM with biasing ratio 0, and their respective lower bounds. To obtain the lower bounds, we used `CVX`, a package for specifying and solving convex programs [24], to solve Equation (70). The resulting EVM curves for DCO-OFDM are plotted in Figure 15. The resulting EVM curves for ACO-OFDM are plotted in Figure 16. We see that the EVM for ACO-OFDM achieves its lower bound, thus corroborating the discussion in "Optimality for ACO-OFDM" section. For DCO-OFDM, the gap above the lower bound increases with the clipping ratio (i.e., with increasing dynamic range of the LED). This implies that there exists another (more complicated) way of mapping $x^D[n]$ into a limited dynamic range signal $\hat{x}[n]$ that can yield a lower EVM.

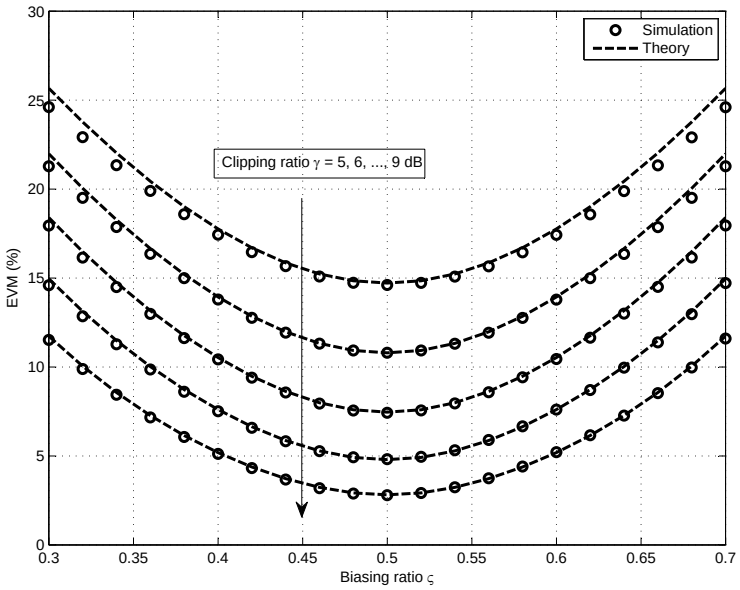

Figure 14: EVM as a function of biasing ratio for DCO-OFDM with clipping ratio = 5, 6, ..., 9 dB.

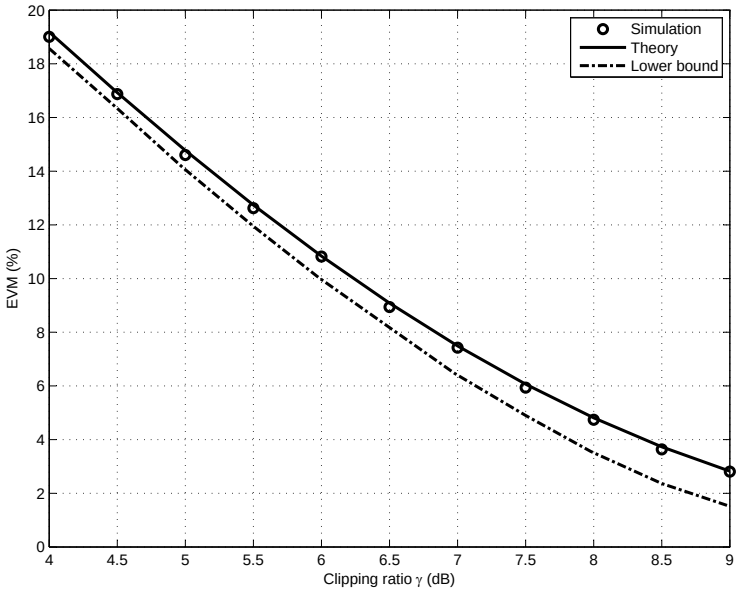

Figure 15: EVM as a function of the clipping ratio γ for DCO-OFDM along with the EVM lower bound for a given dynamic range limit $2\gamma\sigma_x$.

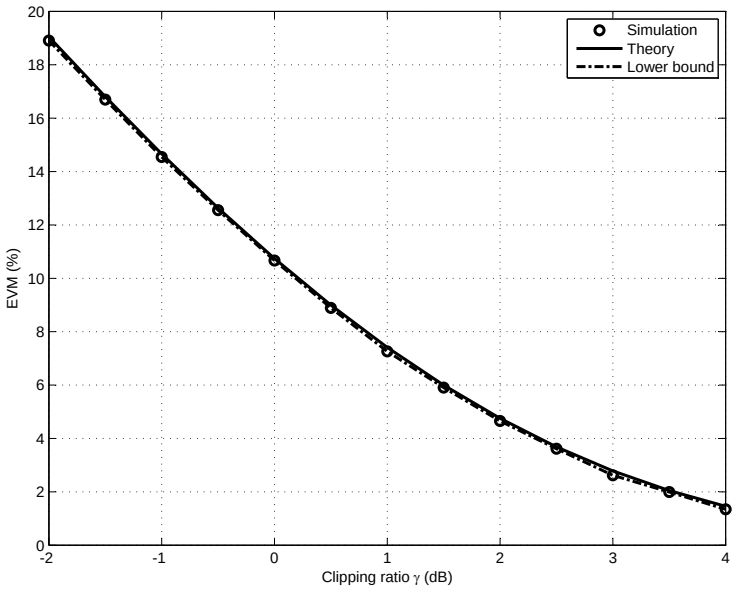

Figure 16: EVM as a function of the clipping ratio γ for ACO-OFDM along with the EVM lower bound for a given dynamic range limit $2\gamma\sigma_x$.

CHAPTER V

ACHIEVABLE DATA RATE ANALYSIS OF CLIPPED OFDM SIGNALS IN OWC

In contrast to prior work which investigated the achievable data rates for OWC-OFDM with only average optical power limitation, we will derive the achievable data rates subject to both the average optical power and dynamic optical power constraints. We will first derive the signal-to-distortion ratio (SDR) for a given data-bearing subcarrier based on the Bussgangs theory. Upon the SDR analysis, we will derive the achievable data rates for additive white Gaussian noise (AWGN) channel and frequency-selective channel. Finally, we will compare the performance of two optical OFDM techniques.

5.1 Signal-to-distortion ratio (SDR) analysis

Based on the Bussgang's theorem [19], any nonlinear function of $x[n]$ can be decomposed into a scaled version of $x[n]$ plus a distortion term $d[n]$ that is uncorrelated with $x[n]$. For example, we can write

$$\bar{x}[n] = \alpha \cdot x[n] + d[n], \quad n = 0, \ldots, N-1. \tag{78}$$

Let $R_{xx}[q] = E\{x[n]x[n+q]\}$ denote the auto-correlation function of $x[n]$, and let $R_{xy}[q] = E\{x[n]y[n+q]\}$ denote the cross-correlation function between $x[n]$ and $y[n]$ at lag q. For any given q, the correlation functions satisfy

$$R_{xd}[q] = 0, \tag{79}$$

$$R_{\bar{x}x}[q] = \alpha R_{xx}[q]. \tag{80}$$

Thus, the scaling factor α can be calculated as

$$\alpha = \frac{R_{\bar{x}x}[0]}{R_{xx}[0]} = \frac{E\{\bar{x}[n]x[n]\}}{\sigma_x^2} = \frac{1}{\sigma_x^2}\int_{-\infty}^{\infty} \bar{x}x \cdot p(x)dx. \tag{81}$$

Let $f(\cdot)$ denote the function linking the original signal to the clipped signal, it is shown in [26] that the output auto-correlation function $R_{\bar{x}\bar{x}}[q]$ is related to the input auto-correlation function $R_{xx}[q]$ via

$$R_{\bar{x}\bar{x}}[q] = \sum_{\ell=0}^{\infty} \frac{b_\ell^2}{\ell!} \left[\frac{R_{xx}[q]}{\sigma_x^2} \right]^\ell, \tag{82}$$

where the coefficients

$$b_\ell = \frac{(-1)^\ell \sigma_x^{\ell-1}}{\sqrt{2\pi}} \int_{-\infty}^{\infty} f(x) \frac{d^\ell [\exp(-\frac{x^2}{2\sigma_x^2})]}{dx^\ell} dx. \tag{83}$$

The input auto-correlation function $R_{xx}[q]$ can be obtained from taking IDFT of the input power spectrum density (PSD) as

$$R_{xx}[q] = \text{IDFT}\{P_{X,k}\}_q, \quad q = 0, \ldots, N-1, \tag{84}$$

where $P_{X,k} = E[|X_k|^2]$ is the expected value of the power on the kth subcarrier before clipping. Then it is straightforward to calculate the output PSD by taking the DFT of the auto-correlation of the output signal:

$$P_{\bar{X},k} = \text{DFT}\{R_{\bar{x}\bar{x}}[q]\}_k, \quad k = 0, \ldots, N-1. \tag{85}$$

Taking the DFT of Equation (78), the data at the kth subcarrier are expressed as

$$\begin{aligned} \bar{X}_k &= \text{DFT}\{\alpha \cdot x[n]\}_k + \text{DFT}\{d[n]\}_k \\ &= \alpha \cdot X_k + D_k, \quad k \in \mathcal{K}_d. \end{aligned} \tag{86}$$

Here, we assume that D_k is Gaussian distributed, which is the common assumption when N is large [60]. The SDR at the kth subcarrier is given by

$$\text{SDR}_k = \frac{E[|\alpha \cdot X_k|^2]}{E[|D_k|^2]} = \frac{\alpha^2 P_{X,k}}{P_{D,k}} = \frac{\alpha^2 P_{X,k}}{P_{\bar{X},k} - \alpha^2 P_{X,k}}, \quad k \in \mathcal{K}_d, \tag{87}$$

where $P_{D,k} = E[|D_k|^2] = P_{\bar{X},k} - \alpha^2 P_{X,k}$ is the average power of the distortion on the kth subcarrier. According to Equation (81), we can obtain the scaling factor α as a

function of the clipping ratio γ and the biasing ratio ς:

$$\begin{aligned}\alpha &= \frac{1}{\sigma_x^2}\int_{-\infty}^{\infty}\bar{x}x\cdot p(x)dx \\ &= \frac{1}{\sigma_x^2}\int_{c_l}^{c_u} z^2\frac{1}{\sigma_x}\phi\left(\frac{z}{\sigma_x}\right)dz+\frac{1}{\sigma_x^2}\int_{-\infty}^{c_l} c_l z\frac{1}{\sigma_x}\phi\left(\frac{z}{\sigma_x}\right)dz+\frac{1}{\sigma_x^2}\int_{c_u}^{\infty} c_u z\frac{1}{\sigma_x}\phi\left(\frac{z}{\sigma_x}\right)dz \\ &= \Phi\left(2\gamma(1-\varsigma)\right)-\Phi\left(-2\gamma\varsigma\right).\end{aligned} \tag{88}$$

According to Equation (83), we can obtain the coefficient b_ℓ as a function of the clipping ratio γ and the biasing ratio ς:

$$b_\ell=\begin{cases}\sigma_x\phi(2\gamma\varsigma)-\sigma_x\phi\left(2\gamma(1-\varsigma)\right)-2\sigma_x\gamma\varsigma\Phi\left(-2\gamma\varsigma\right)+2\sigma_x\gamma(1-\varsigma)\Phi\left(-2\gamma(1-\varsigma)\right), & \ell=0\\ \sigma_x\Phi\left(2\gamma(1-\varsigma)\right)-\sigma_x\Phi(-2\gamma\varsigma), & \ell=1\\ \frac{\sigma_x}{\sqrt{2\pi}}\exp\left(-2\gamma^2\varsigma^2\right)He_{(\ell-2)}\left(-2\gamma\varsigma\right)-\frac{\sigma_x}{\sqrt{2\pi}}\exp\left(-2\gamma^2(1-\varsigma)^2\right)He_{(\ell-2)}\left(2\gamma(1-\varsigma)\right), & \ell>1\end{cases} \tag{89}$$

where $He_n(t)=(-1)^\ell\exp\left(\frac{t^2}{2}\right)\frac{d^\ell[\exp(-\frac{t^2}{2})]}{dt^\ell}$ is the probabilists' Hermite polynomials [5].

5.2 Achievable data rate

In OWC, average optical power and dynamic optical power are two main constraints. In the optical communication literature, the average optical power of the LED input signal y[n] is defined as

$$O_{y[n]}=E\{y[n]\}. \tag{90}$$

We can obtain the average optical power of $\bar{y}[n]$ as

$$\begin{aligned}O_{\bar{y}[n]} &= E\{\bar{y}[n]\} \\ &= E\{\bar{x}[n]\}+B \\ &= \int_{c_l}^{c_u} z\frac{1}{\sigma_x}\phi\left(\frac{z}{\sigma_x}\right)dz+c_u\int_{c_u}^{\infty}\frac{1}{\sigma_x}\phi\left(\frac{z}{\sigma_x}\right)dz+c_l\int_{-\infty}^{c_l}\frac{1}{\sigma_x}\phi\left(\frac{z}{\sigma_x}\right)dz-c_l \\ &= \sigma_x\Big(\phi(2\gamma\varsigma)-\phi\left(2\gamma(1-\varsigma)\right)-2\gamma\varsigma\Phi\left(-2\gamma\varsigma\right)+2\gamma(1-\varsigma)\Phi\left(-2\gamma(1-\varsigma)\right)+2\gamma\varsigma\Big).\end{aligned} \tag{91}$$

Let $\sigma_w^2 = E\{w^2[n]\}$ denote the power of AWGN $w[n]$, we define the optical signal-to-noise ratio (OSNR) as

$$\text{OSNR} \triangleq \frac{O_{\bar{y}[n]}}{\sigma_w}. \tag{92}$$

We can obtain the dynamic range of $\bar{y}[n]$ as

$$G_{\bar{y}} = \max(\bar{y}[n]) - \min(\bar{y}[n]) = c_u - c_l = 2\sigma_x\gamma. \tag{93}$$

We define the dynamic signal-to-noise ratio (DSNR) as

$$\text{DSNR} = \frac{G_{\bar{y}}}{\sigma_w}. \tag{94}$$

Let $\eta_{\text{OSNR}} = I_{\text{avg}}/\sigma_w$ denote the OSNR constraint and $\eta_{\text{DSNR}} = D/\sigma_w$ denote the DSNR constraint, we have

$$\frac{\sigma_x}{\sigma_w} \leq \frac{\eta_{\text{OSNR}}}{O_{\bar{y}}/\sigma}, \tag{95}$$

$$\frac{\sigma_x}{\sigma_w} \leq \frac{\eta_{\text{DSNR}}}{G_{\bar{y}}/\sigma}. \tag{96}$$

Thus, the maximum σ_x/σ_w value can be obtained as

$$\frac{\sigma_x}{\sigma_w} = \tag{97}$$
$$\min\left(\frac{\eta_{\text{OSNR}}}{\phi(2\gamma\varsigma) - \phi\left(2\gamma(1-\varsigma)\right) - 2\gamma\varsigma\Phi\left(-2\gamma\varsigma\right) + 2\gamma(1-\varsigma)\Phi\left(-2\gamma(1-\varsigma)\right) + 2\gamma\varsigma}, \frac{\eta_{\text{DSNR}}}{2\gamma}\right).$$

by substituting (91) and (93) into the right-hand side of (95) and (96), respectively. The ratio $\eta_{\text{DSNR}}/\eta_{\text{OSNR}} = D/I_{\text{avg}}$ is determined by specific system requirements.

5.2.1 AWGN channel

For AWGN channel, recall from Equation (49), The received data on the kth subcarrier can be expressed as

$$R_k = \bar{X}_k + W_k = \alpha X_k + D_k + W_k, \quad k \in \mathcal{K}_d. \tag{98}$$

The signal-to-noise-and-distortion ratio (SNDR) for the kth subcarrier is given by

$$\begin{aligned} \mathrm{SNDR}_k &= \frac{\alpha^2 E\{|X_k|^2\}}{E\{|D_k|^2\} + E\{|W_k|^2\}} \\ &= \frac{\alpha^2 P_{X,k}}{P_{D,K} + \sigma_w^2} \\ &= \frac{1}{\mathrm{SDR}_k^{-1} + \sigma_w^2 \cdot \frac{1}{\alpha^2 P_{X,k}}}. \end{aligned} \tag{99}$$

In this dissertation, we assume the power is equally distributed on all data-carrying subcarriers,

$$P_{X,k} = \frac{N\sigma_x^2}{|\mathcal{K}_d|}, \tag{100}$$

then Equation (99) is reduced to

$$\mathrm{SNDR}_k = \frac{1}{\mathrm{SDR}_k^{-1} + \frac{\sigma_w^2}{\sigma_x^2} \cdot \frac{|\mathcal{K}_d|}{N\alpha^2}}. \tag{101}$$

By substituting Equation (97) into (163), we obtain the reciprocal of SNDR at the kth subcarrier:

$$\begin{aligned} &(\mathrm{SNDR}_k)^{-1} = (\mathrm{SDR}_k)^{-1} + \frac{|\mathcal{K}_d|}{N\alpha^2} \\ &\cdot \max\left(\frac{\left(\phi(2\gamma\varsigma) - \phi\left(2\gamma(1-\varsigma)\right) - 2\gamma\varsigma\Phi\left(-2\gamma\varsigma\right) + 2\gamma(1-\varsigma)\Phi\left(-2\gamma(1-\varsigma)\right) + 2\gamma\varsigma\right)^2}{\eta_{\mathrm{OSNR}}^2}, \quad \frac{4\gamma^2}{\eta_{\mathrm{DSNR}}^2} \right). \end{aligned} \tag{102}$$

Therefore, the achievable data rate, as a function of clipping ratio γ, ς, η_{OSNR}, and η_{DSNR}, is given by

$$\mathcal{R}\left(\gamma, \varsigma, \eta_{\mathrm{OSNR}}, \eta_{\mathrm{DSNR}}\right) = \frac{1}{2N} \sum_{k \in \mathcal{K}_d} \log_2\left(1 + \mathrm{SNDR}_k\right) \frac{\mathrm{bits}}{\mathrm{Hz}}. \tag{103}$$

5.2.2 Frequency-selective channel

In the presence of frequency-selective channel, the received data on the kth subcarrier obey the following in the frequency-domain:

$$R_k = H_k \bar{X}_k + W_k = H_k(\alpha X_k + D_k) + W_k, \quad k \in \mathcal{K}_d. \tag{104}$$

From Equation (104), the SNDR is given by

$$\mathrm{SNDR}_k(H_k) = \frac{|H_k|^2\alpha^2 E\{|X_k|^2\}}{|H_k|^2 E\{|D_k|^2\} + E\{|W_k|^2\}} \tag{105}$$

$$= \frac{1}{\mathrm{SDR}_k^{-1} + \sigma_w^2 \cdot \frac{1}{|H_k|^2\alpha^2 P_{X,k}}}. \tag{106}$$

With the assumption of equal power distribution, we can obtain the 1/SNDR as

$$(\mathrm{SNDR}_k)^{-1} = (\mathrm{SDR}_k)^{-1} + \frac{|\mathcal{K}_d|}{N|H_k|^2\alpha^2} \tag{107}$$

$$\cdot \max\left(\frac{\left(\phi(2\gamma\varsigma) - \phi\left(2\gamma(1-\varsigma)\right) - 2\gamma\varsigma\Phi\left(-2\gamma\varsigma\right) + 2\gamma(1-\varsigma)\Phi\left(-2\gamma(1-\varsigma)\right) + 2\gamma\varsigma\right)^2}{\eta_{\mathrm{OSNR}}^2}, \quad \frac{4\gamma^2}{\eta_{\mathrm{DSNR}}^2} \right).$$

The achievable data rate, in the presence of frequency-selective channel, is given by

$$\mathcal{R}\left(\gamma, \varsigma, \eta_{\mathrm{OSNR}}, \eta_{\mathrm{DSNR}}, \mathbf{H}\right) = \frac{1}{2N} \sum_{k \in \mathcal{K}_d} \log_2\left(1 + \mathrm{SNDR}_k(H_k)\right) \frac{\text{bits}}{\text{subcarrier}}. \tag{108}$$

5.3 Numerical results

We now show achievable data rates of clipped OFDM signals under various average optical power and dynamic optical power constraints. The number of subcarriers was $N = 512$. For the frequency-selective channel, we consider the ceiling bounce channel model [47] given by

$$h(t) = H(0)\frac{6a^6}{(t+a)^7}u(t), \tag{109}$$

where $H(0)$ is the gain constant, $a = 12\sqrt{11/23}\mathcal{D}_{rms}$ and $u(t)$ is the unit step function. $\mathcal{D}_{rms}$ denotes the rms delay. We chose the rms delay spread $\mathcal{D}_{rms} = 10\,\mathrm{ns}$ and sampling frequency 100 MHz. The normalized frequency response for each subcarrier is shown in Figure 17.

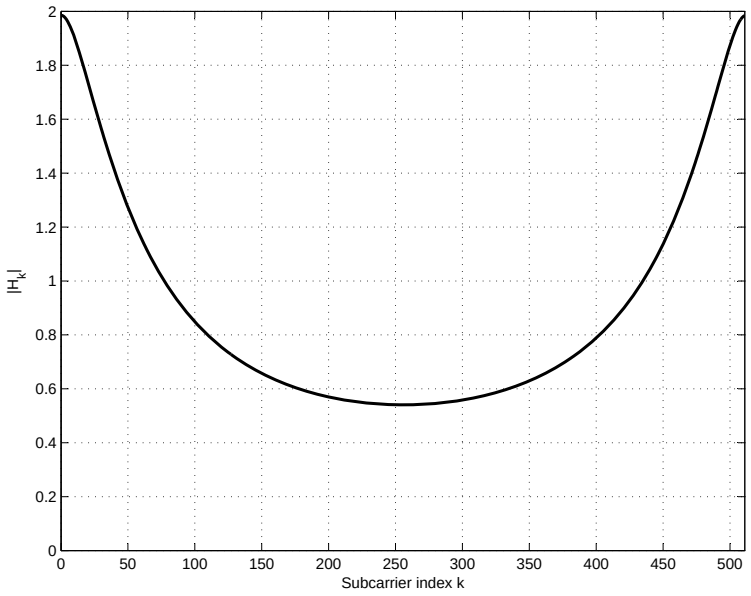

Figure 17: Normalized frequency response for each subcarrier (rms delay spread $\mathcal{D}_{rms} = 10$ ns, 100 MHz sampling rate).

As examples, we chose $\eta_{\mathrm{OSNR}} = 20\,\mathrm{dB}$, $\eta_{\mathrm{DSNR}} = 32\,\mathrm{dB}$. Figures 20 and 21 show the achievable data rate as a function of the clipping ratio and the biasing ratio for DCO-OFDM and ACO-OFDM, respectively. We see that for given η_{OSNR} and η_{DSNR} values, a pair of optimum clipping ratio $\gamma^{\ddagger}$ and optimum biasing ratio $\varsigma^{\ddagger}$ exist that maximize the achievable data rate. It is worthwhile to point out that the optimum biasing ratio $\varsigma^{\ddagger}$ is different from $\varsigma^{\star}$ (recall that $\varsigma^{\star}$ minimizes the EVM). If the system is only subject to the dynamic power constraint, $\varsigma^{\ddagger}$ should be equal to $\varsigma^{\star}$. If the dominant constraint is the average power, $\varsigma^{\ddagger}$ should be less than or equal to $\varsigma^{\star}$ because reducing the biasing ratio can make the signal average power lower. The existence of optimum can be explained that the less the clipping ratio and biasing ratio, the lower the average optical power and dynamic optical power, but the more the distortion introduced. Therefore, there is trade-off between the average optical power, or dynamic optical power and the non-linear distortion. We can obtain the optimum clipping ratio and

biasing ratio for given $\eta_{\mathrm{OSNR}}, \eta_{\mathrm{DSNR}}$ by

$$(\gamma^{\ddagger}, \varsigma^{\ddagger}) = \underset{(\gamma,\varsigma)}{\operatorname{argmax}} \quad \mathcal{R}|_{\eta_{\mathrm{OSNR}},\eta_{\mathrm{DSNR}}} \tag{110}$$

Figure 18 (a) shows the optimal clipping ratio as a function of η_{OSNR} for DCO-OFDM. Figure 18 (b) shows the optimum biasing ratio as a function of η_{OSNR} for DCO-OFDM. Similar plots are shown as Figure 19 (a), (b) for ACO-OFDM. In all cases, η_{OSNR} varied from 0 to 25 dB in step size of 1 dB, $\eta_{\mathrm{DSNR}}/\eta_{\mathrm{OSNR}} = 18$ dB, and the channel was AWGN. The main observation is, with a lower average optical power constraint, the clipping ratio and the biasing ratio can be increased to achieve higher data rates. Intuitively, when η_{OSNR} is large, the channel noise has little effect and the nonlinear distortion dominates.

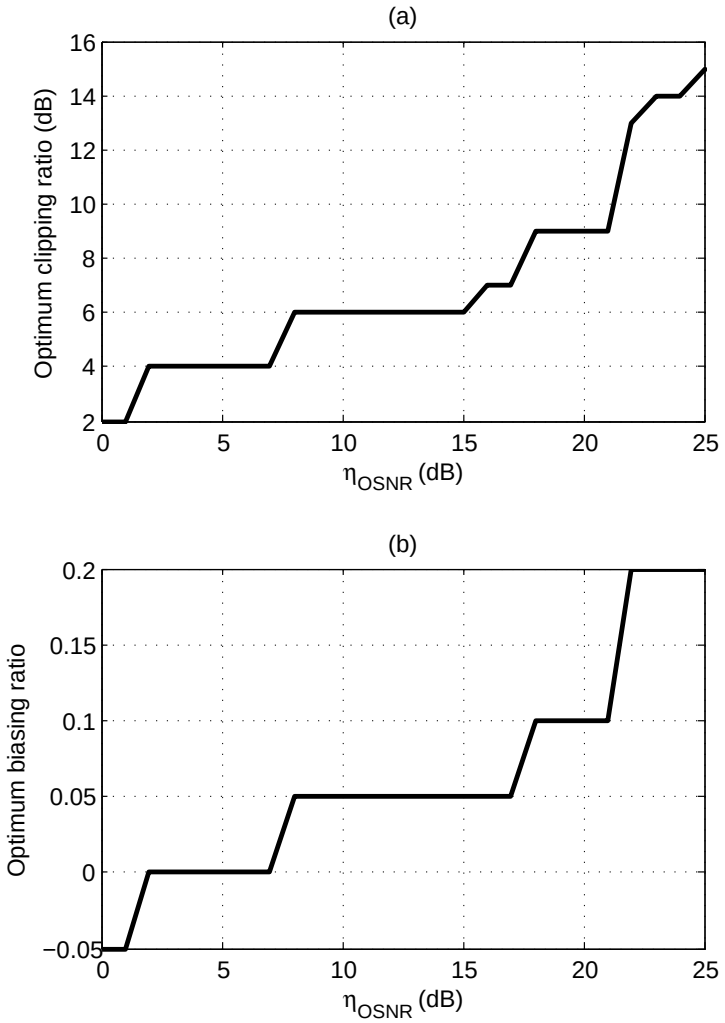

Figure 18: Optimal clipping ratio and biasing ratio of DCO-OFDM for $\eta_{\mathrm{OSNR}} = 0, 1, ..., 25$ dB (in step size of 1 dB), $\eta_{\mathrm{DSNR}}/\eta_{\mathrm{OSNR}} = 18$ dB, and AWGN channel.

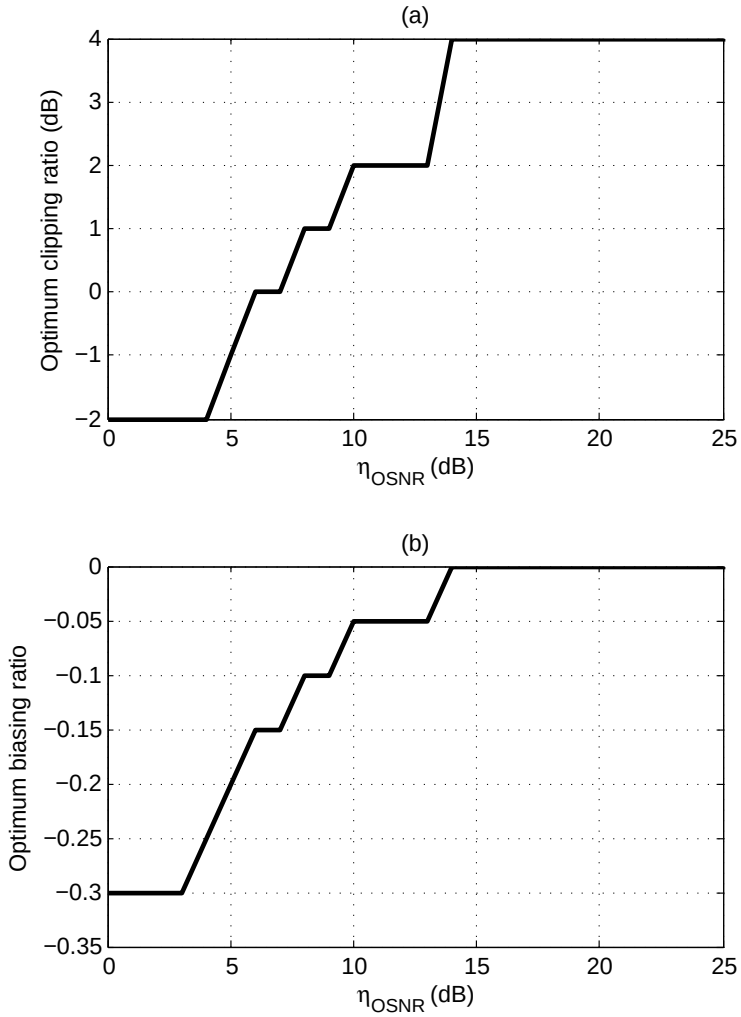

Figure 19: Optimal clipping ratio and biasing ratio of ACO-OFDM for $\eta_{\mathrm{OSNR}} = 0, 1, ..., 25$ dB (in step size of 1 dB), $\eta_{\mathrm{DSNR}}/\eta_{\mathrm{OSNR}} = 18$ dB, and AWGN channel.

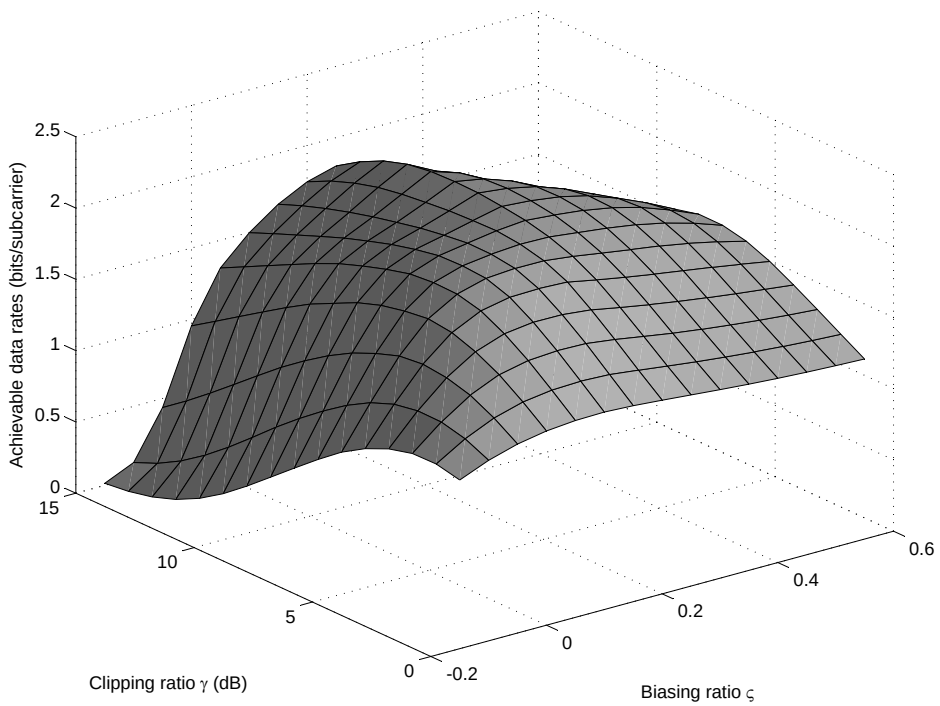

Figure 20: Achievable data rate as a function of the clipping ratio and the biasing ratio for DCO-OFDM with $\eta_{\mathrm{OSNR}} = 20$ dB, $\eta_{\mathrm{DSNR}} = 32$ dB.

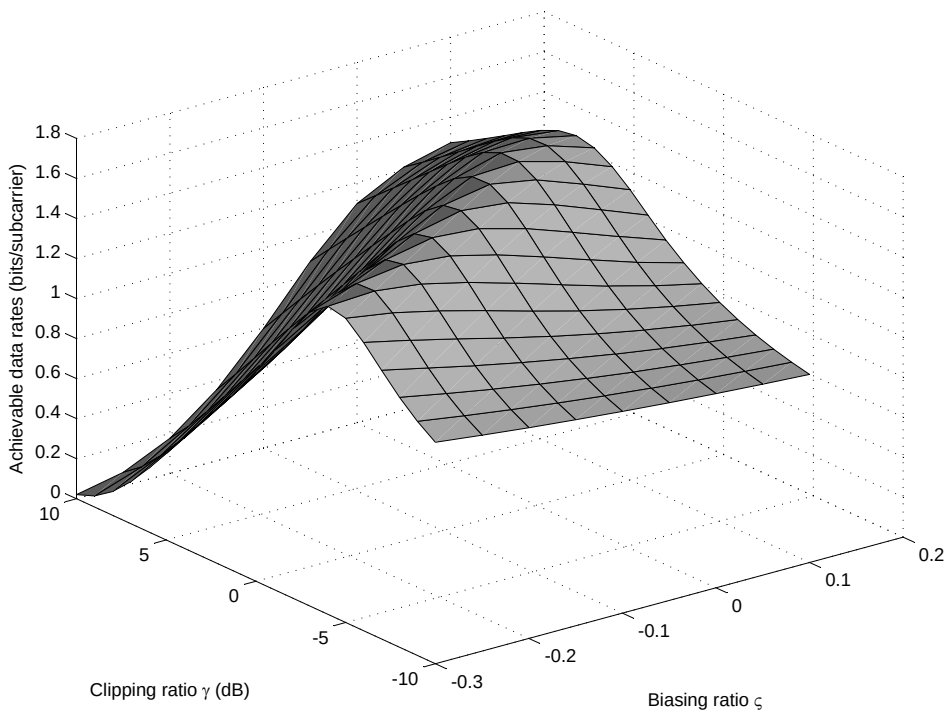

Figure 21: Achievable data rate as a function of the clipping ratio and the biasing ratio for ACO-OFDM with $\eta_{\mathrm{OSNR}} = 20$ dB, $\eta_{\mathrm{DSNR}} = 32$ dB.

Next, we chose the ratio $\eta_{\mathrm{DSNR}}/\eta_{\mathrm{OSNR}}$ from 6 dB and 12 dB. For each pair of η_{OSNR} and η_{DSNR}, we can calculate the optimum clipping ratio $\gamma^{\ddagger}$ and biasing ratio $\varsigma^{\ddagger}$ according to Equation (110) and the corresponding achievable data rates. Figures 22 shows the achievable data rates with optimal clipping ratio and biasing ratio for the case $\eta_{\mathrm{DSNR}}/\eta_{\mathrm{OSNR}} = 6$ dB and 12 dB. We observe that the performance of ACO-OFDM and DCO-OFDM depends on the specific optical power constraints scenario. In general, DCO-OFDM outperforms ACO-OFDM for all the cases. With the increase of the ratio $\eta_{\mathrm{DSNR}}/\eta_{\mathrm{OSNR}}$, the average optical power becomes the dominant constraint. The ACO-OFDM moves closer to the DCO-OFDM.

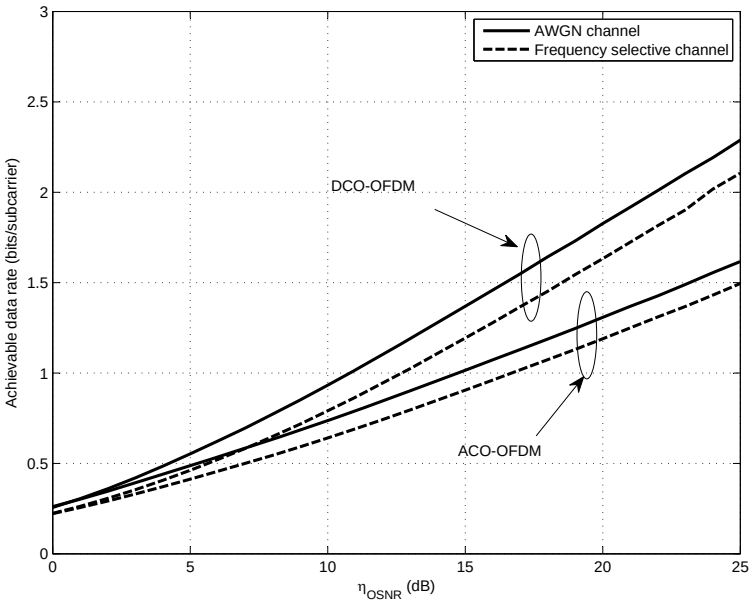

Figure 22: Achievable data rate with optimal clipping ratio and optimal biasing ratio for $\eta_{\mathrm{OSNR}} = 0, 1, ..., 25$ dB (in step size of 1 dB), and $\eta_{\mathrm{DSNR}}/\eta_{\mathrm{OSNR}} = 6$, 12 dB.

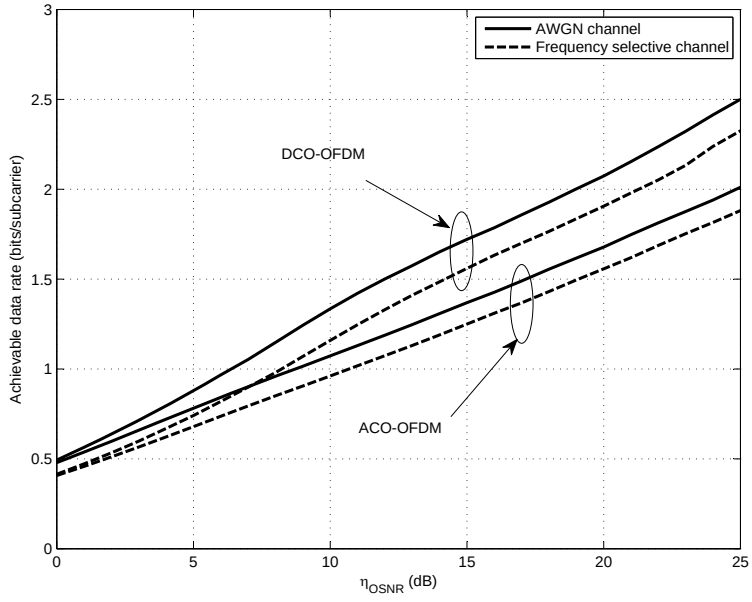

Figure 23: Achievable data rate with optimal clipping ratio and biasing ratio for $\eta_{\mathrm{OSNR}} = 0, 1, ..., 25$ dB (in step size of 1 dB), and $\eta_{\mathrm{DSNR}}/\eta_{\mathrm{OSNR}} = 12$ dB.

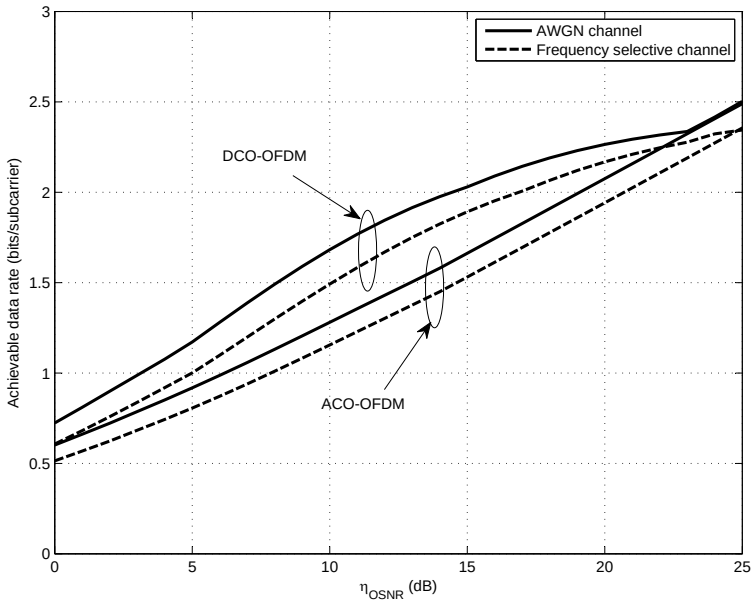

Figure 24: Achievable data rate with optimal clipping ratio and biasing ratio for $\eta_{\text{OSNR}} = 0, 1, ..., 25$ dB (in step size of 1 dB), and no η_{DSNR} constraint.

As seen in Figure 24, when there is no DSNR constraint and the OSNR constraint is large, the DCO-OFDM curve closely matches the ACO-OFDM curve. This is in contrast to the performance curves in Figures 22 and 23. The reason for the curve coincidence in Figure 24 is twofold. First, we have already discussed that the performance difference between DCO-OFDM and ACO-OFDM is less when the OSNR constraint dominates, which is the case for Figure 24. Second, the suddenness of the convergence of the two curves can be explained by the fact that with only OSNR constraint, there will be more flexibility in the signal optimization to adjust the clipping ratio and biasing ratio to achieve the best performance. That means that the achievable data rates in the middle-OSNR region (5–22 dB) are improved significantly compared with Figures 22 and 23. However, for high-OSNR region (greater than 22 dB), since the nonlinear distortion is negligible, the improvement becomes less pronounced compared to Figures 22 and 23. Therefore, the transition from the

middle-OSNR region to the high-OSNR region will become sharper with only an OSNR constraint.

CHAPTER VI

ILLUMINATION-TO-COMMUNICATION EFFICIENCY (ICE) ANALYSIS IN VLC-OFDM

Visible light communication (VLC) systems can provide illumination and communication simultaneously via light emitting diodes (LEDs). Orthogonal frequency division multiplexing (OFDM) waveforms transmitted in a VLC system will have high peak-to-average power ratios (PAPRs). Since the transmitting LED is dynamic-range limited, peaks of the OFDM waveform can be clipped causing signal degradation. This same phenomenon also occurs in RF communication system, although in RF systems it is straightforward to quantify the performance in terms of RF power conversion efficiency. Results on quantifying VLC performance are scarce. Specifically, because VLC differs from RF communication in system constraint, baseband signal format, and nonlinearity characteristic of the transmitter, it is not obvious how PAPR is related to illumination-to-communication conversion efficiency in VLC. In this chapter, we will attempt to quantify the illumination-to-communication conversion efficiency and clarify how PAPR is related to efficiency in VLC systems. We also present a method to improve the efficiency of VLC OFDM systems.

6.1 Introduction

Orthogonal frequency division multiplexing (OFDM) has a well-known disadvantage of high peak-to-average power ratio (PAPR). In the transmitter, to avoid nonlinear distortions, an OFDM signal has to be backed-off to the linear region of a power amplifier (PA), suppressing DC-to-RF power conversion efficiency of the PA. PAPR is an important metric because it impacts directly the power efficiency of a radio

frequency (RF) communication system [59, 78]. A number of techniques have been proposed to reduce the PAPR of OFDM [42, 16, 22, 7, 18, 6, 74, 27], in order to improve the power efficiency in RF communication systems and to reduce the sensitivity to nonlinear system components.

A major constraint in a VLC system is not the electrical power consumption as in RF communication, but the average radiated optical power, which is determined by illumination level. Thus, instead of being concerned with the DC-to-RF power conversion efficiency, we are interested in the illumination-to-communication conversion efficiency. The high PAPR problem also exists in visible light OFDM systems because LEDs are dynamic range limited devices [29]. However, since VLC differs from RF communication in system constraint, baseband signal format, and nonlinearity characteristic of front-end devices, it is not obvious how the PAPR is related to the illumination-to-communication conversion efficiency.

The objectives of this chapter are three-fold: i) to define the illumination-to-communication conversion efficiency metric, ii) to clarify how PAPR is related to efficiency in a VLC system, iii) to investigate methods to improve the efficiency of visible light OFDM systems.

6.2 Review of power efficiency in RF OFDM system

In RF OFDM systems, the time-domain signal $x[n]$ is generated by applying inverse discrete Fourier transform to the frequency-domain signal:

$$x[n] = \frac{1}{\sqrt{N}} \sum_{k=0}^{N-1} X_k e^{j2\pi kn/N}, \quad 0 \leq k \leq N-1, \tag{111}$$

where N is number of subcarriers. It is well-known that the OFDM time-domain signal has high peak-to-average power ratio (PAPR) [17], which is defined as

$$\text{PAPR} = \frac{\max |x[n]|^2}{E[|x[n]|^2]}, \tag{112}$$

Power amplifiers (PAs) are peak power limited devices. Figure 25 shows the input-

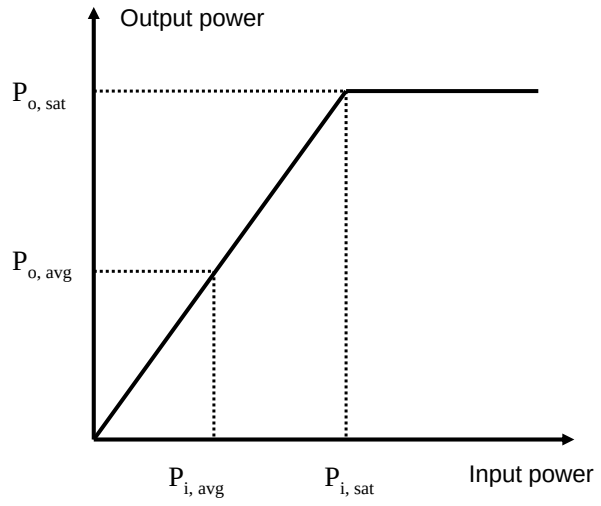

Figure 25: Input-output relationship of an ideal linear PA.

output characteristic of an ideal linear PA [78]. The DC-to-RF power conversion efficiency is

$$\zeta \triangleq \frac{P_{o,\text{avg}}}{P_{\text{dc}}}, \tag{113}$$

where $P_{o,\text{avg}}$ is the average output power, and P_{dc} is the power drawn from the DC source. We can linearly scale the peak power of the input signal to the saturation level $P_{i,\text{sat}}$ to deliver the maximum power efficiency. For a class A PA, $P_{\text{dc}} = 2P_{o,\text{sat}}$, where $P_{o,\text{sat}}$ denotes the output saturation power [78]. As such, the efficiency of a class A PA is

$$\zeta = \frac{P_{o,\text{avg}}}{P_{\text{dc}}} = \frac{P_{o,\text{avg}}}{2P_{o,\text{sat}}} = \frac{P_{i,\text{avg}}}{2P_{i,\text{sat}}} = \frac{0.5}{\text{PAPR}}. \tag{114}$$

6.3 Efficiency analysis in visible light OFDM System

In VLC, LEDs are the main source of non-linearity. With predistortion, the input-output characteristic of the LED can be linearized, but only within a limited interval $[I_L, I_H]$, where I_L denotes the turn on current/voltage and I_H denotes the saturation input current/voltage [29]. Figure 26 shows the input-output characteristic of an ideal LED. O_H denotes the maximum output optical power. The illumination level determines the average optical power, which is fixed to a value O_{avg}. Denote by I_{avg}

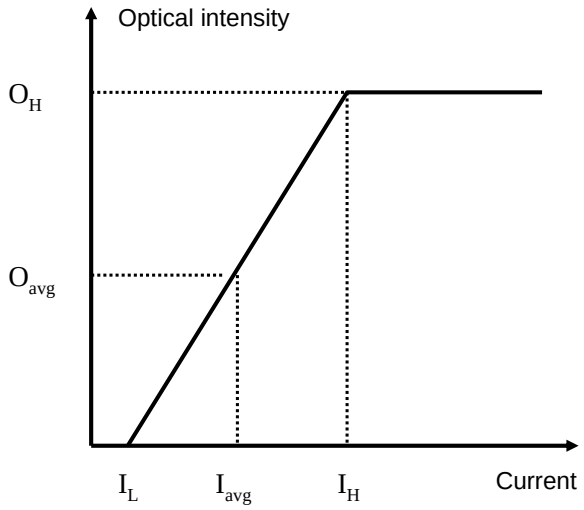

Figure 26: Ideal linear LED characteristic.

the input average voltage corresponding to O_{avg}. Thus, the input signal $y[n]$ must satisfy

$$E[y[n]] = I_{\text{avg}}. \tag{115}$$

The VLC constraint in (115) differs from the peak power constraint in RF systems. Accordingly the power conversion efficiency is not an appropriate metric for VLC systems. In VLC, considering the system constraint is the average optical power, the DC power consumption to RF power conversion efficiency defined in RF communication is not suitable any more. Instead, we define the illumination-to-communication conversion efficiency (ICE) in VLC as

$$\Gamma \triangleq \frac{D_o}{O_{\text{avg}}} = \frac{D_i}{I_{\text{avg}} - I_L}, \tag{116}$$

where $D_i = \sqrt{E[y^2[n]] - (E[y[n]])^2}$ denotes the standard deviation of the input electrical signal, and D_o denotes the corresponding standard deviation of the output optical intensity.

6.4 Linear scaling and biasing

The forward signal $y[n]$ is obtained from the OFDM signal $x[n]$ after both a linear scaling and a biasing operation such that

$$y[n] = \epsilon x[n] + B, \tag{117}$$

where ϵ and B are both real-valued. The resulting signal, $y[n]$, has a mean value B and a standard deviation $D_i = |\epsilon|\sigma_x$. We set $B = I_{\text{avg}}$. The standard deviation D_i can be maximized by selecting a scaling factor with the greatest absolute value $|\epsilon|$. To ensure $y[n]$ is within the dynamic range of LED, when ϵ is positive, we can obtain an ϵ with the greatest absolute value as

$$\epsilon^{(+)} = \min\left\{\frac{I_H - I_{\text{avg}}}{\max x[n]}, \frac{I_L - I_{\text{avg}}}{\min x[n]}\right\}. \tag{118}$$

When ϵ is negative, we can obtain an ϵ with the greatest absolute value as

$$\epsilon^{(-)} = \max\left\{\frac{I_H - I_{\text{avg}}}{\min x[n]}, \frac{I_L - I_{\text{avg}}}{\max x[n]}\right\}. \tag{119}$$

In summary, a ϵ with the maximum absolute value can be obtained as

$$\epsilon = \begin{cases} \epsilon^{(+)}, & \text{if} \quad |\epsilon^{(+)}| \geq |\epsilon^{(-)}| \\ \epsilon^{(-)}, & \text{if} \quad |\epsilon^{(+)}| < |\epsilon^{(-)}| \end{cases}. \tag{120}$$

Let us recall the upper peak-to-average power ratio of $x[n]$ as

$$\text{UPAPR} \triangleq \frac{(\max x[n])^2}{E[x^2[n]]}, \tag{121}$$

the lower peak-to-average power ratio of $x[n]$ as

$$\text{LPAPR} \triangleq \frac{(\min x[n])^2}{E[x^2[n]]}. \tag{122}$$

Define the brightness factor

$$\lambda \triangleq \frac{O_{\text{avg}}}{O_H} = \frac{I_{\text{avg}} - I_L}{I_H - I_L}, \tag{123}$$

where $\lambda \in [0, 1]$ theoretically. However, in practical scenario, λ has to be less than a value $\lambda_{\max}$, which is constrained by the maximum permissible DC current of LED. Thus, we can obtain the illumination-to-communication conversion efficiency as

$$\begin{aligned} \Gamma\{x[n]\} &= \frac{|\epsilon|\sigma_x}{I_{\text{avg}} - I_L} \qquad (124) \\ &= \frac{\sqrt{E[x^2[n]]}}{I_{\text{avg}} - I_L} \max\ \left\{\epsilon^{(+)},\ -\epsilon^{(-)}\right\} \\ &= \max\left\{ \min\left\{ \frac{1-\lambda}{\lambda} \frac{1}{\sqrt{\text{UPAPR}}}, \frac{1}{\sqrt{\text{LPAPR}}} \right\}, \min\left\{ \frac{1-\lambda}{\lambda} \frac{1}{\sqrt{\text{LPAPR}}}, \frac{1}{\sqrt{\text{UPAPR}}} \right\} \right\} \end{aligned}$$

We can observe that the efficiency depends on three factors: (i) illumination level and LED dynamic range; (ii) upper PAPR of OFDM signals; (iii) lower PAPR of OFDM signals.

Figure 27 is a plot of the mean illumination-to-communication conversion efficiency with varying brightness factors and numbers of subcarriers. Observe that the efficiency decreases with increasing illumination level. In Eq. (124), when λ tends to 0, the efficiency approaches $\max\left\{1/\sqrt{\text{LPAPR}},\ 1/\sqrt{\text{UPAPR}}\right\}$.

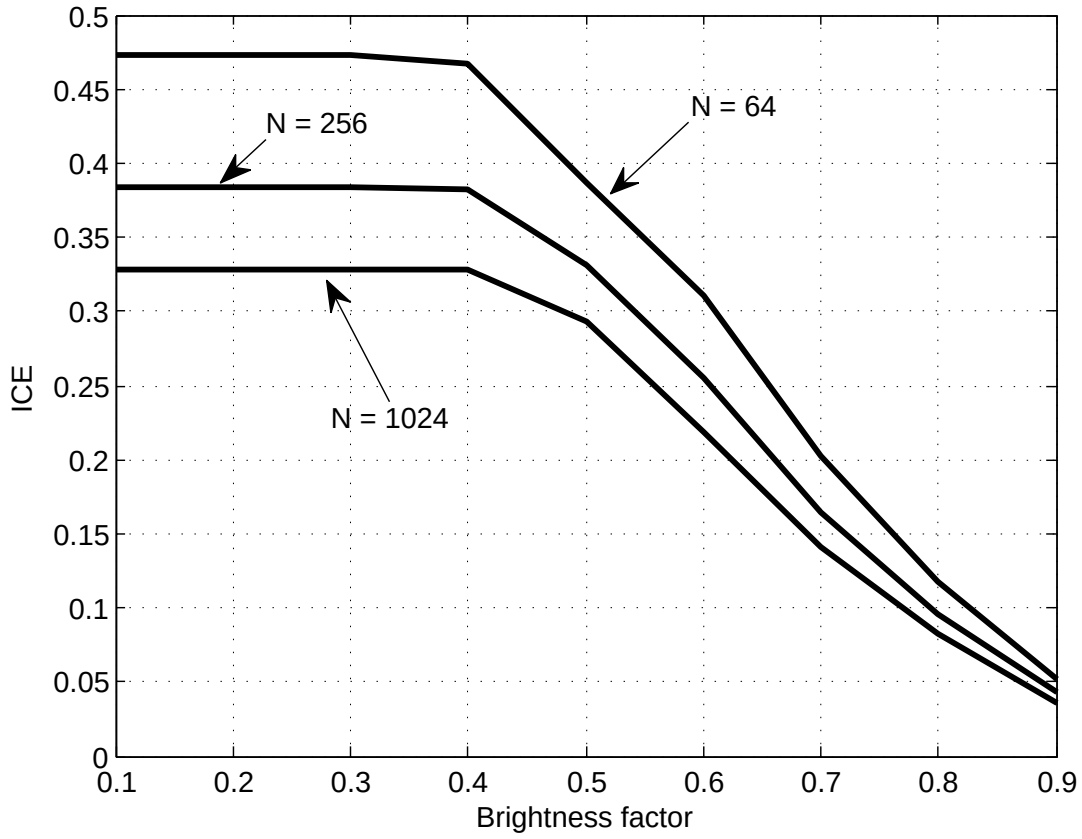

Figure 27: Illumination-to-communication conversion efficiency with varying brightness factors and numbers of subcarriers.

6.5 Efficiency improvement with selected mapping

In RF communication, DC-to-RF power conversion efficiency can be improved by reducing the PAPR. However, in VLC, the relationship between efficiency and PAPR is not as straightforward as that in RF. We are interested in investigating methods to improve the illumination-to-communication conversion efficiency. In this proposal, we consider the selected mapping (SLM) method [16].

In SLM, The assumption is that the same phase table $\{\vartheta_k^{(m)}\}$, $1 \leq k \leq N/2 - 1$, $1 \leq m \leq M$, where $\vartheta_k^{(1)} = 0$, $\forall\, 1 \leq k \leq N/2-1$, is available to both the transmitter and the receiver. We first rotate the phase of X_k as

$$X_k^{(m)} = X_k e^{j\vartheta_k^{(m)}},\ 1 \leq k \leq N/2 - 1, \tag{125}$$

and the corresponding time-domain signal can be obtained as

$$x^{(m)}[n] = \frac{2}{\sqrt{N}} \sum_{k=1}^{N/2-1} \left(\Re\left(X_k^{(m)}\right) \cos\left(\frac{2\pi kn}{N}\right) - \Im\left(X_k^{(m)}\right) \sin\left(\frac{2\pi kn}{N}\right) \right). \quad (126)$$

Instead of selecting the mapped signal $x^{(m)}[n]$ with the lowest PAPR [16], we select the $x^{(m)}[n]$ with the maximum illumination-to-communication conversion efficiency

$$m^* = \arg\max_{1 \le m \le M} \quad \Gamma\{x^{(m)}[n]\} \quad (127)$$

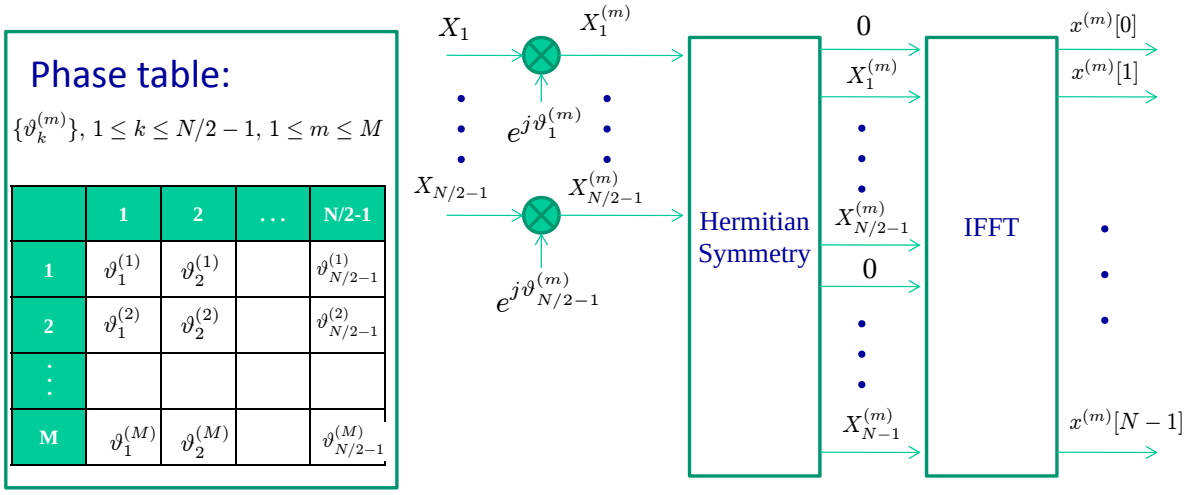

Figure 28: Selected mapping (SLM) method to improve the illumination-to-communication conversion efficiency (ICE) in VLC.

6.6 Numerical results

As an example, we generated the phase table randomly from the set $\{0, \pm\pi/2, \pi\}$ with equal probability, and $M = 8$ or $M = 64$. We chose QPSK modulation and generated 10000 DCO-OFDM symbols with $N = 64$ or $N = 256$. Figure 29 shows the illumination-to-communication conversion efficiency improvement with the selected mapping method. We can see that the efficiency can be improved more when N is small and λ is low.

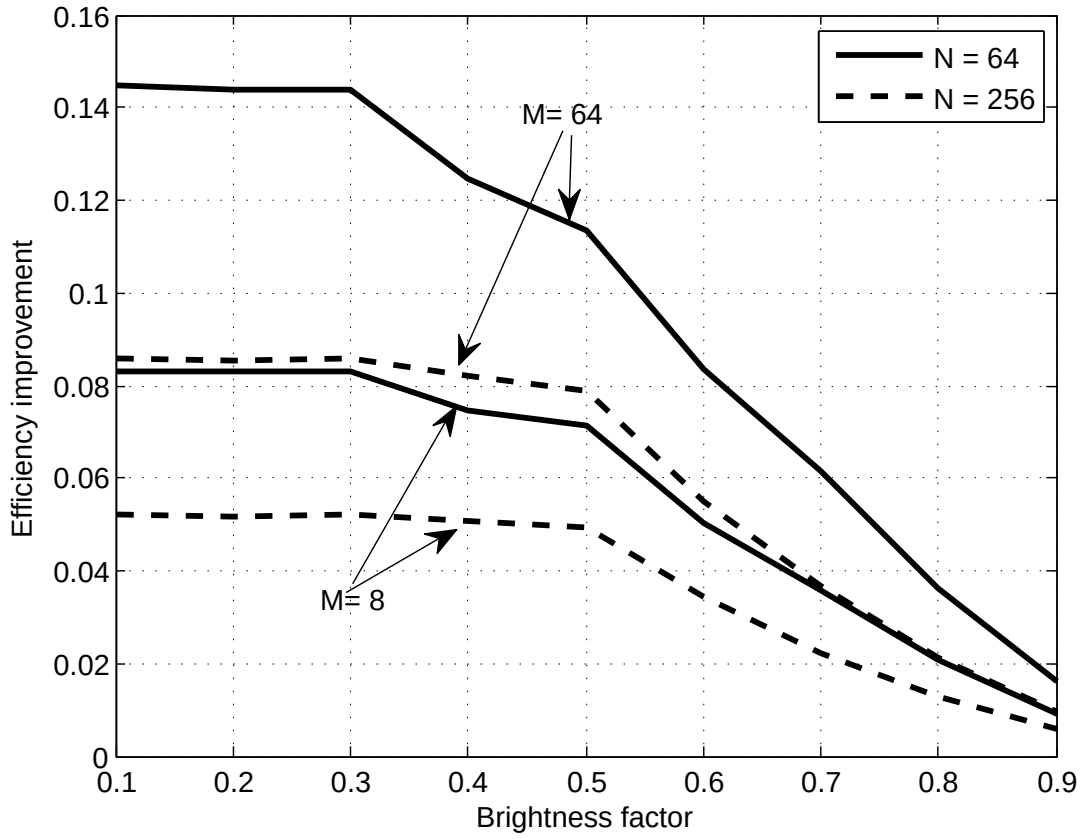

Figure 29: Illumination-to-communication conversion efficiency improvement with selected mapping method (10000 DCO-OFDM symbols, QPSK modulation).

6.7 Conclusion

In this chapter, we investigated the concept of illumination-to-communication conversion efficiency under the average optical power constraint in visible light OFDM systems. We discussed the relationship between efficiency and the positive PAPR, negative PAPR and the illumination coefficient. Finally, we proposed the SLM as a means of improving the illumination-to-communication conversion efficiency.

CHAPTER VII

BRIGHTNESS CONTROL IN DYNAMIC RANGE CONSTRAINED VLC-OFDM

VLC is dynamic range constrained due to the characteristics of LED. OFDM signals have to be either appropriately scaled or clipped to work with the dynamic range constraints. VLC has to support brightness control while transmitting information. Illumination requirements in turn place a constraint on the average amplitude of the OFDM signal. Designing an illumination compatible VLC-OFDM is still an open challenge. In this chapter, we will analyze the performance of dynamic range constrained visible light OFDM systems with brightness control. We will combine the two bipolar-to-unipolar models, namely, linear scaling & biasing model, and clipping & biasing model, with the biasing adjustments and pulse width modulation (PWM) schemes. The achievable data rates will be derived and compared.

7.1 Introduction

Applying OFDM in VLC are faced with two major challenges. First, OFDM is known for its disadvantage of high peak-to-average power ratio (PAPR) and thus is very sensitive to nonlinear distortions. The LED is the main source of nonlinearity in VLC. Although LEDs can be linearized by a predistorter [29], the dynamic range is limited by the turn-on current and maximum permissible alternating current. Second, VLC has to support brightness control while transmitting information. Illumination requirements in turn place a constraint on the average amplitude of the OFDM signal. Designing an illumination compatible VLC-OFDM is still an open challenge.

To make the OFDM signal work with the dynamic range constrained VLC system,

OFDM signal has to be either appropriately scaled or clipped. A linear scaling and biasing model has been proposed in [77, 76]. The scaling factor depends on upper PAPR and lower PAPR of OFDM signal, and biasing level is determined by illumination demand. However, the scaling and biasing method is too "conservative" in trying to avoid any distortion and thus not delivering sufficient signal power. Additionally, the joint distribution of upper PAPR and lower PAPR is also unknown, which prevents the theoretical analysis of achievable data rates. A distortion-based clipping and biasing model is used in [75]. The clipping ratio and biasing ratio are optimized given dynamic range and optical power constraints to maximize achievable data rates. The clipping effects on VLC-OFDM are also studied in [28, 69].

Brightness control is essential for the illumination function of VLC. Generally, there are two ways to control the brightness: (i) adjust the average forward voltage or current; (ii) change the duty cycle of pulse width modulation (PWM). For single carrier pulsed modulation, the standard IEEE 802.15.7 [63] has applied the above two ways to control the brightness for on-off keying (OOK) and variable pulse position modulation (VPPM). A multiple pulse position modulation is proposed in [51], which controls the brightness by changing the number of pulses in one symbol duration. Reference [21] studied the optical power distribution, eye diagrams, and bit error rates of the PWM-based position modulation (PPM). A brightness control scheme was proposed in [13] for overlapping PPM. Brightness control has also being investigated for the OFDM. In [57], PWM is combined with OFDM by sending the product of the OFDM and PWM waveforms. In reference [66], the authors adjusted the average optical power of asymmetrically clipped optical OFDM (ACO-OFDM) and studied the nonlinearity of LED. A reverse polarity OFDM was proposed in reference [33] to combine ACO-OFDM with PWM. In reference [71], the authors investigated the performance of M-QAM OFDM with PWM brightness control. To the best of our knowledge, however, only the references [66, 33] considered the dynamic range

constraints. Moreover comparison between the average forward current adjusting method and the PWM method is still lacking.

In this chapter, we will analyze the performance of dynamic range constrained visible light OFDM systems with various combinations of brightness control methods and bipolar-to-unipolar models. We will focus on DC biased optical OFDM (DCO-OFDM) [44]. Linear scaling & model and clipping & biasing model will be both considered. We will apply the biasing adjustment method and PWM duty cycle adjustment method to DCO-OFDM and compare achievable data rates.

7.2 Bipolar-to-unipolar conversion

A bipolar-to-unipolar block convert the zero-mean bipolar signal $x[n]$ to a unipolar signal $y[n]$, which has to be within the dynamic range of LED. In this chapter, we consider two bipolar-to-unipolar signal shaping models based on whether distortions are allowed, i.e., 1) linear scaling and biasing model; 2) clipping and biasing model.

7.2.1 Linear scaling and biasing

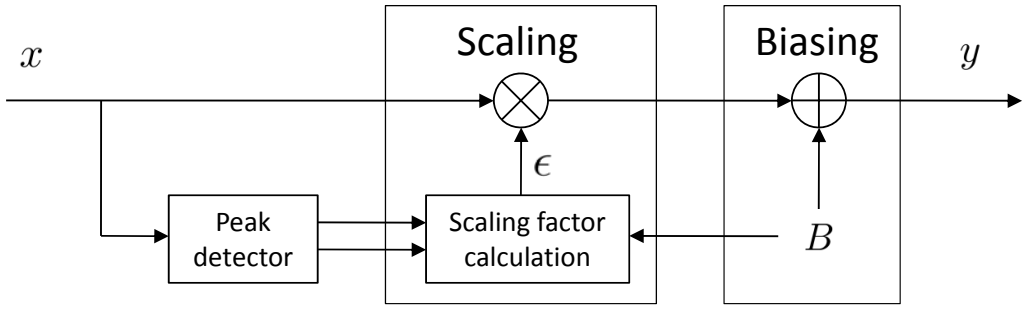

Figure 30: Linear scaling and biasing model.

In order to avoid non-linear distortion, the forward signal $y[n]$ can be obtained from the OFDM signal $x[n]$ after both a linear scaling and a biasing operation; i.e.,

$$y[n] = \epsilon x[n] + B, \quad 0 \leq n \leq N-1, \tag{128}$$

where ϵ and B are both real-valued. The resulting signal, $y[n]$, has a mean value B and a variance $\sigma_y^2 = E[\epsilon^2]\sigma_x^2$. Fig. 30 shows the linear scaling and biasing model. Assume ϵ is positive. The variance σ_y^2 can be maximized by selecting ϵ with the greatest value for each OFDM symbol. To ensure $y[n]$ is within the dynamic range of the LED, we can obtain an ϵ with the greatest value as

$$\epsilon = \min \left\{ \frac{I_H - B}{\max\limits_{0 \le n \le N-1} x[n]}, \frac{I_L - B}{\min\limits_{0 \le n \le N-1} x[n]} \right\} \tag{129}$$

Recall the definition of biasing ratio as

$$\zeta \triangleq \frac{B - I_L}{I_H - I_L}. \tag{130}$$

We can obtain the variance of $y[n]$ as

$$\begin{aligned} & \sigma_y^2 = \sigma_x^2 E[\epsilon^2] \\ = \; & D^2 E_{\mathcal{U},\mathcal{L}} \left[\min \left\{ \frac{(1-\zeta)^2}{\mathcal{U}}, \frac{\zeta^2}{\mathcal{L}} \right\} \right] \\ = \; & D^2 \int_0^\infty \int_0^\infty \min \left\{ \frac{(1-\zeta)^2}{r_u}, \frac{\zeta^2}{r_l} \right\} f_{\mathcal{L},\mathcal{U}}(r_l, r_u) dr_l dr_u, \end{aligned} \tag{131}$$

where $f_{\mathcal{L},\mathcal{U}}(r_l, r_u)$ is the joint PDF of UPAPR and LPAPR from Eq. (36). We can observe that the variance σ_y^2 depends on three factors: biasing ratio, upper PAPR of the OFDM signal and lower PAPR of the OFDM signal. Note that the dynamic range D is a fixed value, which is determined by characteristics of LEDs. The scaling factor ϵ varies symbol by symbol since $\mathcal{U}$ and $\mathcal{L}$ are both random variables. We treat ϵ as part of the channel and assume that ϵ for each symbol can be perfectly estimated at the receiver.

7.2.2 Clipping and biasing

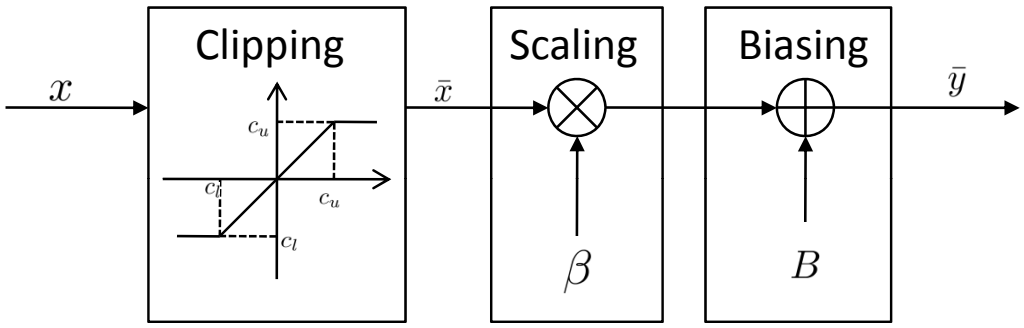

Figure 31: Clipping and biasing model.

The scaling and biasing method may be too "conservative" in trying to avoid any distortion and thus not delivering sufficient signal power. Fig. 31 shows the clipping and biasing model considered in this section. In order to reduce the dynamic range of $x[n]$, we can deliberately clip the $x[n]$, i.e.,

$$\bar{x}[n] = \begin{cases} c_u, & x[n] > c_u \\ x[n], & c_l \le x[n] \le c_u \\ c_l, & x[n] < c_l \end{cases} \tag{132}$$

where c_u denotes the upper clipping level, and c_l denotes the lower clipping level. To facilitate the analysis, we define the upper clipping ratio γ_u and the lower clipping ratio γ_l as

$$\gamma_u \triangleq \frac{c_u}{\sigma_x}, \quad \gamma_l \triangleq \frac{c_l}{\sigma_x}. \tag{133}$$

After clipping, the expectation of $\bar{x}[n]$ become

$$\begin{aligned} & E\{\bar{x}[n]\} \\ = & \int_{c_l}^{c_u} z\frac{1}{\sigma_x}\phi\left(\frac{z}{\sigma_x}\right)dz + c_u\int_{c_u}^{\infty}\frac{1}{\sigma_x}\phi\left(\frac{z}{\sigma_x}\right)dz \\ & + c_l\int_{-\infty}^{c_l}\frac{1}{\sigma}\phi\left(\frac{z}{\sigma_x}\right)dz - c_l \\ = & \sigma_x\Big(\phi(\gamma_l) - \phi\left(\gamma_u\right) + \gamma_l\Phi\left(\gamma_l\right) + \gamma_u\Phi\left(-\gamma_u\right)\Big). \end{aligned} \tag{134}$$

Next, we investigate how much distortions falling on each subcarrier of the OFDM signal. Based on the Bussgang's theorem [19], any nonlinear function of $x[n]$ can be decomposed into a scaled version of $x[n]$ plus a distortion term $d[n]$ that is uncorrelated with $x[n]$. For example, we can write

$$\bar{x}[n] = \alpha x[n] + d[n], \quad n = 0, \ldots, N-1. \tag{135}$$

Let $R_{xx}[q] = E\{x[n]x[n+q]\}$ denote the auto-correlation function of $x[n]$, and let $R_{\bar{x}x}[q] = E\{\bar{x}[n]x[n+q]\}$ denote the cross-correlation function between $\bar{x}[n]$ and $x[n]$ at lag q. For any given q, the correlation functions satisfy

$$R_{xd}[q] = 0, \;\; R_{\bar{x}x}[q] = \alpha R_{xx}[q]. \tag{136}$$

Thus, the scaling factor α can be calculated as a function of the upper clipping ratio γ_u and the lower clipping ratio γ_l:

$$\begin{aligned} \alpha &= \frac{R_{\bar{x}x}[0]}{R_{xx}[0]} = \frac{E\{\bar{x}[n]x[n]\}}{\sigma^2} \\ &= \frac{1}{\sigma_x^2}\int_{-\infty}^{\infty} \bar{x}x \cdot p(x)dx \\ &= \frac{1}{\sigma_x^2}\left(\int_{-\infty}^{c_l} \frac{c_l x}{\sigma_x}\phi\left(\frac{x}{\sigma_x}\right)dx + \int_{c_l}^{c_u} \frac{x^2}{\sigma_x}\phi\left(\frac{x}{\sigma_x}\right)dx \right. \\ &\quad \left. + \int_{c_u}^{\infty} \frac{c_u x}{\sigma_x}\phi\left(\frac{x}{\sigma_x}\right)dx\right) \\ &= \Phi(\gamma_u) - \Phi(\gamma_l). \end{aligned} \tag{137}$$

It is shown in [26] that the output auto-correlation function $R_{\bar{x}\bar{x}}[q]$ is related to the input auto-correlation function $R_{xx}[q]$ via

$$R_{\bar{x}\bar{x}}[q] = \sum_{\ell=0}^{\infty} \frac{b_\ell^2}{\ell!}\left[\frac{R_{xx}[q]}{\sigma_x^2}\right]^\ell, \tag{138}$$

where the coefficients

$$b_\ell = \frac{(-1)^\ell \sigma_x^{\ell-1}}{\sqrt{2\pi}}\int_{-\infty}^{\infty} \bar{x}\frac{d^\ell[\exp(-\frac{x^2}{2\sigma_x^2})]}{dx^\ell}dx. \tag{139}$$

From Eq. (135) and Eq. (139), we can obtain the coefficient b_ℓ as a function of the upper clipping ratio γ_u and the lower clipping ratio γ_l for three cases:

i) $\ell = 0$

$$b_\ell = \sigma_x \left(\phi(\gamma_l) - \phi\left(\gamma_u\right) - \gamma_l \Phi\left(\gamma_l\right) + \gamma_u \Phi\left(-\gamma_u\right)\right), \tag{140}$$

ii) $\ell = 1$

$$b_\ell = \sigma_x \left(\Phi\left(\gamma_u\right) - \Phi(\gamma_l)\right), \tag{141}$$

iii) $\ell > 1$

$$b_\ell = \frac{\sigma_x}{\sqrt{2\pi}} \left(e^{-\frac{\gamma_l^2}{2}} He_{(\ell-2)}\left(\gamma_l\right) - e^{-\frac{\gamma_u^2}{2}} He_{(\ell-2)}\left(\gamma_u\right)\right), \tag{142}$$

where $He_n(t) = (-1)^\ell \exp\left(\frac{t^2}{2}\right) \frac{d^\ell[\exp(-\frac{t^2}{2})]}{dt^\ell}$ is the probabilists' Hermite polynomials [5].

The input auto-correlation function $R_{xx}[q]$ can be obtained from taking IDFT of the input power spectrum density (PSD)

$$R_{xx}[q] = \text{IDFT}\{P_{X,k}\}_m, \quad q = 0, \ldots, N-1, \tag{143}$$

where $P_{X,k} = E[|X_k|^2]$ is the expected value of the power on the kth subcarrier before clipping. Then it is straightforward to calculate the output PSD by taking the DFT of the auto-correlation of the output signal:

$$P_{\bar{X},k} = \text{DFT}\{R_{\bar{x}\bar{x}}[q]\}_k, \quad k = 0, \ldots, N-1. \tag{144}$$

Taking the DFT of Equation (135), the data at the kth subcarrier are expressed as

$$\begin{aligned} \bar{X}_k &= \text{DFT}\{\alpha \cdot x[n]\}_k + \text{DFT}\{d[n]\}_k \\ &= \alpha \cdot X_k + D_k. \end{aligned} \tag{145}$$

Here, we assume that D_k is Gaussian distributed, which is the common assumption when N is large [60]. The SDR at the kth subcarrier is given by

$$\text{SDR}_k = \frac{E[|\alpha \cdot X_k|^2]}{E[|D_k|^2]} = \frac{\alpha^2 P_{X,k}}{P_{D,k}} = \frac{\alpha^2 P_{X,k}}{P_{\bar{X},k} - \alpha^2 P_{X,k}}, \tag{146}$$

where $P_{D,k} = E[|D_k|^2] = P_{\bar{X},k} - \alpha^2 P_{X,k}$ is the average power of the distortion on the kth subcarrier.

After clipping operation, the forward signal $\bar{y}[n]$ can be obtained from the clipped signal $\bar{x}[n]$ after linear scaling and a biasing as

$$\bar{y}[n] = \beta \bar{x}[n] + B, \quad 0 \leq n \leq N-1. \tag{147}$$

To ensure $\bar{y}[n]$ is within the dynamic range of the LED, we can obtain an β with the greatest value as

$$\beta = \min \left\{ \frac{I_H - B}{c_u}, \frac{I_L - B}{c_l} \right\} \tag{148}$$

Note that scaling does not affect the SDR on each subcarrier and the biasing only changes the DC component.

7.3 Brightness control

In this section, we will analyze the performance of VLC OFDM with or without clipping when brightness control is treated as a system constraint. To control the brightness of LED, we have to make the average input forward signal equal to I_{avg}, which corresponds to the desired emitted average optical intensity O_{avg}. Let us recall the definition of brightness factor

$$\lambda \triangleq \frac{O_{\text{avg}}}{O_H} = \frac{I_{\text{avg}} - I_L}{I_H - I_L}. \tag{149}$$

Without loss of generality, we only consider brightness factor in the range $0 \leq \lambda \leq 0.5$, because any forward signal $s[n]$ with brightness factor $\lambda > 0.5$ can be created from $y[n]$, which has brightness factor $1-\lambda < 0.5$ and is within the dynamic range $[I_L, I_H]$, by $s[n] = I_H + I_L - y[n]$.

We consider two schemes to implement brightness control for DCO-OFDM: (i) biasing adjustment; (ii) pulse width modulation. For each scheme, we discuss both "without clipping" and "with clipping" bipolar-to-unipolar models.

7.3.1 Biasing adjustment

7.3.1.1 Without clipping

According to Eq. (37), since the mean value of the scaled and biased signal $y[n]$ is equal to B, it is straightforward to set the biasing level equal to I_{avg} for each DCO-OFDM symbol; i.e., $B = I_{\text{avg}}$, $\zeta = \lambda$. Replacing ζ with λ in Eq. (131), we can obtain the variance of a scaled DCO-OFDM symbol as

$$\sigma_y^2 = D^2 E_{\mathcal{U},\mathcal{L}} \left[\min \left\{ \frac{(1-\lambda)^2}{\mathcal{U}}, \frac{\lambda^2}{\mathcal{L}} \right\} \right]. \tag{150}$$

Define the dynamic-range-to-noise power ratio

$$\text{DNR} \triangleq \frac{D^2}{\sigma_w^2}, \tag{151}$$

where σ_w^2 denotes variance of the additive white Gaussian noise (AWGN) $w[n]$. Thus, according to Eq. (131) , the signal to noise power ratio (SNR) for each scaled DCO-OFDM symbol can be obtained as

$$\text{SNR} \triangleq \frac{\sigma_y^2}{\sigma_w^2} = \text{DNR} \cdot E_{\mathcal{U},\mathcal{L}} \left[\min \left\{ \frac{(1-\lambda)^2}{\mathcal{U}}, \frac{\lambda^2}{\mathcal{L}} \right\} \right]. \tag{152}$$

Using the Shannon capacity formula and taking expectation with respect to $\mathcal{U}$ and $\mathcal{L}$, we can obtain the achievable ergodic rates as a function of DNR and λ as

$$\begin{aligned} & \mathcal{R}(\text{DNR}, \lambda) \\ = \; & \frac{1}{2} E_{\mathcal{U},\mathcal{L}} \left[\log_2 \left(1 + \text{DNR} \cdot \min \left\{ \frac{(1-\lambda)^2}{\mathcal{U}}, \frac{\lambda^2}{\mathcal{L}} \right\} \right) \right], \end{aligned} \tag{153}$$

where the 1/2 degradation is due to the Hermitian symmetry requirement for X_k in the DCO-OFDM system.

7.3.1.2 With clipping

According to Eq. (134), the mean value of the clipped and biased signal $\bar{y}[n]$ becomes

$$E\{\bar{y}[n]\} = \beta\sigma L(\gamma_l, \gamma_u) + B, \tag{154}$$

where $L(\gamma_l, \gamma_u) = \left(\phi(\gamma_l) - \phi(\gamma_u) + \gamma_l \Phi(\gamma_l) + \gamma_u \Phi(-\gamma_u) \right)$. Equating right hand side of (154) to I_{avg}, we can obtain the biasing level as

$$B = I_{\text{avg}} - \beta \sigma_x L(\gamma_l, \gamma_u). \tag{155}$$

Substituting (155) into (148), we obtain $\beta\sigma_x/D$

$$\begin{aligned} \beta\sigma_x/D = \cdot \min \Big\{ & \frac{1-\lambda}{\gamma_u} + \frac{\beta\sigma_x/D}{\gamma_u} L(\gamma_l, \gamma_u), \\ & \frac{-\lambda}{\gamma_l} + \frac{\beta\sigma_x/D}{\gamma_l} L(\gamma_l, \gamma_u) \Big\} \end{aligned} \tag{156}$$

If $\frac{1-\lambda}{\gamma_u} + \frac{\beta\sigma_x/D}{\gamma_u} L(\gamma_l, \gamma_u) < \frac{-\lambda}{\gamma_l} + \frac{\beta\sigma_x/D}{\gamma_l} L(\gamma_l, \gamma_u)$, we can solve $\beta\sigma_x/D$ as

$$\left(\frac{\beta\sigma_x}{D} \right)^{\dagger} = \frac{1-\lambda}{\gamma_u - L(\gamma_l, \gamma_u)}. \tag{157}$$

If $\frac{1-\lambda}{\gamma_u} + \frac{\beta\sigma_x/D}{\gamma_u} L(\gamma_l, \gamma_u) \geq \frac{-\lambda}{\gamma_l} + \frac{\beta\sigma_x/D}{\gamma_l} L(\gamma_l, \gamma_u)$, we can solve $\beta\sigma_x/D$ as

$$\left(\frac{\beta\sigma_x}{D} \right)^{\star} = \frac{-\lambda}{\gamma_l - L(\gamma_l, \gamma_u)}. \tag{158}$$

By choosing the smaller one between (157) and (158), We can obtain $\beta\sigma_x/D$ as a function of γ_l, γ_u, and λ

$$\begin{aligned} \beta\sigma_x/D &= J(\gamma_u, \gamma_l, \lambda) \\ &= \min \left\{ \frac{1-\lambda}{\gamma_u - L(\gamma_l, \gamma_u)}, \frac{-\lambda}{\gamma_l - L(\gamma_l, \gamma_u)} \right\} \end{aligned} \tag{159}$$

For AWGN channel, according to Eq. (145), the received data on the kth subcarrier can be expressed as

$$R_k = \beta \bar{X}_k + W_k = \beta\alpha X_k + \beta D_k + W_k, \quad 1 \leq k \leq N/2 - 1, \tag{160}$$

where $W_k = \text{DFT}\{w[n]\}_k$ denotes the noises on the kth subcarrier. The signal-to-noise-and-distortion power ratio (SNDR) for the kth subcarrier is given by

$$\begin{aligned} \text{SNDR}_k &= \frac{\beta^2\alpha^2 E\{|X_k|^2\}}{\beta^2 E\{|D_k|^2\} + E\{|W_k|^2\}} \\ &= \frac{\beta^2\alpha^2 P_{X,k}}{\beta^2 P_{D,K} + \sigma_N^2} \\ &= \frac{1}{\text{SDR}_k^{-1} + \sigma_w^2 \cdot \frac{1}{\beta^2\alpha^2 P_{X,k}}}. \end{aligned} \tag{161}$$

In this chapter, we assume the power is equally distributed on all data-carrying sub-carriers,

$$P_{X,k} = \frac{N\sigma_x^2}{N-2}, \tag{162}$$

then Equation (161) is reduced to

$$\begin{aligned} \mathrm{SNDR}_k &= \frac{1}{\mathrm{SDR}_k^{-1} + \frac{\sigma_w^2}{\beta^2\sigma_x^2} \cdot \frac{N-2}{N\alpha^2}} \\ &= \frac{1}{\mathrm{SDR}_k^{-1} + \mathrm{DNR}^{-1} J^{-2}(\gamma_u, \gamma_l, \lambda) \cdot \frac{N-2}{N\alpha^2}}. \end{aligned} \tag{163}$$

Using the Shannon capacity formula, the achievable data rate, as a function of DNR, λ, γ_u, γ_l, is given by

$$\bar{\mathcal{R}}\left(\mathrm{DNR}, \lambda, \gamma_u, \gamma_l\right) = \frac{1}{N} \sum_{k=1}^{N/2-1} \log_2\left(1 + \mathrm{SNDR}_k\right), \tag{164}$$

where DNR and λ are system constraints. The optimum upper and lower clipping ratios can found by

$$\{\gamma_u^*, \gamma_l^*\} = \arg\max_{\gamma_u, \gamma_l} \quad \bar{\mathcal{R}}\,|_{\mathrm{DNR},\lambda}. \tag{165}$$

7.3.2 Pulse width modulation

PWM is an efficient way to control the brightness of LED. A PWM signal with period N_{pwm} is expressed as

$$p[n] = \begin{cases} I_{\mathrm{pwm}}, & 0 \le n < N \\ 0, & N \le n < N_{\mathrm{pwm}} \end{cases}, \tag{166}$$

where N is the "on" duration and $N_{\mathrm{pwm}} - N$ is the "off" duration. I_{pwm} denotes the input forward current during the "on" interval. Let us define the PWM forward ratio

$$\mu \triangleq \frac{I_{\mathrm{pwm}} - I_L}{I_H - I_L}. \tag{167}$$

The output optical intensity can be adjusted by changing the duty cycle defined as $\rho \triangleq N/N_{\mathrm{pwm}}$. To generate the optical intensity with average power O_{avg}, the duty

cycle of PWM is chosen to be

$$\rho = \frac{I_{\text{avg}} - I_L}{I_{\text{pwm}} - I_L} = \frac{\lambda}{\mu}, \tag{168}$$

where $\rho \leq 1$, $\lambda \leq \mu$, and $I_{\text{pwm}} \geq I_{\text{avg}}$.

7.3.2.1 Without clipping

We propose to combine the OFDM signal $x[n]$ with PWM as

$$y[n] = \begin{cases} \epsilon x[n] + I_{\text{pwm}}, & 0 \leq n < N \\ 0, & N \leq n < N_{\text{pwm}} \end{cases}, \tag{169}$$

which can be seen as a DCO-OFDM symbol with biasing level $B = I_{\text{pwm}}$ followed by $N_{\text{pwm}} - N$ length "0" compensations. To avoid flicker, the PWM period T_{pwm} has to be less than $1/f_T$, where f_T denotes the frequency threshold, below which human may be aware of the flicker. Let $T_{\text{OFDM}} = 1/\Delta f$ denote the duration of one OFDM symbol, where Δf if the subcarrier frequency spacing. To make $T_{\text{pwm}} < 1/f_T$, the duty cycle has to satisfy

$$\rho > \frac{f_T}{\Delta f}. \tag{170}$$

which is very easy to be achieved since $\Delta f >> f_T$.

During the "on" interval, the biasing ratio is actually $\mu = \lambda/\rho$. By replacing λ with μ in Eq. (152), we can obtain the SNR for each scaled DCO-OFDM symbol during the "on" interval as

$$\text{SNR} = \text{DNR} \cdot E_{\mathcal{U},\mathcal{L}} \left[\min \left\{ \frac{(1 - \lambda/\rho)^2}{\mathcal{U}}, \frac{\lambda^2/\rho^2}{\mathcal{L}} \right\} \right]. \tag{171}$$

Since we do not transmit data in the "off" interval, the achievable ergodic rates can be obtained as

$$\mathcal{R}_{\text{pwm}}(\text{DNR}, \lambda, \rho) = \rho \cdot R(\text{DNR}, \lambda/\rho). \tag{172}$$

Given system constraints DNR and λ, we can obtain an optimum ρ^* that maximize the achievable ergodic rates as

$$\rho^* = \arg\max_{\rho} \quad \mathcal{R}_{\text{pwm}} \,|_{\text{DNR},\lambda}. \tag{173}$$

7.3.2.2 With clipping

If we allow distortion, we can combine the clipped OFDM signal $\bar{x}[n]$ from Eq. (132) with PWM as

$$\bar{y}[n] = \begin{cases} \beta\bar{x}[n] + I_{\text{pwm}} - \beta\sigma_x L(\gamma_l, \gamma_u), & 0 \le n < N \\ 0, & N \le n < N_{\text{pwm}} \end{cases}, \tag{174}$$

where the term $-\beta\sigma_x L(\gamma_l, \gamma_u)$ is used to cancel the deviation of mean value of $\bar{x}[n]$ caused by clipping, which is similar with Eq. (155). Then the β is chose by replacing λ with $\mu = \lambda/\rho$ in Eq. (159). Also, by replacing λ with $\mu = \lambda/\rho$ in Eq. (163), we can obtain the SNDR for each clipped DCO-OFDM symbol during the "on" interval as

$$\text{SNDR}_k = \frac{1}{\text{SDR}_k^{-1} + \text{DNR}^{-1} J^{-2}(\gamma_u, \gamma_l, \lambda/\rho) \cdot \frac{N-2}{N\alpha^2}} \tag{175}$$

Since we do not transmit data in the "off" interval, the achievable data rates can be obtained as

$$\bar{\mathcal{R}}_{\text{pwm}}\left(\text{DNR}, \lambda, \rho, \gamma_u, \gamma_l\right) = \rho \cdot \bar{\mathcal{R}}\left(\text{DNR}, \lambda/\rho, \gamma_u, \gamma_l\right) \tag{176}$$

Given system constraints DNR and λ, the optimum duty cycle, upper and lower clipping ratios can found by

$$\{\rho^*, \gamma_u^*, \gamma_l^*\} = \arg\max_{\rho, \gamma_u, \gamma_l} \quad \bar{\mathcal{R}}_{\text{pwm}} \,|_{\text{DNR},\lambda}. \tag{177}$$

7.3.3 Examples

As an example, suppose that we need to transmit five OFDM symbols with $N = 256$. We assume the brightness factor λ to be 0.25. Fig. 32 shows the input signals of LED

with four scenarios: i) biasing adjustment, without clipping; ii) biasing adjustment, with clipping, $\gamma_u = 1.5$, $\gamma_l = -0.5$; iii) PWM, without clipping, $\rho = 0.625$; iv) PWM, with clipping, $\rho = 0.78$, $\gamma_u = 1.5$, $\gamma_l = -0.5$.

- brightness factor $\lambda = 0.25$, $N = 256$
- biasing adjustment, without clipping
- biasing adjustment, with clipping, $\gamma_u = 1.5$, $\gamma_l = -0.5$
- PWM, without clipping, $\rho = 0.625$
- PWM, with clipping, $\rho = 0.78$, $\gamma_u = 1.5$, $\gamma_l = -0.5$

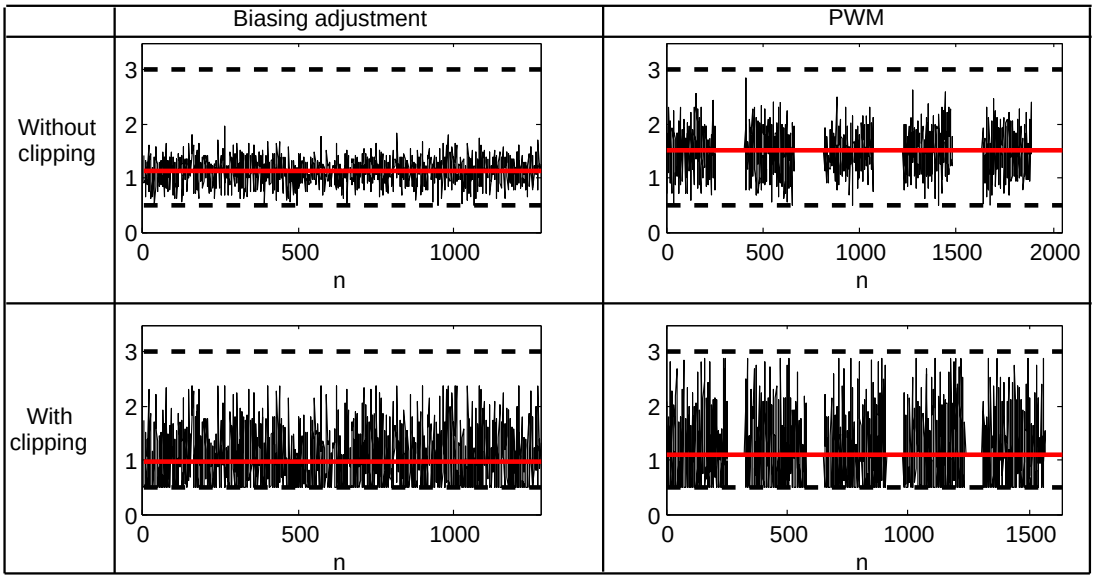

Figure 32: An example of transmitting five OFDM symbols with brightness control (Dash lines: dynamic range of LED; Solid line: biasing level).

7.4 Numerical results

In this section, we will compare achievable data rates of biasing adjustment method and PWM scheme under various illumination and bipolar-to-unipolar conversion scenarios.

First, let us look at the results of biasing adjustment methods. Fig. 33 shows the achievable data rates as a function of DNR with $\lambda = 0.25$. Four sets of bipolar-to-unipolar conversion parameters are selected. We can see that the performance depends on specific DNR. Fig. 34 shows the achievable data rates as a function of γ_u and γ_l with DNR = 14 dB, and $\lambda = 0.25$. This figure demonstrates that given DNR and illumination requirements λ, a pair of optimum upper and lower clipping ratios exist to maximize the data rates. Fig. 35 plots the optimum upper and lower clipping ratios γ_u^* and γ_l^* as a function of DNR with $\lambda = 0.2$ or 0.4. With increasing DNR, the nonlinear distortion caused by clipping become dominant. Thus, the absolute value of optimum upper and lower clipping ratios increase, which means less peaks are clipped. The lower peaks are always clipped more than upper peaks ($|\gamma_l^*| < |\gamma_u^*|$) because the λ is less than 0.5.

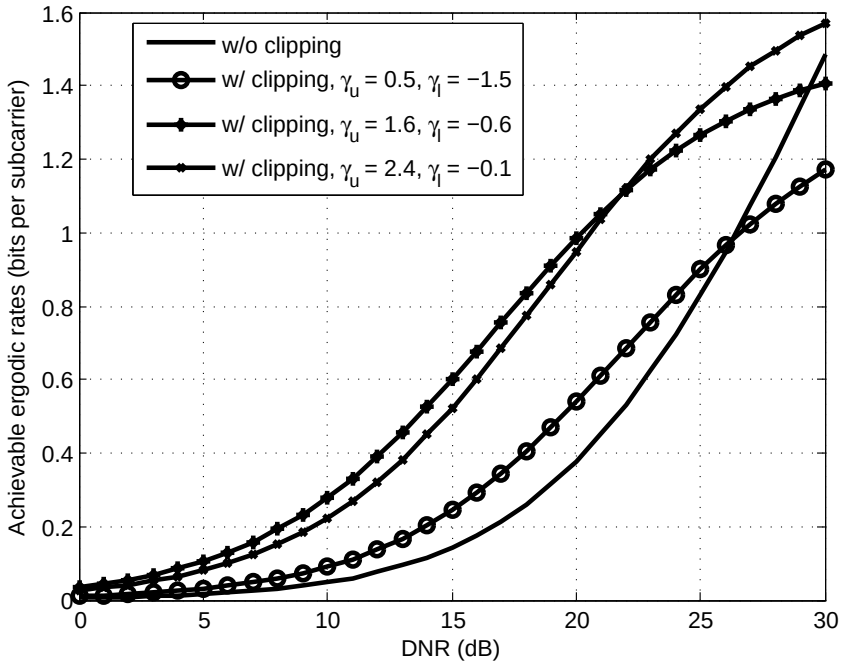

Figure 33: Achievable data rates as a function of DNR with biasing adjustment method and $\lambda = 0.25$.

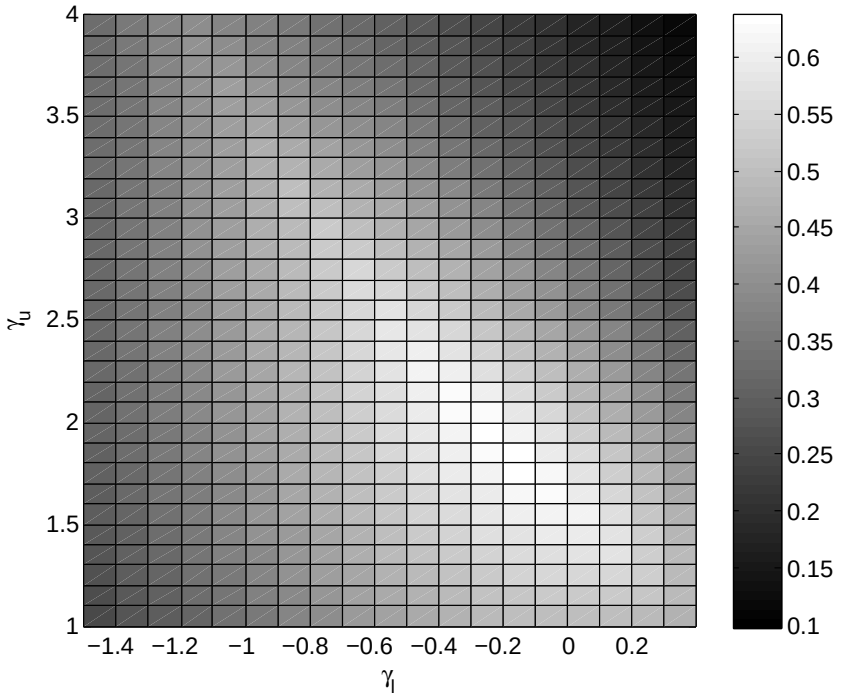

Figure 34: Achievable data rates as a function of γ_u and γ_l with biasing adjustment method, DNR = 14 dB, and $\lambda = 0.25$.

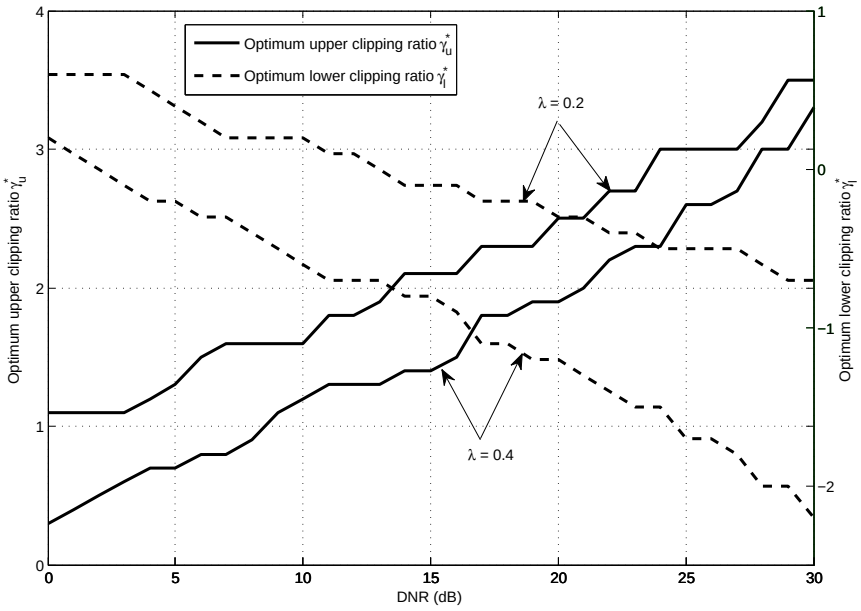

Figure 35: Optimum clipping ratios γ_u^* and γ_l^* as a function of DNR with biasing adjustment method, $\lambda = 0.2, 0.4$.

Next, let us look at PWM scheme. Fig. 36 shows the achievable data rates as a function of DNR with $\lambda = 0.2$. The PWM duty cycle ρ is chosen from 0.8, 0.67 and 0.57. Both "without clipping" and "with clipping" (clipping ratios are optimized given DNR and PWM duty cycle) cases are plotted. We can see that the performance depends on the specific λ and DNR. Fig. 39 plots the optimum PWM duty cycle ρ^* as a function of DNR with $\lambda = 0.25$ and 0.35. For the "without clipping" case, with increasing DNR, the optimum PWM duty cycle ρ^* approaches 1. For the "with clipping" case, the optimum PWM duty cycle ρ^* is equal to 1 for most of DNR. Note that the biasing adjustment method can be seen as a special case of PWM scheme with $\rho = 1$. Thus, $\rho^* = 1$ indicates that biasing adjustment method is preferred. Fig. 38 compare the achievable data rates of biasing adjustment method and PWM scheme for both "without clipping" and "with clipping" cases, $\lambda = 0.25$, or 0.35, where the duty cycle, upper and lower clipping ratios are all optimized. Generally, "with clipping" outperforms "without. Since biasing adjustment is a special case of the PWM method, PWM with optimum duty cycle will be always better than or the same with biasing adjustment. For the "without clipping" case, PWM scheme outperforms biasing adjustment method. When the brightness factor λ or DNR is larger, the difference become less noticeable. For the "with clipping" case, since the optimum PWM duty cycle ρ^* is equal to or nearly equal to 1, the achievable data rates of biasing adjustment and PWM are the same, which means that PWM is not preferred.

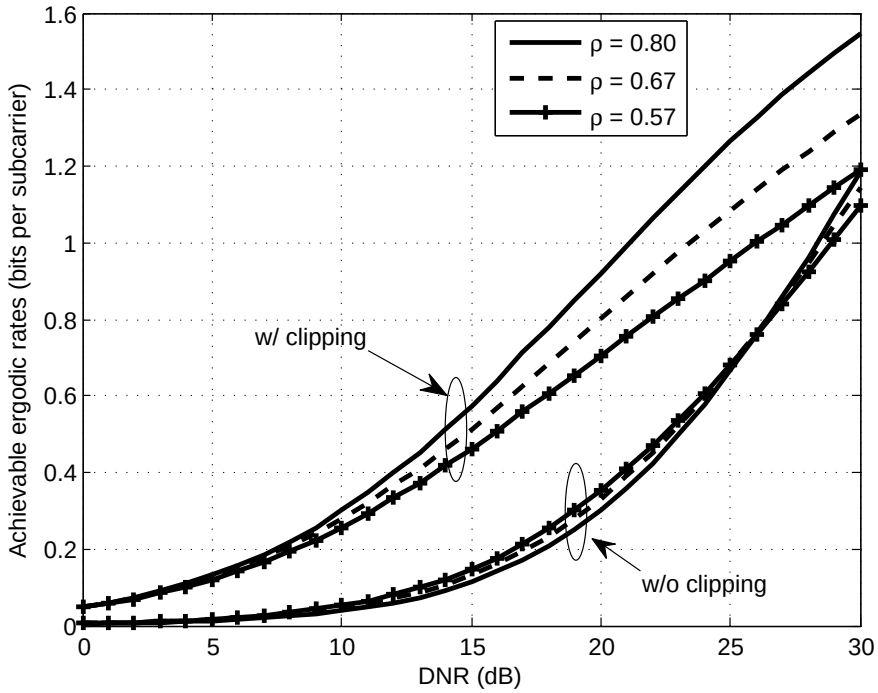

Figure 36: Achievable data rates as a function of DNR with PWM scheme and $\lambda = 0.2$.

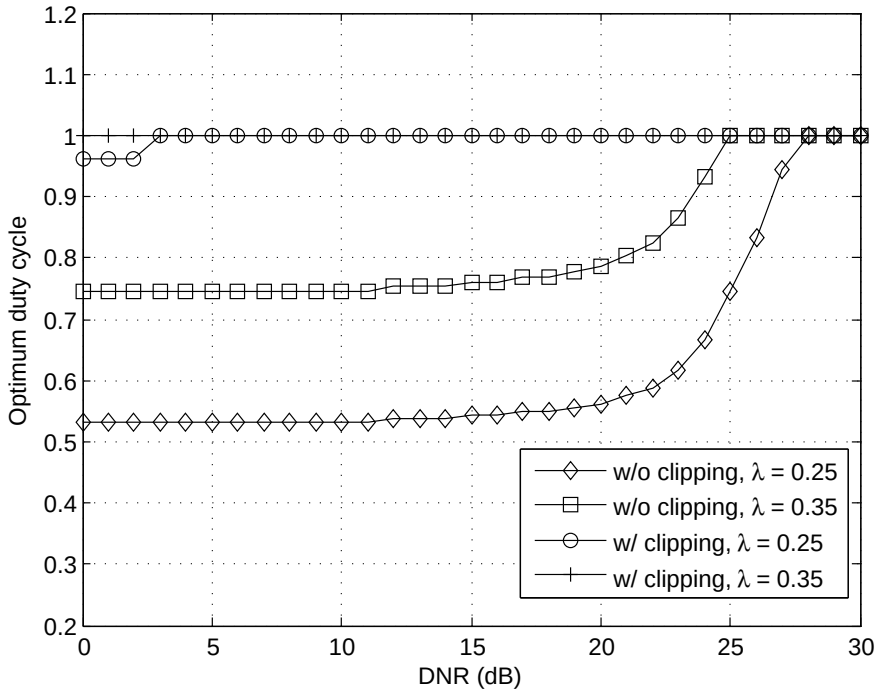

Figure 37: Optimum duty cycle as a function of DNR with $\lambda = 0.25$, and 0.35.

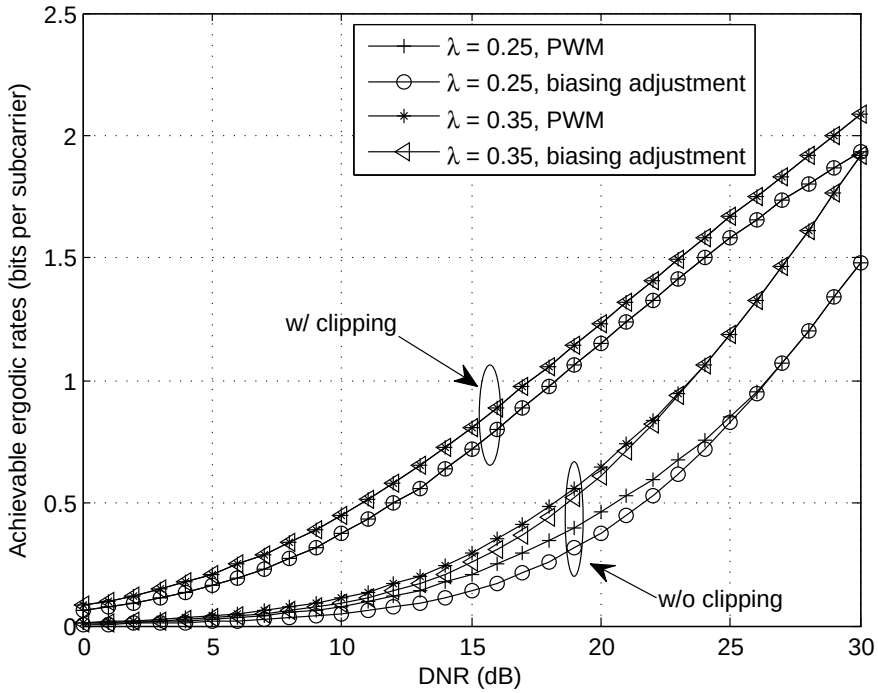

Figure 38: Achievable data rates as a function of DNR with optimum duty cycle and $\lambda = 0.25$, and 0.35.

7.5 Conclusion

In this chapter, we have proposed biasing adjustment and PWM schemes to control brightness in dynamic range constrained visible light OFDM systems. Both distortion-less and distortion-based bipolar-to-unipolar models are considered. We have optimized the clipping ratios for distortion-based model, and PWM duty cycle for PWM scheme. We have compared the achievable date rates with various combinations of brightness control methods and bipolar-to-unipolar models. Distortion-based case is generally better than distortion-less case. Biasing adjustment scheme is preferred for distortion-based case, while PWM with optimum duty cycle is favored for distortion-less case.

CHAPTER VIII

DYNAMIC RANGE CONSTRAINED CLIPPING IN VLC-OFDM CONSIDERING ILLUMINATION

Brightness control and flicker mitigation are two main challenges for the illumination function. OFDM waveforms have high peak-to-average power ratio, and will be clipped if its magnitude is beyond the dynamic range of LEDs. Clipping can cause the performance degradation of communication as well as illumination. In this paper, we will propose an iterative clipping method considering brightness control and flicker mitigation. We will investigate the performance in terms of error vector magnitude (EVM) as well as computational complexity. We will formulate the EVM minimization problem as a convex optimization problem to compare with the iterative clipping method.

8.1 Introduction

Brightness control and flicker mitigation are two main challenges for the illumination function in VLC. Generally, there are two ways to control the brightness: (i) adjust the average forward voltage or current; (ii) change the duty cycle of pulse width modulation (PWM). The standard IEEE 802.15.7 [63] has applied the above two ways to control the brightness for on-off keying (OOK) and variable pulse position modulation (VPPM). Flicker refers to the situation that the changing variations of the light intensity is noticeable to human eye. Run length limited (RLL) code is utilized in IEEE 802.15.7 [63] to mitigate flicker for OOK and VPPM.

OFDM is known for its disadvantage of high peak-to-average power ratio (PAPR) and thus is very sensitive to nonlinear distortions. The LED is the main source of

non-linearity in VLC. Although LEDs can be linearized by a predistorter [29], the dynamic range is limited by the turn-on voltage (TOV) and maximum permissible alternating current. The input signal outside this range will be clipped. Clipping will not only degrade the performance of communication, but also affect the brightness control and cause inter-symbol flicker.

In this chapter, we will propose an iterative clipping method considering brightness control and flicker mitigation. We will focus on DC biased optical OFDM (DCO-OFDM) [44]. We will investigate the performance in terms of error vector magnitude (EVM) as well as computational complexity. We will formulate the EVM minimization problem as a convex optimization problem to compare with the iterative clipping method.

8.2 Clipping effects on illumination

Since $y[n]$ is constrained by the dynamic range $[I_L, I_H]$, the constraints will in turn apply to $x[n]$ as $[I_L - B, I_H - B]$. Therefore, the maximum $x[n]$ is limited by $I_H - B$, and the minimum $x[n]$ is limited by $I_L - B$. The clipped signal $\bar{y}[n]$ in (132) can be written as

$$\bar{y}[n] = \bar{x}[n] + B, \tag{178}$$

where $\bar{x}[n]$ denotes the clipped version of $x[n]$ as

$$\bar{x}[n] = \begin{cases} I_H - B, & x[n] > I_H - B \\ x[n], & I_L - B \leq x[n] \leq I_H - B \\ I_L - B, & x[n] < I_L - B \end{cases} \tag{179}$$

Fig. 39 shows the histogram of the ratio $\mathcal{U}/\mathcal{L}$, from 50000 DCO-OFDM symbols. We chose QPSK modulation and $N = 256$. In the histogram, the maximum probability occurs around the ratio $\mathcal{U}/\mathcal{L} = 0$ dB since DCO-OFDM are symmetric distributed. We can observe that the ratio $\mathcal{U}/\mathcal{L}$ has a wide range, which means that the difference between UPAPR and LPAPR can be very large for some symbols.

Therefore, depending on the biasing ratio, UPAPR, and LPAPR, the clipping effects vary symbol by symbol.

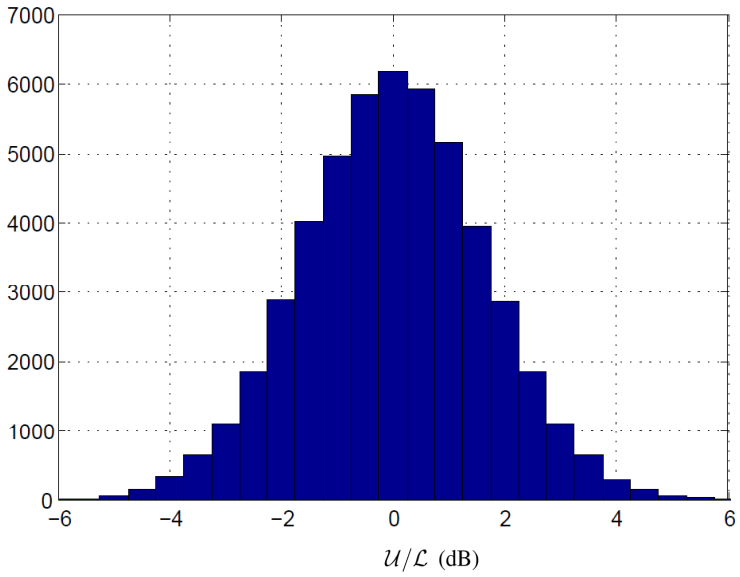

Figure 39: Histogram of the ratio $\mathcal{U}/\mathcal{L}$ from 50000 DCO-OFDM symbols (QPSK modulation, $N = 256$).

After clipping, the average value of the clipped signal $\bar{y}[n]$ will become

$$\frac{1}{N}\sum_{n=0}^{N-1}\bar{y}[n] = B + \frac{1}{N}\sum_{n=0}^{N-1}\bar{x}[n]. \tag{180}$$

where $\frac{1}{N}\sum_{n=0}^{N-1}\bar{x}[n]$, the average value of $\bar{x}[n]$, will not necessarily equal to zero. For example, when the LED is dimly lit, the biasing level B will be very close to I_L. Then the absolute value of upper clipping level $|I_H - B|$ will be much greater than the absolute value of lower clipping level $|I_L - B|$. Because $x[n]$ are symmetric distributed, the $x[n]$ will be clipped at the negative tails more than at the positive tails. In this case, the average value of $\bar{x}[n]$ will be greater than zero. Besides, because the $\mathcal{U}$ and $\mathcal{L}$ are random variables, the average value of $\bar{x}[n]$ will change symbol by symbol. In summary, the clipping can affect the illumination function in two ways. First, the emitted average optical power will deviate the desired value O_{des} because

the average value of the clipped symbol $\bar{y}[n]$ is not equal to B. Second, the clipping may cause LED to flicker since the average value of $\bar{y}[n]$ changes symbol by symbol.

8.3 Iterative clipping method

To avoid the deviation of the output optical power and flicker, an iterative clipping method is proposed in the paper. The objective is to generate a forward signal $\tilde{y}[n]$ as

$$\tilde{y}[n] = \tilde{x}[n] + B, \tag{181}$$

where $\tilde{x}[n]$ has a zero average value and a limited dynamic range as

$$\frac{1}{N}\sum_{n=0}^{N-1} \tilde{x}[n] = 0, \tag{182}$$

$$I_L - B \leq \tilde{x}[n] \leq I_H - B. \tag{183}$$

Let $\tilde{x}^{(i-1)}[n]$ denote the output signal from the $(i-1)$th iteration, which has a zero average value. In the ith iteration, we first compare max $\tilde{x}^{(i-1)}[n]$ with $I_H - B$, and compare min $\tilde{x}^{(i-1)}[n]$ with $I_L - B$.

If max $\tilde{x}^{(i-1)}[n] > I_H - B$ and min $\tilde{x}^{(i-1)}[n] < I_L - B$, we operate upper clipping and lower clipping separately as

$$\bar{x}^u[n] = \begin{cases} I_H - B, & \tilde{x}^{(i-1)}[n] > I_H - B \\ \tilde{x}^{(i-1)}[n], & \tilde{x}^{(i-1)}[n] \leq I_H - B \end{cases} \tag{184}$$

$$\bar{x}^l[n] = \begin{cases} I_L - B, & \tilde{x}^{(i-1)}[n] < I_L - B \\ \tilde{x}^{(i-1)}[n], & \tilde{x}^{(i-1)}[n] \geq I_L - B \end{cases} \tag{185}$$

Then we take FFT of both $\bar{x}^u[n]$ and $\bar{x}^l[n]$ to obtain the frequency-domain signal $\bar{X}_k^u$ and $\bar{X}_k^l$, respectively. We compare the distortions power $\bar{P}^u = \sum_{k=1}^{N/2-1} |\bar{X}_k^u - X_k|^2$ and $\bar{P}^l = \sum_{k=1}^{N/2-1} |\bar{X}_k^l - X_k|^2$, and obtain $\tilde{x}^{(i)}[n]$ as

$$\tilde{x}^{(i)}[n] = \begin{cases} \bar{x}^u[n], & \bar{P}^u < \bar{P}^l \\ \bar{x}^l[n], & \text{otherwise} \end{cases} \tag{186}$$

If $\max \tilde{x}^{(i-1)}[n] > I_H - B$, and $\min \tilde{x}^{(i-1)}[n] \geq I_L - B$, we only operate upper clipping and obtain $\tilde{x}^{(i)}[n]$ as $\tilde{x}^{(i)}[n] = \bar{x}^u[n]$.

If $\max \tilde{x}^{(i-1)}[n] \leq I_H - B$, and $\min \tilde{x}^{(i-1)}[n] < I_L - B$, we only operate lower clipping and obtain $\tilde{x}^{(i)}[n]$ as $\tilde{x}^{(i)}[n] = \bar{x}^l[n]$.

Second, we remove the DC component from $\tilde{x}^{(i)}[n]$ as

$$\tilde{x}^{(i)}[n] = \tilde{x}^{(i)}[n] - \frac{1}{N}\sum_{n=0}^{N-1} \tilde{x}^{(i)}[n]. \tag{187}$$

Third, examine whether $\tilde{x}^{(i)}[n]$ satisfies the dynamic range as

$$I_L - B \leq \tilde{x}^{(i)}[n] \leq I_H - B. \tag{188}$$

If it does not, go to the next iteration; otherwise, we obtain the desired signal $\tilde{x}[n] = \tilde{x}^{(i)}[n]$.

In practice, to facilitate the convergence of the iteration, the upper clipping level $I_H - B$ in (184) and lower clipping level $I_L - B$ in (185) are both multiplied by a scaling factor β which is very close to 1.

8.4 EVM minimization

EVM is a figure-of-merit for distortions. Let $\mathbf{X}^\dagger = [X_0^\dagger, X_1^\dagger, \ldots, X_{N-1}^\dagger]$ denote the N-length FFT of the modified time-domain symbol $\mathbf{x}^\dagger = [x^\dagger[0], x^\dagger[1], \ldots, x^\dagger(N-1)]$. EVM can be defined as

$$\xi(\mathbf{X}, \mathbf{X}^\dagger) \triangleq \sqrt{\frac{\sum_{k=1}^{N/2-1} |X_k - X_k^\dagger|^2}{\sum_{k=1}^{N/2-1} |X_k|^2}}, \tag{189}$$

Let us consider the setting

$$\hat{x}[n] = x[n] + c[n], \quad 0 \leq n \leq N-1, \tag{190}$$

where $c[n]$ is a distortion signal, and the resulting $\hat{x}[n]$ is expected to be zero average value and have a limited dynamic range as

$$\frac{1}{N}\sum_{n=0}^{N-1} \hat{x}[n] = 0, \tag{191}$$

$$I_L - B \leq \hat{x}[n] \leq I_H - B. \tag{192}$$

Clipping can produce one such $\hat{x}[n]$ signal, but there are other less straightforward algorithms that can generate other $\hat{x}[n]$ waveforms that also satisfy (191) and (192). In the frequency-domain,

$$\hat{X}_k = X_k + C_k. \tag{193}$$

Since $x[n]$, $c[n]$, and $\hat{x}[n]$ are all real-valued, X_k, C_k, and $\hat{X}_k$ all should satisfy the Hermitian symmetry condition (13). Therefore, $c[n]$ has the form

$$\begin{aligned} c[n] = \frac{2}{\sqrt{N}} \sum_{k=1}^{N/2-1} \Bigg(& \Re(C_k) \cos\left(\frac{2\pi kn}{N}\right) \\ & -\Im(C_k) \sin\left(\frac{2\pi kn}{N}\right) \Bigg) + \frac{1}{\sqrt{N}} C_0 + \frac{1}{\sqrt{N}} C_{N/2} \cos(\pi n). \end{aligned} \tag{194}$$

The condition (191) implies $\frac{1}{N}\sum_{n=0}^{N-1} c[n] = 0$. Hence, we have $C_0 = 0$.

We are interested in knowing the lowest possible EVM,

$$\xi = \sqrt{\frac{\sum_{k=1}^{N/2-1} |C_k|^2}{\sum_{k=1}^{N/2-1} |X_k|^2}}, \tag{195}$$

among all such $\hat{x}[n]$ waveforms.

We formulate the following convex optimization problem:

$$\begin{aligned} \text{minimize} \quad & \sum_{k=1}^{N/2-1} |C_k|^2 \\ \text{subject to} \quad & \hat{x}[n] \leq I_H - B \\ & \hat{x}[n] \geq I_L - B \\ & \hat{x}[n] = x[n] + \frac{2}{\sqrt{N}} \sum_{k=1}^{N/2-1} \Bigg(\Re(C_k) \cos\left(\frac{2\pi kn}{N}\right) \\ & \quad - \Im(C_k) \sin\left(\frac{2\pi kn}{N}\right) \Bigg) + \frac{1}{\sqrt{N}} C_{N/2} \cos(\pi n), \\ & 0 \leq n \leq N-1 \\ & C_{N/2} \in \mathbb{R} \end{aligned} \tag{196}$$

When the distortion of each OFDM symbol is minimized by the above convex optimization approach, the corresponding EVM of $\hat{x}[n]$ (which is proportional to $\sqrt{\sum_{k=1}^{N/2-1} |C_k|^2}$) serves as the lower bound for the given dynamic range. The convex optimization problem can be solved by the interior point method (IPM) as in [6, 52, 74]. In this work we used CVX, a package for specifying and solving convex programs [24, 40]. Fig. 40 compared the EVM between iterative clipping method and EVM minimization scheme with various power back-off and biasing ratios. In the simulation, we generated 1000 DCO-OFDM symbols with QPSK modulation and $N = 256$. The ς is assumed between 0 and 0.5. We can observe that the EVM has a minimum value at biasing ratio $\varsigma = 0.5$ regardless of the power back-off. When $\varsigma = 0.5$, we infer that $I_H - B = -(I_L - B)$, i.e., when the $x[n]$ waveform is symmetrically clipped at the negative and positive tails, the clipping error power is always less than that when the two tails are asymmetrically clipped. The proposed iterative clipping method has a no more than 4% gap compared with EVM minimization scheme. Fig. 40 can serve as a reference for choosing an appropriate biasing ratio and power back-off pair given the EVM threshold. For example, if the EVM threshold is 20%, for a power back-off $\Lambda = 15$ dB, the biasing ratio has to be chosen greater than 0.4 with iterative clipping method or 0.4 with EVM minimization scheme. However, the biasing adjustment method does not have the freedom to choose the biasing ratio since it is determined by the illumination requirement. The PWM method can increase or decrease the biasing ratio in the "on" interval while keeping the brightness unchanged by decreasing or increasing the duty cycle.

8.5 Complexity analysis

In this section, we will investigate the complexity of the proposed iterative clipping algorithm. The computational complexity will be quantified by the number of instructions per OFDM symbol and iteration.

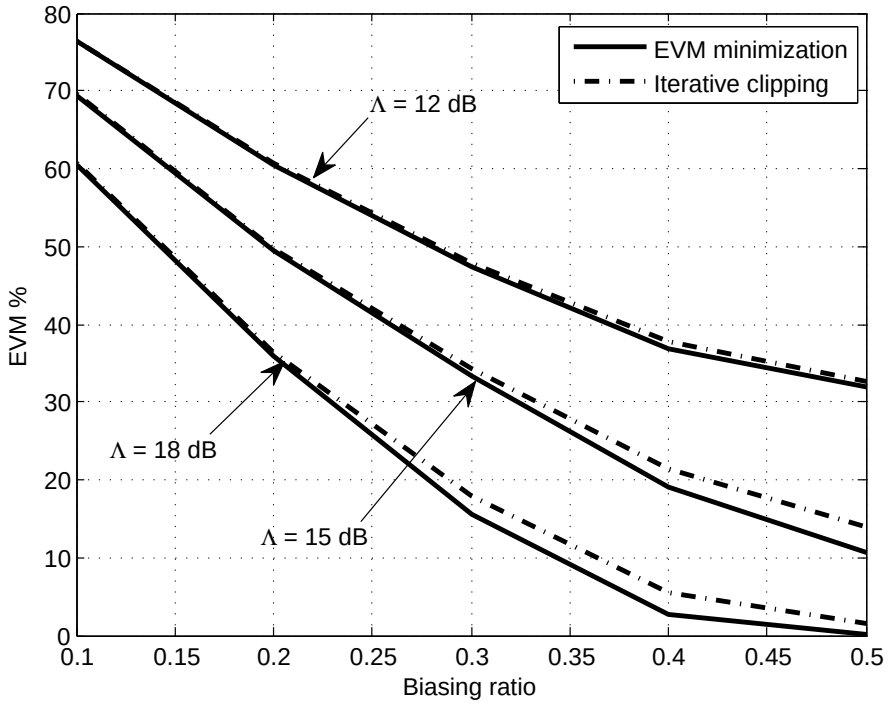

Figure 40: EVM comparison between iterative clipping method and EVM minimization scheme (QPSK modulation, N = 256).

At the first step, $2N$ comparisons were made to decide which samples need to be upper clipped or lower clipped. Assume that the number of clipped sample is K_t, there are K_t assignment operations. Assuming either comparison operation or assignment operation only requires a single instruction, the number of instructions required to implement clipping is $I_{\text{clipping}} = 2N + K_t$. If $\max \tilde{x}^{(i-1)}[n] > I_H - B$ and $\min \tilde{x}^{(i-1)}[n] < I_L - B$, the FFT has be operated. It is known that a N-point FFT requires $N \log N$ multiplication and $N \log N$ additions. In order to calculate $\bar{P}_u$ and $\bar{P}_l$, we need $4(N/2-1)$ subtractions, $4(N/2-1)$ multiplications, and $4(N/2-1)$ additions. Assuming that the multiplication operation requires α_M instructions and addition/subtraction operation requires α_A instruction, the total number of additional instructions for the case "$\max \tilde{x}^{(i-1)}[n] > I_H - B$ and $\min \tilde{x}^{(i-1)}[n] < I_L - B$" is $I_p = \alpha_M(N \log N + 2N - 4) + \alpha_A(N \log N + 4N - 8)$. Actually, the case "$\max \tilde{x}^{(i-1)}[n] > I_H - B$ and $\min \tilde{x}^{(i-1)}[n] < I_L - B$" can only happen in the first iteration. The

probability depends on the power back-off and biasing ratio.

At the second step, N additions and one multiplication are required to calculate the DC component and N subtractions required to remove the DC-component. Thus, the number of instructions required for the second step is $I_{\text{dc}} = 2\alpha_A N + \alpha_M$.

At the third step, we need $2N$ comparisons to examine whether the dynamic range is obeyed. Hence, the number of instructions required for the third step is $I_{\text{comp}} = 2N$.

In summary, the overall computational complexity of the iterative clipping algorithm is $I_{\text{total}} = I_{\text{clipping}} + I_p + I_{\text{dc}} + I_{\text{comp}}$, where $I_p = 0$ after the first iteration. Either the parameter K_t or the number of iterations depends on the power back-off and biasing ratio. Table 4 shows the average number of iterations of 1000 OFDM symbols ($N = 256$ subcarriers, QPSK modulation, and $\beta = 0.998$) with various power back-off and biasing ratio.

When solving (196) with IPM, the computation is dominated by one FFT and inversion of a $N \times N$ matrix per iteration. Therefore, the complexity has the order $O(N \log N + N^3)$, which is much more complicated than the iterative clipping method, which has a complexity of order $O(N \log N + N)$.

Table 4: Average number of iterations

Power back-off \ Biasing ratio	0.1	0.2	0.3	0.4	0.5
12 dB	9.29	6.01	6.64	9.42	11.49
15 dB	6.55	3.00	2.06	1.97	2.28
18 dB	4.82	2.00	1.11	0.19	0.02

8.6 Conclusion

In this chapter, we investigated the clipping effects on illumination in visible light OFDM systems. To avoid brightness deviation and flicker of simple clipping, we proposed an iterative clipping method. We formulated the EVM minimization problem as a convex optimization problem, which requires high-complexity computation to

solve. The simulation shows that, compared with the EVM minimization method, the iterative clipping method has a less than 4% EVM gap.

CHAPTER IX

USING DELTA-SIGMA MODULATORS IN VLC-OFDM

Simple two-level on-off keying (OOK) and pulse-position modulation (PPM) are supported in IEEE standard due to their compatibility with existing constant current LED drivers, but their low spectral efficiency have limited the achievable data rates of VLC. VLC-OFDM inherits the disadvantage of high peak-to-average power ratio (PAPR) from RF-OFDM. Besides, the continuous magnitude of OFDM signals requires complicated mixed-signal digital-to-analog converter (DAC) and modification of LED drivers. We propose the use of delta-sigma modulators in visible light OFDM systems to convert continuous magnitude OFDM symbols into LED driver signals. The proposed system has the communication theory advantages of OFDM along with the practical analog and optical advantages of simple two level driver signals. Simulation results are provided to illustrate the proposed system.

9.1 Introduction

Single-carrier unipolar and real-valued modulations, such as on-off keying (OOK), variable pulse-position modulation (VPPM), and pulse amplitude modulation (PAM), are adopted in VLC [31, 37]. Recently, orthogonal frequency division multiplexing (OFDM) has been considered for VLC due to its ability to boost data rates and efficiently combat inter-symbol-interference (ISI) [32, 48, 41]. OFDM can easily support multiple access (OFDMA), which is essential for multi-user broadcasting. However, transmitting OFDM symbols requires the driving circuits of a white LED to support continuous magnitude inputs, and the mixed-signal digital-to-analog converter (DAC) design is complicated. In IEEE 802.15.7 standard [2], only two-level modulations (OOK and VPPM) are supported because their seamless compatibility with

most constant-current LED drivers [1]. Since the primary function of the VLC is providing illumination, modification of driving circuits of LED will be not beneficial to the application and commercialization of VLC. Moreover, the high peak to average power ratio (PAPR) makes OFDM signals sensitive to LED nonlinearities [34].

In this chapter, we propose using a delta-sigma modulator [65, 64] to convert the OFDM signal into a two level representation and directly drive the LED. Most of the quantization noises will be pushed to the out-of-band, and the in-band subcarriers can be simply recovered at the receiver. Section 9.2 reviews modulation techniques in VLC and basic concept of delta-sigma digital to analog converters (DACs). Section 9.3 describes the delta-sigma modulator based VLC-OFDM system and discusses the advantages. Numerical results are shown in Section 9.4 and conclusions are provided in Section 9.5.

9.2 Background

In this section, we review delta-sigma digital to analog converters (DACs).

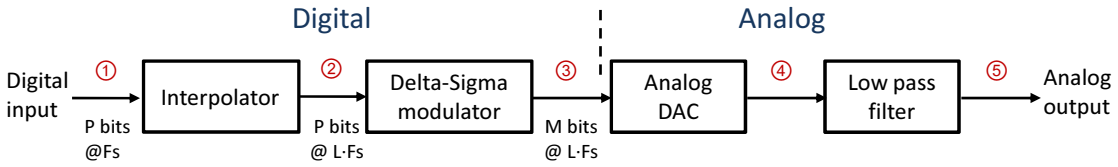

Figure 41: System diagram of delta-sigma DAC.

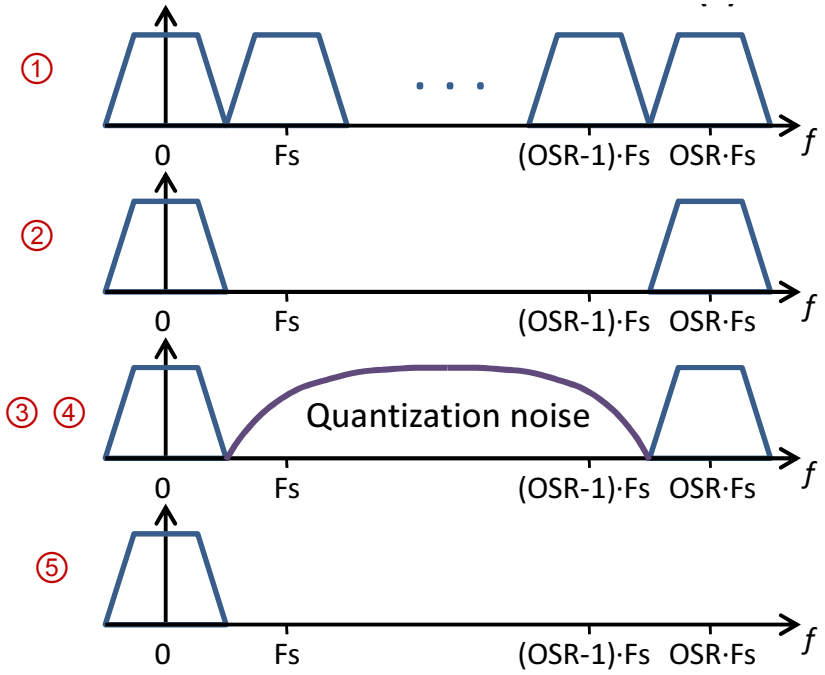

Figure 42: Signal spectrum at different stages of delta sigma DAC.

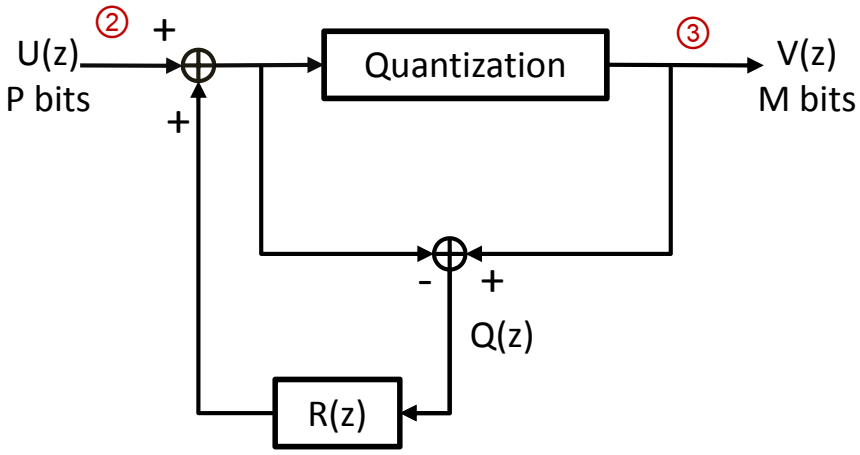

Figure 43: Delta sigma modulator.

Fig. 41 is block diagram of a delta-sigma DAC and Fig. 42 shows the signal spectrum at different stages. A delta-sigma DAC [65] generally comprises a interpolator,

delta-sigma modulator, a mixed signal DAC core and an analog filter. The input is a digital signal sampled at rate F_s with a resolution of P bits. The interpolator up-samples the signal to sampling rate $L \cdot F_S$, where L is the over sampling ratio (OSR), and suppress the spectral replicas centered at F_s, $2F_s$ ..., $(L-1)F_s$.

The role of a delta-sigma modulator is to convert a digital signal with 2^P levels into a digital signal with 2^M levels, where $M < P$, while maintaining a high in-band signal-to-noise power ratio. Converting to a signal with only a few levels makes the analog DAC more tolerant to component mismatch and nonlinearities. Fig. 43 shows the block diagram of a delta-sigma modulator. The operation of delta-sigma modulator can be expressed in the z domain as

$$V(z) = U(z) + (1 + R(z))Q(z) \tag{197}$$

where $U(Z)$, $V(Z)$, and $Q(Z)$ denote the z transform of the input, output and quantization error of the delta-sigma modulator, respectively. $1 + R(z)$ is noise transfer function (NTF).

The delta-sigma modulator pushes quantization noise out of the signal band through the appropriate design of the NTF. A mixed signal DAC reproduces the 2^M level digital signal at its input and an analog lowpass filter removes most of the out-of-band noise power and creates a P bit resolution analog signal.

9.3 Visible light OFDM transmission based on a delta-sigma modulator

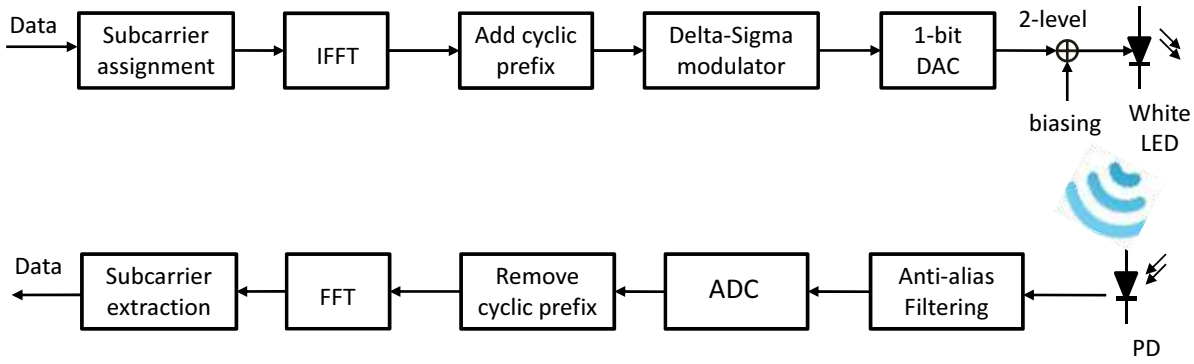

Figure 44: Visible light OFDM transmitter based on delta-sigma modulator .

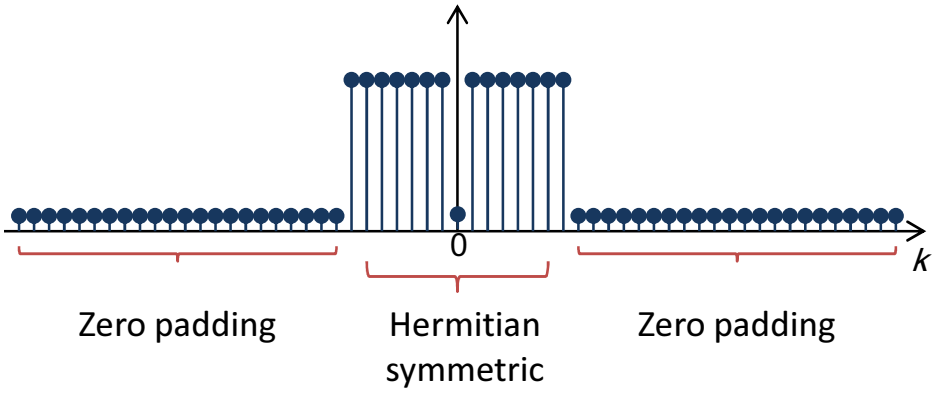

Figure 45: Subcarrier assignment for oversampled VLC-OFDM signal.

Fig. 44 is a block diagram of visible light OFDM transmission that uses a delta-sigma modulator. In a delta-sigma DAC, interpolation is used for generating oversampled signals at the input of the delta-sigma modulator. In our proposed framework, we obtain the oversampled OFDM signals by zero padding in the frequency domain. Define the in-band indices to be the set $\mathcal{I} = [-N/2, N/2-1]$, and the out-of-band indices to be the set $\mathcal{O} = [-NL/2, -N/2-1] \cup [N/2, LN/2-1]$. The zero padded

version of X_k can be expressed as

$$X_k^{(L)} = \begin{cases} X_k, & k \in \mathcal{I} \\ 0, & k \in \mathcal{O} \end{cases}. \tag{198}$$

Fig. 45 shows the subcarrier assignment for oversampled VLC-OFDM signal. An LN length IFFT is used to convert the frequency domain sequence $\{X_k^{(L)}\}_{k=-LN/2}^{LN/2-1}$ into a L times oversampled time-domain sequence $\{x^{(L)}[n]\}_{n=0}^{LN-1}$.

The delta-sigma modulator is then used to convert the continuous magnitude time domain OFDM digital samples $\{x^{(L)}[n]\}_{n=0}^{LN-1}$ into one bit signals $\{y^{(L)}[n]\}_{n=0}^{LN-1}$, where $y^{(L)}[n] \in \{-1, 1\}$. According to Eq. (197) , the data on the frequency-domain subcarriers of $y^{(L)}[n]$ can be expressed as

$$\begin{aligned} Y_k^{(L)} &= X_k^{(L)} + \mathrm{NTF}_k Q_k \\ &= \begin{cases} X_k + \mathrm{NTF}_k Q_k, & k \in \mathcal{I} \\ \mathrm{NTF}_k Q_k, & k \in \mathcal{O} \end{cases}, \end{aligned} \tag{199}$$

where NTF_k denotes the noise transfer function on the kth subcarrier and Q_k denotes the quantization noise on the kth subcarrier, respectively. Since NTF is actually a high-pass filter, very few distortions fall on the in-band subcarriers. We use error vector magnitude (EVM) to quantify the in-band distortions

$$\begin{aligned} \mathrm{EVM} &= \frac{\sum_{k=1}^{N/2-1} |Y_k^{(L)} - X_k^{(L)}|^2}{\sum_{k=1}^{N/2-1} |X_k^{(L)}|^2} \\ &= \frac{\sum_{k=1}^{N/2-1} |\mathrm{NTF}_k Q_k|^2}{\sum_{k=1}^{N/2-1} |X_k|^2}. \end{aligned} \tag{200}$$

The proposed DAC has a single bit digital input and a two level analog output. To ensure that the input of the LED is positive, a bias is added to the two level analog signal, which only affects the DC component. Note that this bias could be built into the DAC.

We directly use the two level DAC output signal (after biasing) that contains out-of-band quantization noise to drive the LED for two reasons. First, most of the

existing driving circuits of white LEDs used for the purposes of illumination are not compatible with continuous amplitude driving voltages. However, a two level input signal, like a pulse width modulation (PWM) or OOK signal, is widely accepted [2]. Second, out-of-band inference is not a concern in VLC because the LED acts as a low pass filter (similar to a speaker in a class D amplifier audio system [25]) and no out-of-band information is transmitted simultaneously.

As an example, the most popular white LED, which uses a blue emitter in combination with a phosphor that emits yellow light, has limited bandwidth. The frequency response of emitted white light and the blue part of a typical white light (Luxeon S-TAR) LED is shown in Fig. 2 [50]. The bandwidth of the white light response is only 2.5 MHz. Any remaining out-of-band noise can be removed or ignored at the receiver, either with a low pass anti-aliasing filter or by ignoring out-of-band subcarriers after the FFT.

The delta-sigma modulator based transmitter also has some advantages over a conventional visible light OFDM transmitter. First, the structure of a 1 bit mixed signal DAC is very simple and its linearity is theoretically perfect. Second, the drawback of the high PAPR of OFDM signal is avoided. Third, it is unnecessary to design a customized driving circuit for the LED to support continuous or multiple amplitude level input signals.

9.4 Numerical results

To illustrate the proposed system, we choose $N = 256$ subcarriers with a spacing of $\Delta f = 15$ kHz, and 4-QAM modulation. The bandwidth of the OFDM signal, 1.875 MHz, is within the 3 dB bandwidth of the white LED from [50]. The NTF of the delta-sigma modulator was obtained from the Matlab toolbox associated with [65]. Fig. 46 plots a section of the input and output of the delta-sigma modulator and Fig. 47 plots the power spectral density (PSD) of the input and output of the LED with

a fourth order NTF and $L = 8$. Note that most of the noise falls out of the signal band.

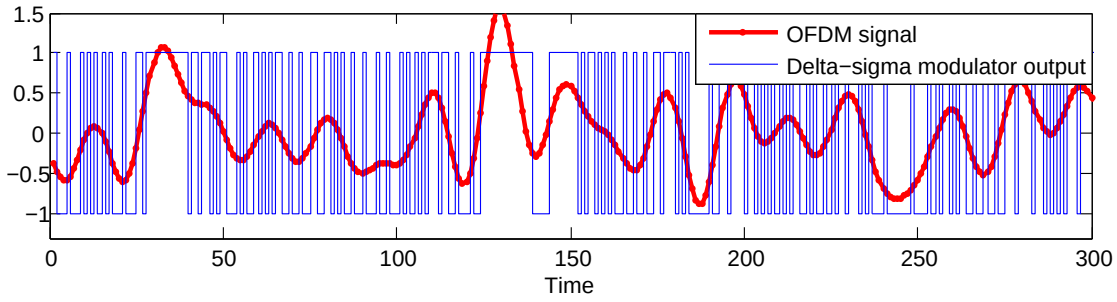

Figure 46: Input and output sequence of delta-sigma modulator (L = 8).

Fig. 48 plots the EVM of transmitted signals with various OSRs and orders of NTF. By increasing the OSR, less in-band noise is observed. However, increasing the order of NTF does not always guarantee better performance because the stability of the loop filter in a delta-sigma modulator may become a problem. Different loop filter designs can be created to address this issue. We can see that the EVM can be as low as 1% - 3% if we choose oversampling ratio greater than 12. Compared with conventional two-level OOK signal, when SNR is low (less than 10 dB), EVM is much less than channel noise, which means the degradation due to delta-sigma is negligible. When SNR is high, delta-sigma output will obviously outperform OOK since higher-order modulations can be adopted.

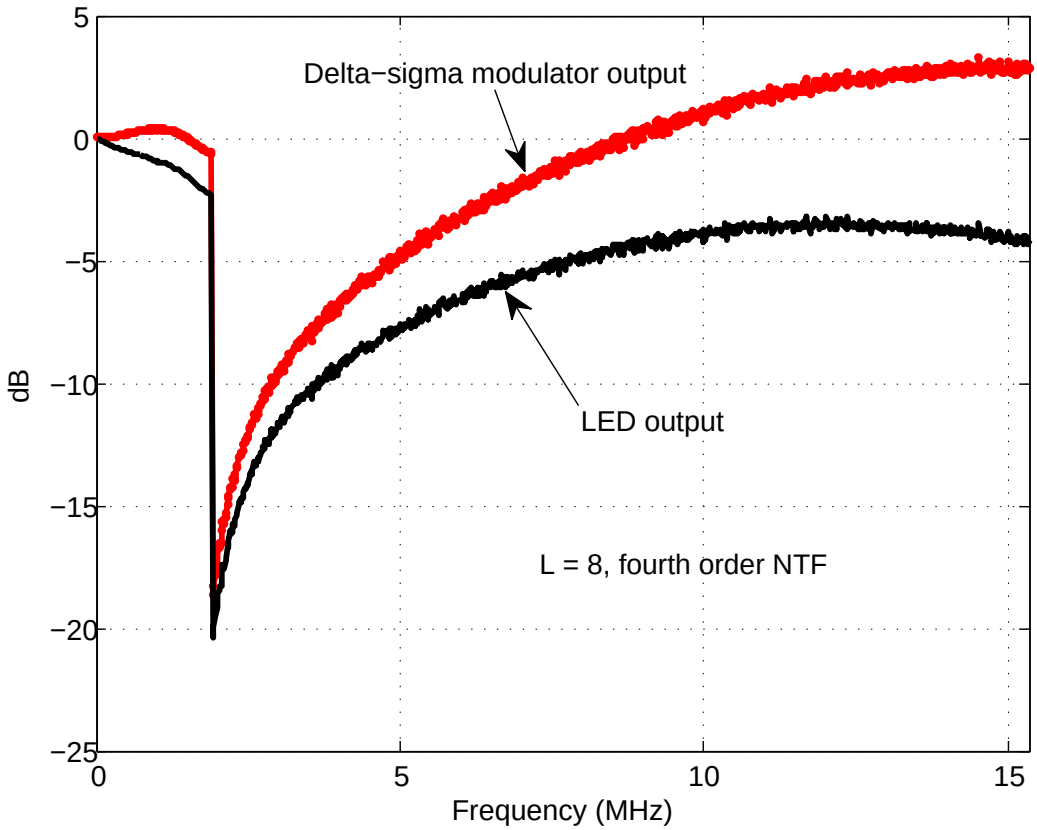

Figure 47: PSD of input and output of LED.

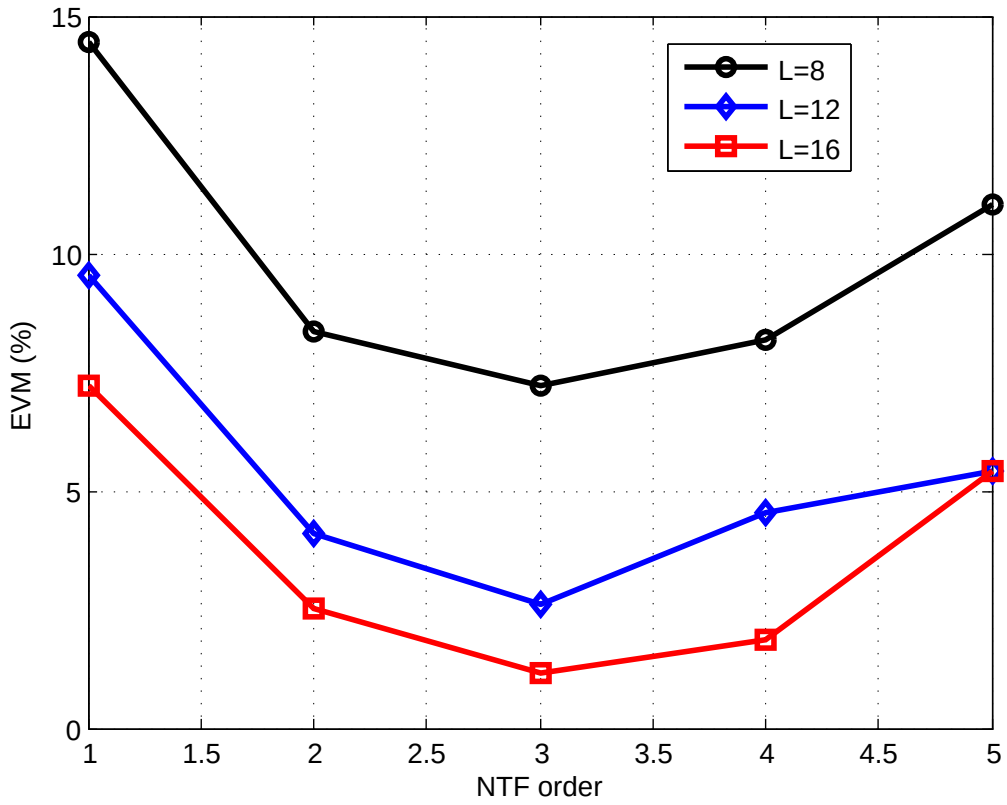

Figure 48: Error vector magnitude of transmitted signals.

9.5 Conclusions

We used a delta-sigma modulator to convert a continuous magnitude OFDM digital signal into a two level analog signal that can directly serve as the input of a LED. This scheme eases the design of the mixed signal DAC and driving circuits, as well as avoids nonlinear distortion due to a high PAPR.

CHAPTER X

CONCLUSIONS

10.1 Contributions

In this dissertation, we have analyzed and designed optical power and dynamic range constrained OWC-OFDM systems. Primary contributions of this dissertation are summarized here:

- Derived individual and joint distributions of upper PAPR and lower PAPR of real-valued OWC-OFDM signals.
- Derived closed-form EVM expressions of clipped DCO-OFDM and ACO-OFDM signals. Lower-bound are obtained through linear programming. Proved the optimality of ACO-OFDM in the term of EVM.
- Analyzed SDR and achievable data rates of clipped DCO-OFDM and ACO-OFDM under both optical power and dynamic range constraints.
- Investigated the illumination-to-communication efficiency (ICE) in VLC-OFDM. Extended the selected-mapping method (SLM) as a means of improving the ICE.
- Proposed brightness control schemes for VLC-OFDM under dynamic range constraints.
- Investigated the clipping effects on the performance degradation of communication as well as illumination in VLC-OFDM. Proposed an iterative clipping method considering brightness control and flicker mitigation.

- Proposed using delta-sigma modulators in VLC-OFDM system. The proposed system has the communication theory advantages of OFDM along with the practical analog and optical advantages of simple two-level driving signals.

10.2 Suggestions for future work

The following is a list of interesting research topics that can be pursued as an extension of this dissertation:

- Investigate nonlinear model of LEDs and design digital pre-distortion techniques that account for memory and thermal effects.
- Design post-distorter at the receiver to mitigate the nonlinear distortions.
- Design PWM modulators to convert the OFDM signals into two-level signals, and compare with delta-sigma modulators.

APPENDIX A

PROOF THAT ACO-OFDM IS OPTIMUM FOR EQ. (76)

Denote by $u(c[n])$ the objective function for the problem in (76):

$$u(c[n]) = \sum_{n=0}^{N/2-1} \left(c[n]\right)^2, \tag{201}$$

and denote by $g_i(c[n])$ the ith constraint function for the problem in (76):

$$g_i(c[n]) = \begin{cases} x^{(A)}[i] + c[i] - 2\gamma\sigma_x, & 0 \leq i \leq \frac{N}{2} - 1 \\ -x^{(A)}[i - N/2] - c[i - N/2], & \frac{N}{2} \leq i \leq N - 1 \end{cases}. \tag{202}$$

Let μ_i denote the ith KT multiplier. We inter that

$$\nabla u(c[n]) = [2c[0], 2c[1], \ldots, 2c[N/2 - 1]], \tag{203}$$

$$\sum_{i=0}^{N-1} \mu_i \nabla g_i(c[n]) = \left[\mu_0 - \mu_{N/2}, \mu_i - \mu_{N/2+1}, \ldots, \mu_{N/2-1} - \mu_{N-1}\right]. \tag{204}$$

Next, we prove that $c^\star[n] = x^{(A)}[n] - \bar{x}^{(A)}[n]$ satisfies the Kuhn-Tucker (KT) conditions [49]:

Stationarity

$$\nabla u(c[n]) + \sum_{i=0}^{N-1} \mu_i \nabla g_i(c[n]) = 0, \tag{205}$$

Primary feasibility

$$\mu_i \geq 0, \quad \forall i = 0, 1, \ldots, N-1, \tag{206}$$

Dual feasibility

$$g_i(c[n]) \leq 0, \quad \forall i = 0, 1, \ldots, N-1, \tag{207}$$

Complementary slackness

$$\mu_i g_i(c[n]) = 0, \quad \forall i = 0, 1, \ldots, N-1. \tag{208}$$

Substituting $c^\star[n]$ into Eq. (205), we obtain,

$$\mu_i - \mu_{i+N/2} = -2x^{(A)}[i] + 2\bar{x}^{(A)}[i], \quad i = 0, 1, \ldots, \frac{N}{2} - 1. \tag{209}$$

In order to satisfy all the other conditions (206)-(208), we can choose μ_i as follows

(1) if $x^{(A)}[i] = \bar{x}^{(A)}[i]$,

$$\mu_i = \mu_{i+N/2} = 0; \tag{210}$$

(2) if $x^{(A)}[i] > 2\gamma\sigma_x$ and $\bar{x}^{(A)}[i] = 2\gamma\sigma_x$,

$$\mu_i = 2\bar{x}^{(A)}[i], \quad \mu_{i+N/2} = 2x^{(A)}[i]; \tag{211}$$

(3) if $x^{(A)}[i] < 0$ and $\bar{x}^{(A)}[i] = 0$,

$$\mu_i = -2x^{(A)}[i], \quad \mu_{i+N/2} = -2\bar{x}^{(A)}[i]. \tag{212}$$

Therefore, there exits constants $\mu_i\,(i = 0, 1, \ldots, N-1)$ that make $c^\star[n] = x^{(A)}[n] - \bar{x}^{(A)}[n]$ satisfy the KT conditions. It was shown in reference [43] that if the objective function and the constraint functions are continuously differentiable convex functions, KT conditions are sufficient for optimality. It is obvious that u and g are all continuously differentiable convex functions. Therefore, $c^\star[n]$ is optimal for the minimization problem (76).

REFERENCES

[1] "Constant current led driver." Texas Instruments, TPS61042 datasheet, Dec. 2002 [Revised Mar. 2007].

[2] *IEEE Standard for Local and Metropolitan Area Networks–Part 15.7: Short-Range Wireless Optical Communication Using Visible Light*. 2011.

[3] "Sorry, America: Your wireless airwaves are full." *CNN Money*, Feb. 2012.

[4] "Visible Light Communication (VLC)/Li-Fi Technology Market worth $6,138.02 Million - 2018." *New International*, Nov. 2013.

[5] Abramowitz, M. and Stegun, I., *Handbook of mathematical functions with formulas, graphs, and mathematical tables*, vol. 55. Dover publications, 1964.

[6] Aggarwal, A. and Meng, T. H., "Minimizing the peak-to-average power ratio of OFDM signals using convex optimization," *IEEE Transactions on Signal Processing*, vol. 54, pp. 3099–3110, Aug. 2006.

[7] Armstrong, J., "Peak-to-average power reduction for OFDM by repeated clipping and frequency domain filtering," *Electronics Letters*, vol. 38, p. 246, Feb. 2002.

[8] Armstrong, J. and Lowery, A. J., "Power efficient optical OFDM," *Electronics Letters*, vol. 42, no. 6, pp. 370–372, 2006.

[9] Armstrong, J. and Schmidt, B., "Comparison of asymmetrically clipped optical OFDM and dc-biased optical OFDM in AWGN," *IEEE Communications Letters*, vol. 12, no. 5, pp. 343–345, 2008.

[10] Armstrong, J., "OFDM for Optical Communications," *Journal of Lightwave Technology*, vol. 27, pp. 189–204, Feb. 2009.

[11] Audeh, M. D., Kahn, J. M., and Barry, J. R., "Performance of pulse-position modulation on measured non-directed indoor infrared channels," *Communications, IEEE Transactions on*, vol. 44, no. 6, pp. 654–659, 1996.

[12] Azhar, A., Tran, T., and O'Brien, D., "A Gigabit/s Indoor Wireless Transmission Using MIMO-OFDM Visible-Light Communications," *Photonics Technology Letters, IEEE*, vol. 25, no. 2, pp. 171–174, 2013.

[13] Bai, B., Xu, Z., and Fan, Y., "Joint LED dimming and high capacity visible light communication by overlapping PPM," in *Wireless and Optical Communications Conference (WOCC), 2010 19th Annual*, pp. 1–5, IEEE, 2010.

[14] Banelli, P. and Cacopardi, S., "Theoretical analysis and performance of OFDM signals in nonlinear awgn channels," *IEEE Transactions on Communications*, vol. 48, no. 3, pp. 430–441, 2000.

[15] Barros, D. J. F., Wilson, S. K., and Kahn, J. M., "Comparison of Orthogonal Frequency-Division Multiplexing and Pulse-Amplitude Modulation in Indoor Optical Wireless Links," *IEEE TRANSACTIONS ON COMMUNICATIONS*, vol. 60, no. 1, pp. 153–163, 2012.

[16] Bauml, R., Fischer, R., and Huber, J., "Reducing the peak-to-average power ratio of multicarrier modulation by selected mapping," *Electronics Letters*, vol. 32, no. 22, p. 2056, 1996.

[17] Baxley, R. J. and Zhou, G. T., "Peak-to-Average Power Ratio Reduction," in *Digital Signal Processing Handbook* (Madisetti, V., ed.), CRC Press, 2nd ed., 2009.

[18] Baxley, R. J., Zhao, C., and Zhou, G. T., "Constrained Clipping for Crest Factor Reduction in OFDM," *IEEE Transactions on Broadcasting*, vol. 52, pp. 570–575, Dec. 2006.

[19] Bussgang, J., "Crosscorrelation functions of amplitude-distorted gaussian signals," *NeuroReport*, vol. 17, no. 2, 1952.

[20] Campello, J., "Optimal discrete bit loading for multicarrier modulation systems," in *Information Theory, 1998. Proceedings. 1998 IEEE International Symposium on*, p. 193, IEEE, 1998.

[21] Choi, J.-H., Ghassemlooy, Z., and Lee, C. G., "PWM-based PPM format for dimming control in visible light communication system," *2012 8th International Symposium on Communication Systems, Networks & Digital Signal Processing (CSNDSP)*, pp. 1–5, July 2012.

[22] Cimini, L. J. and Sollenberger, N. R., "Peak-to-average power ratio reduction of an OFDM signal using partial transmit sequences," *IEEE Communications Letters*, vol. 4, pp. 86–88, Mar. 2000.

[23] Cossu, G., Khalid, A., Choudhury, P., Corsini, R., Ciaramella, E., and others, "3.4 Gbit/s visible optical wireless transmission based on RGB LED," *Optics express*, vol. 20, no. 26, pp. B501–6, 2012.

[24] CVX Research, I., "CVX: Matlab software for disciplined convex programming, version 2.0 beta," Sept. 2012.

[25] Dapkus, D., "Class-d audio power amplifiers: an overview," in *Consumer Electronics, 2000. ICCE. 2000 Digest of Technical Papers. International Conference on*, pp. 400–401, IEEE, 2000.

[26] Davenport, W. and Root, W., *An introduction to the theory of random signals and noise*. IEEE Press, 1987.

[27] De Maio, A., Huang, Y., Piezzo, M., Zhang, S., and Farina, A., "Design of optimized radar codes with a peak to average power ratio constraint," *IEEE Transactions on Signal Processing*, vol. 59, pp. 2683–2697, June 2011.

[28] Dimitrov, S., Sinanovic, S., and Haas, H., "Clipping Noise in OFDM-Based Optical Wireless Communication Systems," *IEEE Transactions on Communications*, vol. 60, pp. 1072–1081, Apr. 2012.

[29] Elgala, H., Mesleh, R., and Haas, H., "Non-linearity effects and predistortion in optical OFDM wireless transmission using LEDs," *International Journal of Ultra Wideband Communications and Systems*, vol. 1, no. 2, pp. 143–150, 2009.

[30] Elgala, H., Mesleh, R., and Haas, H., "A study of LED nonlinearity effects on optical wireless transmission using OFDM," in *International Conference on Wireless and Optical Communications Networks*, pp. 1–5, IEEE, 2009.

[31] Elgala, H., Mesleh, R., and Haas, H., "Indoor optical wireless communication: potential and state-of-the-art," *IEEE Communications Magazine*, vol. 49, no. 9, pp. 56–62, 2011.

[32] Elgala, H., Mesleh, R., Haas, H., and Pricope, B., "OFDM Visible Light Wireless Communication Based on White LEDs," in *2007 IEEE 65th Vehicular Technology Conference*, pp. 2185–2189, IEEE, Apr. 2007.

[33] Elgala, H. and Little, T. D. C., "Reverse polarity optical-OFDM (RPO-OFDM): dimming compatible OFDM for gigabit VLC links.," *Optics express*, vol. 21, pp. 24288–24299, Oct. 2013.

[34] Elgala, H., Mesleh, R., and Haas, H., "An led model for intensity-modulated optical communication systems," *Photonics Technology Letters, IEEE*, vol. 22, no. 11, pp. 835–837, 2010.

[35] Elgala, H., Mesleh, R., and Haas, H., "Indoor optical wireless communication: potential and state-of-the-art," *IEEE Communications Magazine*, vol. 49, pp. 56–62, Sept. 2011.

[36] Fernando, N., Hong, Y., and Viterbo, E., "Flip-OFDM for optical wireless communications," in *Proc. IEEE Information Theory Workshop, 2011*, pp. 5–9, IEEE, 2011.

[37] Gancarz, J., Elgala, H., and Little, T. D., "Impact of lighting requirements on vlc systems," *Communications Magazine, IEEE*, vol. 51, no. 12, pp. 34–41, 2013.

[38] Gfeller, F. and Bapst, U., "Wireless in-house data communication via diffuse infrared radiation," *Proceedings of the IEEE*, vol. 67, no. 11, pp. 1474–1486, 1979.

[39] Goeckel, D. and Kelly, P., "A modern extreme value theory approach to calculating the distribution of the peak-to-average power ratio in OFDM systems," in *2002 IEEE International Conference on Communications.*, vol. 3, pp. 1686–1690, Ieee, 2002.

[40] Grant, M. and Boyd, S., "Graph implementations for nonsmooth convex programs," in *Recent Advances in Learning and Control* (Blondel, V., Boyd, S., and Kimura, H., eds.), Lecture Notes in Control and Information Sciences, pp. 95–110, Springer-Verlag Limited, 2008.

[41] Grobe, L., Paraskevopoulos, A., Hilt, J., Schulz, D., Lassak, F., Hartlieb, F., Kottke, C., Jungnickel, V., and Langer, K.-D., "High-speed visible light communication systems," *Communications Magazine, IEEE*, vol. 51, no. 12, pp. 60–66, 2013.

[42] Han, S. H. and Lee, J. H., "An overview of peak-to-average power ratio reduction techniques for multicarrier transmission," *IEEE Wireless Communications*, vol. 12, pp. 56–65, Apr. 2005.

[43] Hanson, M., "Invexity and the kuhn–tucker theorem," *Journal of mathematical analysis and applications*, vol. 236, no. 2, pp. 594–604, 1999.

[44] Hranilovic, S., "On the design of bandwidth efficient signalling for indoor wireless optical channels," *International Journal of Communication Systems*, vol. 18, no. 3, pp. 205–228, 2005.

[45] Hranilovic, S., *Wireless optical communication systems*. Springer, 2005.

[46] Jiang, T., Guizani, M., and Chen, H.-h., "Derivation of PAPR Distribution for OFDM Wireless Systems Based on Extreme Value Theory," *IEEE Transactions on Wireless Communications*, vol. 7, no. 4, pp. 1298–1305, 2008.

[47] Kahn, J. M. and Barry, J. R., "Wireless Infrared Communications," *Proceedings of the IEEE*, vol. 85, no. 97, pp. 265 – 298, 1997.

[48] Khalid, A. M., Cossu, G., Corsini, R., Choudhury, P., and Ciaramella, E., "1-Gb/s Transmission Over a Phosphorescent White LED by Using Rate-Adaptive Discrete Multitone Modulation," *IEEE Photonics Journal*, vol. 4, pp. 1465–1473, Oct. 2012.

[49] Kuhn, H. and Tucker, A., "Nonlinear programming," in *Proceedings of the second Berkeley symposium on mathematical statistics and probability*, vol. 1, pp. 481–492, California, 1951.

[50] Le Minh, H., O'Brien, D., Faulkner, G., Zeng, L., Lee, K., Jung, D., Oh, Y., and Won, E. T., "100-mb/s nrz visible light communications using a postequalized white led," *Photonics Technology Letters, IEEE*, vol. 21, no. 15, pp. 1063–1065, 2009.

[51] Lee, K. and Park, H., "Modulations for Visible Light Communications With Dimming Control," *IEEE Photonics Technology Letters*, vol. 23, pp. 1136–1138, Aug. 2011.

[52] Liu, Q., Baxley, R., Ma, X., and Zhou, G., "Error vector magnitude optimization for ofdm systems with a deterministic peak-to-average power ratio constraint," *IEEE Journal of Selected Topics in Signal Processing*, vol. 3, no. 3, pp. 418–429, 2009.

[53] Ma, C., Zhang, H., Yao, M., Xu, Z., and Cui, K., "Distributions of PAPR and crest factor of OFDM signals for VLC," *2012 IEEE Photonics Society Summer Topical Meeting Series*, vol. 5, pp. 119–120, July 2012.

[54] Marsh, G. W. and Kahn, J. M., "Performance evaluation of experimental 50-mb/s diffuse infrared wireless link using on-off keying with decision-feedback equalization," *Communications, IEEE Transactions on*, vol. 44, no. 11, pp. 1496–1504, 1996.

[55] Mesleh, R., Elgala, H., and Haas, H., "On the performance of different OFDM based optical wireless communication systems," *Journal of Optical Communications and Networking*, vol. 3, no. 8, pp. 620–628, 2011.

[56] Noshad, M. and Brandt-Pearce, M., "Can Visible Light Communications Provide Gb/s Service?," *arXiv:1308.3217*, pp. 1–7, Aug. 2013.

[57] Ntogari, G., Kamalakis, T., Walewski, J. W., and Sphicopoulos, T., "Combining Illumination Dimming Based on Pulse-Width Modulation With Visible-Light Communications Based on Discrete Multitone," *J. OPT. COMMUN. NETW*, vol. 3, p. 56, Dec. 2010.

[58] O'Brien, D. C., Zeng, L., Le-Minh, H., Faulkner, G., Walewski, J. W., and Randel, S., "Visible light communications: Challenges and possibilities," in *2008 IEEE 19th International Symposium on Personal, Indoor and Mobile Radio Communications*, pp. 1–5, IEEE, Sept. 2008.

[59] Ochiai, H., "Performance analysis of peak power and band-limited OFDM system with linear scaling," *IEEE Transactions on Wireless Communications*, vol. 2, no. 5, pp. 1055–1065, 2003.

[60] Ochiai, H. and Imai, H., "Performance analysis of deliberately clipped OFDM signals," *IEEE Transactions on Communications*, vol. 50, no. 1, pp. 89–101, 2002.

[61] Ochiai, H. and Imai, H., "On the distribution of the peak-to-average power ratio in OFDM signals," *IEEE Transactions on communications*, vol. 49, no. 2, pp. 282–289, 2001.

[62] Peng, F. and Ryan, W., "On the capacity of clipped OFDM channels," in *Information Theory, 2006 IEEE International Symposium on*, pp. 1866–1870, IEEE, 2006.

[63] Rajagopal, S., Roberts, R., and Lim, S.-K., "IEEE 802.15.7 visible light communication: modulation schemes and dimming support," *IEEE Communications Magazine*, vol. 50, no. March, pp. 72–82, 2012.

[64] Redfern, A. J. and Shi, K., "Quantization noise shaping for information maximizing adcs," *arXiv preprint arXiv:1305.2801*, 2013.

[65] Schreier, R., Temes, G. C., and Wiley, J., *Understanding delta-sigma data converters*, vol. 74. IEEE press Piscataway, NJ, 2005.

[66] Stefan, I., Elgala, H., and Haas, H., "Study of dimming and LED nonlinearity for ACO-OFDM based VLC systems," *2012 IEEE Wireless Communications and Networking Conference (WCNC)*, pp. 990–994, Apr. 2012.

[67] Tellado, J., *Multicarrier modulation with low PAR: applications to DSL and wireless*, vol. 587. Springer, 2000.

[68] Tsonev, D., Chun, H., Rajbhandari, S., McKendry, J., Videv, S., Gu, E., Haji, M., Watson, S., Kelly, A., Faulkner, G., and others, "A 3-Gb/s Single-LED OFDM-based Wireless VLC Link Using a Gallium Nitride μLED," 2014.

[69] Tsonev, D., Sinanovic, S., and Haas, H., "Complete Modeling of Nonlinear Distortion in OFDM-Based Optical Wireless Communication," *Journal of Lightwave Technology*, vol. 31, pp. 3064–3076, Sept. 2013.

[70] Wang, Z., Ma, X., and Giannakis, G., "Ofdm or single-carrier block transmissions?," *Communications, IEEE Transactions on*, vol. 52, no. 3, pp. 380–394, 2004.

[71] Wang, Z., Yu, C., Zhong, W.-D., Chen, J., and Chen, W., "Performance of variable M-QAM OFDM visible light communication system with dimming control," in *Opto-Electronics and Communications Conference (OECC), 2012 17th*, no. July, pp. 741–742, 2012.

[72] Wilson, S. and Armstrong, J., "Transmitter and receiver methods for improving asymmetrically-clipped optical OFDM," *IEEE Transactions on Wireless Communications*, vol. 8, no. 9, pp. 4561–4567, 2009.

[73] Yu, H., Chen, M., and Wei, G., "Distribution of PAR in DMT systems," *Electronics Letters*, vol. 39, no. 10, p. 799, 2003.

[74] Yu, Z., Baxley, R. J., and Zhou, G. T., "Generalized interior-point method for constrained peak power minimization of OFDM signals," in *2011 IEEE International Conference on Acoustics, Speech and Signal Processing (ICASSP)*, (Prague, Czech Republic), pp. 3572–3575, IEEE, May 2011.

[75] Yu, Z., Baxley, R. J., and Zhou, G. T., "EVM and achievable data rate analysis of clipped OFDM signals in visible light communication," *EURASIP Journal on Wireless Communications and Networking*, vol. 2012, Oct. 2012.

[76] Yu, Z., Baxley, R. J., and Zhou, G. T., "Brightness Control in Dynamic Range Constrained Visible Light OFDM Systems," *arXiv:1304.0193*, Mar. 2013.

[77] Yu, Z., Baxley, R., and Zhou, G., "Peak-to-Average Power Ratio and Illumination-to-Communication Efficiency Considerations in Visible Light OFDM Systems," in *IEEE Intl. Conference on Acoustics, Speech, and Signal Processing*, (Vancouver, Canada), 2013.

[78] Zhao, C., Baxley, R. J., and Zhou, G. T., "Peak-to-average power ratio and power efficiency considerations in MIMO-OFDM systems," *IEEE Communications Letters*, vol. 12, pp. 268–270, Apr. 2008.

VITA

Zhenhua Yu received the B.S. degree in Information Engineering and M.S. degree in Communication and Information Engineering from Shanghai Jiao Tong University, Shanghai, China, in 2007 and 2010, respectively. He also received a M.S. degree in Electrical and Computer Engineering from Georgia Institute of Technology in 2010. He is currently working towards the Ph.D. degree in Electrical and Computer Engineering at Georgia Institute of Technology, Atlanta, GA. His research interests include OFDM, visible light communications, signal processing, and optimizations.